

NONLINEAR AND NONCLASSICAL PROPERTIES OF DEFORMED QUANTUM STATES

A thesis submitted
in partial fulfillment for the award of the degree of

Doctor of Philosophy

by

Anupama S



**Department of Physics
Indian Institute of Space Science and Technology
Thiruvananthapuram, India**

April 2023

Certificate

This is to certify that the thesis titled *NONLINEAR AND NONCLASSICAL PROPERTIES OF DEFORMED QUANTUM STATES* submitted by **Anupama S**, to the Indian Institute of Space Science and Technology, Thiruvananthapuram, in partial fulfillment for the award of the degree of **Doctor of Philosophy** is a bonafide record of the original work carried out by her under my supervision. The contents of this thesis, in full or in parts, have not been submitted to any other Institute or University for the award of any degree or diploma.

Dr. Sudheesh Chethil
Professor and Head
Department of Physics
Indian Institute of Space Science and Technology
Thiruvananthapuram - 695547
Kerala, India

Thiruvananthapuram
April 2023

Declaration

I declare that this thesis titled *NONLINEAR AND NONCLASSICAL PROPERTIES OF DEFORMED QUANTUM STATES* submitted in partial fulfillment for the award of the degree of **Doctor of Philosophy** is a record of the original work carried out by me under the supervision of **Dr. Sudheesh Chethil**, and has not formed the basis for the award of any degree, diploma, associateship, fellowship, or other titles in this or any other Institution or University of higher learning. In keeping with the ethical practice in reporting scientific information, due acknowledgments have been made wherever the findings of others have been cited.

Place: Thiruvananthapuram

Date: April 2023

Anupama S
(SC16D003)

Acknowledgements

I express my sincere gratitude to my supervisor Dr. Sudheesh Chethil for allowing me to do the research. His patience, motivation, and immense knowledge helped me and made this work possible. Also, his teaching skills and sincerity have extremely inspired me. His words of encouragement strengthened me and helped me to face life as it is.

I thank my doctoral committee members, Dr. R. Arun, Dr. Utpal Roy, Dr. Naveen Surendran, Dr. R. Muruges, and Dr. Samir Mandal, for their efforts and valuable suggestions on different stages of my work. I am grateful to them for their unfailing support and encouragement, which helped me to stay sane through all the difficulties. I would also like to thank Dr. M. Rohith for his time, effort, and suggestions. I want to express my special thanks of gratitude to S. Kannan for the valuable discussions we had and thanks for being like a brother to me more than a colleague. I thank Aditi Pradeep and Adipta Pal for the discussions and support in different stages of my research. Also, a heart full of thanks to the office staff and lab assistants of the department of Physics for their kind cooperation and support.

I further extend my gratitude to all my friends, and I feel proud to say that my life was not the same before I met them. Grateful for their moral support, and thanks for making me who I am. I am incredibly thankful to my family, especially my mother, for their love, care, and support. I would also like to thank my husband for his continuous support and understanding while undertaking the research. Thanks to Yadhu, my little brother, for the endless conversations that helped me stay out of stress.

Last but not least, I would like to express my special gratitude and thanks to my teachers, Lucy K A and Dr. A. P. Jayadevan, who guided me in the right direction while inspiring me to be the best I could be. Your care and time have made all the difference in my world.

Anupama S

Abstract

We begin our work by studying the most general class of oscillators, called ‘ f -deformed oscillators’ or ‘ f -oscillators’. We define the quadrature operator for the f -deformed algebra and hence obtain the deformed quadrature operator eigenstates. We derived a new set of polynomials and derived the deformed oscillator wavefunctions in terms of them. The position probability distributions for three different types of deformations are plotted, and each is compared with the corresponding non-deformed counterpart. The newly obtained quadrature operator eigenstates will be helpful for those who are working in the field of quantum state reconstruction and quantum information processing of deformed states.

Later, we focus mainly on one of the special cases of f -deformation, i.e., the math-type q -deformation. We inquire into the nonclassical properties of the math-type q -deformed states. Here we report the study of squeezing in q -deformed squeezed vacuum states, their superposition, and the superposition of q -deformed squeezed coherent states of a math-type q -deformed oscillator. Quadrature squeezing, higher-order squeezing, and number squeezing are studied. The analysis reveals that the states exhibit squeezing only for a specific range of the deformation parameter q and the squeezing parameter r . We find that the quadrature squeezing coefficient is independent of q , in the q -deformed squeezed vacuum states. The squeezing vanishes when we go for their superposition. We also studied another nonclassical property, the Husimi Q function, for the above mentioned states. Husimi Q function reveals that these states are highly nonclassical irrespective of squeezing. The nonclassicality present in the deformed states is found to be dependent on q , α and r .

We then extend our study of the math-type q -deformed oscillator into its dynamical behavior by analyzing its expectation values. A primary analysis of the system’s dynamics hints at the possibility of chaos in it. Although the search for chaos in quantum systems has been an area of prominent research over the last few decades, the detailed analysis of many inherently chaotic quantum systems based on expectation values of dynamical variables has not been reported in the literature. The system is found to be periodic, quasi-periodic, or chaotic depending on the values of the deformation parameter q and the deformed coherent amplitude α , thus enabling us to explicitly classify the chaotic nature of the system based

on these parameters. A further detailed study using recurrence plots, power spectra, first-return-time distributions, and Lyapunov exponents unambiguously confirmed the chaotic behavior of the system, existing over a specific range of q and α values.

We outstretch the study of the nonclassicality of a math-type q -deformed system to quantum entanglement, one of the most discussed and relevant areas of quantum physics. We deal with the propagation of a single-mode math-type q -deformed field through a nonlinear medium, where the atoms of the medium interact with the deformed field. We measure the entanglement in terms of von Neumann entropy, and its temporal evolution shows that the states are entangled for all the possible deformation values. We have considered the system in two different initial states, whose dynamics exhibit near revivals and fractional revivals. But the revivals die out even for a slight deformation increase. Thus here we provide the analysis of a general deformed system, with an additional degree of freedom, i.e., the deformation parameter q to control its nonlinear and nonclassical properties.

Contents

List of Figures	xi
Nomenclature	xv
1 Introduction	1
2 Quadrature operator eigenstates and energy eigenfunctions of f-deformed oscillators	9
2.1 Introduction	9
2.2 The non-deformed harmonic oscillator	10
2.3 Review of f -oscillators	11
2.4 Deformed position and momentum operators	13
2.5 The f -deformed quadrature operator and wavefunctions of the f -deformed oscillator	14
2.6 Conclusion	22
3 Squeezing and nonclassicality of q-deformed superposition states	25
3.1 Introduction	25
3.2 Squeezing and Husimi Q function	26
3.3 q -deformed squeezed states and their superpositions	31
3.4 Results and discussion	33
3.5 Conclusion	47
4 Dynamics of observables in a q-deformed harmonic oscillator	49
4.1 Introduction	49
4.2 Harmonic oscillator and energy eigenvalues	50
4.3 Time evolution with q -deformation	51

4.4	Results and Discussion	56
4.5	Conclusion	62
5	Entanglement dynamics in q-deformed states	64
5.1	Introduction	64
5.2	Light propagating through a Kerr medium	65
5.3	The model	65
5.4	Entanglement measures and von Neumann entropy	66
5.5	Entanglement dynamics	67
5.6	Conclusion	73
6	Conclusion	74
	Bibliography	75
	List of Publications	87
	Appendices	89
A	The calculation of Husimi Q-function for the state $\xi\rangle_q^m$	89
B	The calculation of $\langle X_q^{m^2} \rangle$ for the deformed squeezed superposition state $\alpha, \xi\rangle_{s,q}^m$	91
C	Calculation of reduced density matrix for the system with initial state $N_q^m; 0\rangle$	93

List of Figures

2.1	Position probability distributions of a non-deformed harmonic oscillator for different values of n , and corresponding energy eigen values.	11
2.2	A schematic representation of the balanced homodyne detection setup.	15
2.3	(a) ground state and (b) first excited state probability distribution functions for the harmonic oscillator (solid), a deformed oscillator with $q = 0.90$ (dotted), $q = 0.80$ (dash-dotted), and $q = 0.30$ (dashed) in the case of math type q -deformation. For $q = 0.3$, we have included insets in Figures 1(a) and 1(b) to show that wavefunctions go to zero moderately.	20
2.4	(a) ground state and (b) first excited state probability distribution functions for the harmonic oscillator (solid), deformed oscillator with $q=1.1$ (dashed), $q=1.5$ (dash-dotted) and $q=1.9$ (dotted) in the case of physics type q -deformation.	21
2.5	(a) ground state and (b) first excited state probability distribution functions for harmonic oscillator(solid), deformed oscillator with $p=1.3$ $q=0.5$ (dashed), $p=1.5$ $q=0.5$ (dash-dotted) and $p=1.9$ $q=0.5$ (dotted) in the case of (p,q) -deformation.	23
3.1	(a) Vacuum state and (b) the coherent state in the phase space representation.	26
3.2	(a) Squeezed vacuum state with $\theta = 0$ and (b) Squeezed vacuum state with $\theta = \pi$ showing squeezing in different quadratures.	29
3.3	(a) Variation of the squeezing coefficient S_X and (b) the variation of S_P when $\theta = 0^\circ$ for the state $ \xi\rangle_q$. It shows that squeezing coefficient is the same for all q values.	35
3.4	(a) Variation of the squeezing coefficient S_X and (b) the variation of S_P when $\theta = 30^\circ$, for the state $ \xi\rangle_q$. Squeezing coefficient is same for any value of q	35

3.5	(a) Variation of the squeezing coefficient S_X^4 when $\theta = 0^\circ$ ($= S_P^4$ when $\theta = 180^\circ$) and (b) shows the variation of S_P^4 when $\theta = 0^\circ$ ($= S_X^4$ when $\theta = 180^\circ$) with r , for the state $ \xi\rangle_q^m$. In contrast to squeezing, the higher order squeezing is different for different q values.	37
3.6	The variation of Q with r for the state $ \xi\rangle_q^m$. Q is different for different q values. The black horizontal line ($Q = 0$) shows Poisson statistics. Number squeezing is shown below this line.	39
3.7	(a) Q function for $q = 0.1$ and (b) Q function for $q = 0.9$ for the state $ \xi\rangle_q^m$, with $r = 0.1$	40
3.8	The variation of Q with r for the superpsition state $ \xi\rangle_{s,q}^m$. Q is different for different q values. Number squeezing is shown below the black horizontal line ($Q = 0$).	41
3.9	(a) Q function for $q = 0.1$ and (b) Q function for $q = 0.9$ for the state $ \xi\rangle_{s,q}^m$, with $r = 0.1$	42
3.10	(a) Variation of the squeezing coefficient S_X and (b) shows the variation of S_P with r for the state $ \alpha, \xi\rangle_{s,q}^m$. Squeezing coefficient is different for different q values and we have taken $\alpha = 1$	43
3.11	(a) The variation of the squeezing coefficient S_X^4 and (b) shows the variation of S_P^4 with r , for the state $ \alpha, \xi\rangle_{s,q}^m$ with $\alpha = 1$	45
3.12	Variation of the Mandel Q -parameter for (a) $\alpha = 1$ and (b) $\alpha = 2$, for the state $ \alpha, \xi\rangle_{s,q}^m$. Q is different for different q values. The sub-Poissonian behavior is shown below $Q = 0$ (black horizontal line).	45
3.13	Q function for $q = 0.5$ with (a) $r = 0.8$, $\alpha = 0.3$ and (b) $r = 1.2$, $\alpha = 0.5$ for the state $ \alpha, \xi\rangle_{s,q}^m$	46
4.1	The energy of a classical harmonic oscillator against its position. The total energy E is the sum of potential and kinetic energies. A and $-A$ are the turning points at which the kinetic energy of the oscillator is zero.	50
4.2	Plot of energy vs n for a (a)non-deformed oscillator and a (b) deformed oscillator with different q values. (b) shows that the energy eigenvalues are distributed in a nonlinear fashion for the q -deformed oscillator which is in contrast to (a) the linearly distributed energy eigenvalues of the non-deformed harmonic oscillator.	52
4.3	Plot of autocorrelation function as a function of time for (a) non-deformed harmonic oscillator and (b) deformed one with $ \alpha ^2 = 1$ and $q = 0.95$. . .	53

4.4	Time evolution of $\langle X(t) \rangle_q^m$ for different q values and $\alpha = 1$	56
4.5	Phase space diagrams $\langle X(t) \rangle_q^m$ vs $\langle P(t) \rangle_q^m$ for different q values and $\alpha = 1$	57
4.6	Phase space diagrams for different values of α and $q=0.95$	58
4.7	Recurrence plots for different q values when $\alpha = 1$. (a) corresponds to periodic data, (b), (d) correspond to quasi-periodic data and (c) corresponds to chaotic data.	59
4.8	Power spectra for $\alpha = 2$ showing (a) chaotic nature ($q = 0.9$), and (b) periodic nature ($q = 0.999$).	60
4.9	First-return-time distributions for different values of q and $\alpha = 1$. (a) corresponds to periodic data, (b), (d) corresponds to quasi-periodic data and (c) corresponds to chaotic data. The solid black line in the first-return-plot represents the fitted exponential curve mentioned in section 4.3.2.	61
4.10	Plots showing (a) variation of largest Lyapunov exponent with q value, and (b) the Lyapunov exponent plot for $\alpha = 1$ and $q = 0.9$ showing the chaotic nature of the system.	62
4.11	Behaviour of a q -deformed oscillator with respect to α and q values.	63
5.1	The variation of von Neumann entropy with q for different values of N , with the values of system parameters representing the action of a beam splitter.	69
5.2	The variation of von Neumann entropy with γt for (a) non-deformed, (b) $q = 0.9$, (c) $q = 0.7$, (d) $q = 0.5$ for the initial state $ 5, 0\rangle$	70
5.3	The variation of von Neumann entropy with γt for (a) non-deformed, (b) $q = 0.9$, (c) $q = 0.7$, (d) $q = 0.5$ for the initial state $ 10, 0\rangle$	70
5.4	The variation of von Neumann entropy with γt for (a) non-deformed, (b) $q = 0.99$, (c) $q = 0.95$, (d) $q = 0.90$ for the initial state $ \alpha, 0\rangle$ for $ \alpha ^2 = 0.5$	72
5.5	The variation of von-Neumann entropy with γt for (a) non-deformed, (b) $q = 0.99$, (c) $q = 0.95$, (d) $q = 0.90$ for the initial state $ \alpha, 0\rangle$ for $ \alpha ^2 = 1$	72

Nomenclature

a, a^\dagger	ladder operators for the non-deformed single-mode electromagnetic field
$ n\rangle$	non-deformed harmonic oscillator energy eigenstates
\hat{n}	the non-deformed number operator
n	eigen value of the non-deformed number operator
\hat{x}_θ	the non-deformed homodyne quadrature operator
x, p	non-deformed position and momentum operators
A_f, A_f^\dagger	f -deformed ladder operators
Q	general deformation parameter
$ n\rangle_f$	f -deformed harmonic oscillator energy eigenstates
\hat{N}_f	the f -deformed number operator
$[n]_f$	eigen value of the f -deformed number operator
H_f	the f -deformed Hamiltonian
X_f, P_f	f -deformed position and momentum operators
$\hat{X}_{\theta,f}$	f -deformed homodyne quadrature operator
$ X_\theta\rangle_f$	the eigenstate of the f -deformed quadrature operator
$\psi_{n,f}(X_\theta)$	the energy eigenfunction of the f -oscillator
q	q -deformation parameter
$A_q^m, A_q^{m\dagger}$	the math-type q -deformed ladder operators
X_q^m, P_q^m	math-type q -deformed position and momentum operators
$\hat{X}_{\theta,q}^m$	math-type q -deformed homodyne quadrature operator
$ X_\theta\rangle_q^m$	the eigenstate of the math-type q -deformed quadrature operator
$\psi_{n,q}^m(X_\theta)$	the energy eigenfunction of the math-type q -oscillator
$E_{q,n}$	energy eigen value of the math-type q -deformed harmonic oscillator
$ \alpha\rangle_q^m$	the math-type q -deformed coherent state
$A_{(p,q)}, A_{(p,q)}^\dagger$	the (p, q) -deformed ladder operators
$A_q^p, A_q^{p\dagger}$	the physics-type q -deformed ladder operators
$H_n(x_\theta)$	the Hermite polynomial

λ_{max}	greatest Lyapunov exponent
S_ξ	the squeezing operator
ξ	the squeezing parameter
$ \xi\rangle_q^m$	q -deformed squeezed vacuum state
$ \xi\rangle_{s,q}^m$	superposition of two q -deformed squeezed vacuum states
$ \alpha, \xi\rangle_q^m$	q -deformed squeezed coherent state
$ \alpha, \xi\rangle_{s,q}^m$	superposition of two q -deformed squeezed coherent state
S_X	the squeezing coefficient in X -quadrature
S_P	the squeezing coefficient in P -quadrature
Q	the Mandel Q-parameter
Q_α	Husimi function, or Q function
ω	the natural frequency of the atomic field
χ	the nonlinearity parameter of the nonlinear medium
γ	the parameter characterizing the strength of coupling between the field and the atoms
S	von Neumann entropy
S_k	von Neumann entropy of the subsystem
ρ_k	time-dependent reduced density matrix for the subsystem

Chapter 1

Introduction

Nonclassical states of light serve as critical resources for the basic understanding of quantum mechanics and also find applications in fields like quantum computation, quantum metrology, etc. Nonclassical states, such as entangled and squeezed states are usually generated using devices like optical parametric oscillators or frequency doublers. They are also generated in systems like a single-atom laser. A squeezed state of light refers to that state with an uncertainty smaller than that of a coherent state, having potential applications in low-noise communications. They find essential applications in gravitational wave detection [1, 2, 3], optical communications [4], quantum metrology [5], laser interferometers [6], etc. Several recent pieces of research regarding the importance of squeezing in quantum physics exist. A recent study [7] introduces squeezed comb states which are less error-prone when subjected to amplitude damping. One of the critical applications of quantum optics, quantum sensing, is found to be enhanced using squeezing techniques [8]. The authors of another recent work [9] unveil an experiment that can shed some ‘squeezed light’ on dark matter, one of the universe’s greatest mysteries. Apart from squeezing, the idea behind quantum entanglement was developed in the early decades of the 20th century. As one of the most discussed areas of quantum physics, quantum entanglement continues to puzzle researchers worldwide. Entanglement finds applications in the emerging fields of quantum physics such as quantum cryptography [10], quantum metrology [11], superdense coding [12], quantum teleportation [13], etc. The generation of new quantum states with different nonclassical properties has increased the investigation of other types of entangled states. Macroscopic entangled coherent states based on circuit QED [14], Entangled squeezed states in BEC [15], and bound entangled Gaussian states [16], to mention a few. Since quantum entanglement has attracted much attention, several important research outcomes have happened in recent years. Quark and gluon entanglement in the proton is studied and reported in a recent work [17]. Recently, a quantum processor has been developed [18]

using the idea of coherent transport of entangled atom arrays, which provides a route to achieve great goals in fields ranging from simulation to metrology.

Another exciting aspect is the study of nonlinear behavior in quantum systems. Chaos is a generic term that describes systems with a strong sensitivity towards initial conditions. In classical chaotic systems such as multiple coupled anharmonic oscillators, asteroid orbits, double rod pendulums, and so on, a small perturbation in the initial conditions manifests itself as an exponential change in the system trajectories over time. Although several chaotic dynamical systems have been studied in the classical regime, the search for its counterpart in the quantum regime posed some consequences. Bohr's correspondence principle, which states that the behavior of quantum systems reproduces their classical counterparts in the limit of large quantum numbers, mandates the appearance of chaos in quantum systems. However, the discreteness of the quantum energy levels and the solutions to the Schrödinger equation restricts them to a quasi-periodic behavior [19]. As a result, a common approach has been to quantize existing classical systems and analyze how these systems behave in a quantized scenario [20, 21]. These systems were reported to show chaotic behavior equivalent to their classical counterparts only for short periods of time. Another relatively popular methodology in this direction has been identifying chaotic analogs from quantum systems in the semi-classical limit. However, these systems showed chaos only under limiting conditions [22, 23]. So, inherent quantum chaos is still an unexplored area of quantum physics. We are interested in studying the nonlinear and nonclassical properties of a quantum harmonic oscillator with a deformed algebra. The motivation for choosing such a system is what follows hereafter.

When we learn classical mechanics, it is known to everyone that the harmonic oscillator is one of the most important systems in the whole of physics. It allows us to study problems ranging from the vibration of strings to the behavior of electronic circuits. The harmonic oscillator plays a similarly central role in quantum mechanics. In the quantum world, it allows us to study the properties ranging from the motion of atoms in solids to the behavior of light. But there is a fundamental reason that the harmonic oscillator plays a key role; it is very effectively used to exemplify important quantum mechanical concepts. It is to be noted that the simple harmonic oscillator is an ideal one that does not fit all of the real-life examples. Considering the deviations or deformations from the ideal case will be far more advantageous. The deformations in the algebra of a simple harmonic oscillator have been an exciting area of research over the last few decades. The most general one is the f -deformation, where the algebra of the oscillator is deformed by a function $f(n)$. f -deformation is an active area of research; a few are mentioned here.

The f -deformed Hamiltonian has been studied for the anti-Jaynes-Cummings model, with applications in quantum optic interferometers [24]. Another recent research shows that the f -deformed Dirac oscillator can describe the electrons in a nonlinear zig-zag graphene nanoribbon causes a significant difference between Landau levels in the f -deformed oscillator and the non-deformed one [25]. A mathematical procedure to obtain analytical expressions for a general class of deformed coherent states associated with the different patterns of the energy spectrum exhibited by the nonlinear f -oscillator was presented in the literature [26], and deformed photon-added nonlinear coherent states were constructed using nonlinear coherent states [27]. Even though f -deformation is the most generalized one of its types, the type of deformation that reported in the literature for the first time was one of its special cases, namely ‘physics-type q -deformation’, formulated by A. J. Macfarlane [28] where the deformed quantum group $SU_q(2)$ was discussed in detail. Some other special cases of f -deformation, such as math-type q -deformation and (p, q) -deformation, exist, which will be discussed later.

Although the general deformed f -oscillators with their different classes have generated much importance in recent years, their wavefunctions remain unknown, which is the prime motivation to begin our work. A notable attempt has been made to derive a generalized wavefunction encompassing the Macfarlane and Dubna type oscillators [29]. However, this expression is limited by its intricate and restricted access to the parameters involved, thus unable to provide a clear-cut wavefunction to study the system. The analytical wavefunction of a non-deformed harmonic oscillator can be easily evaluated from the knowledge of the deformed Hermite polynomials. Unfortunately, an explicit expression for the deformed Hermite polynomials is unknown when subject to f -deformation, but some attempts have been made over the years. In another work [30], the authors have tried to approach the problem by evaluating the analytical form of the q -deformed Hermite polynomial in terms of the position operator \hat{X} . This result is also limited by the lack of knowledge of the nature and form of operator \hat{X} . However, recently, using the expression for the math-type q -deformed quadrature operator \hat{X}_θ , the expression for math-type q -deformed Hermite polynomial has been found [31]. The paper [31] deals only with the math-type q -deformed oscillator but not the general f -deformed case and does not discuss in detail the wavefunctions of the oscillator. The quadrature wavefunctions of quantum systems are essential for better understanding physical systems and reconstruction of quantum systems from experiments. We begin our study by defining the f -deformed quadrature operator and then obtaining the quadrature wavefunctions for different deformed oscillators with different degrees of deformation.

As we move on further, we mainly concentrate on one of the special cases of f -deformation, the math-type q -deformation, which has acquired more attention in the literature than any other type of deformation. It is an area of active research in quantum optics. The math-type q -deformation have been used recently to study the cosmic microwave background radiation [32]. The energy density distribution of bosons obeying the math-type q -deformations of the harmonic oscillator algebra has been studied in [33]. A class of Fibonacci oscillators that uses deformed algebras has found applications in the Debye model to study the thermodynamics of crystalline solids [34] and the Landau diamagnetism [35]. Also, a recent study of the behavior of math-type q -deformed harmonic oscillator clearly shows the signature of chaos in the system [36]. In the case of math-type q -deformation, the algebra of the simple harmonic oscillator $aa^\dagger - a^\dagger a = 1$ is deformed by a parameter q (which is a real number) in such a way that the algebra becomes $AA^\dagger - q^2 A^\dagger A = 1$ with (A, A^\dagger) and (a, a^\dagger) being the deformed and non-deformed ladder operators respectively. Since it is crucial to understand the physical meaning and interpretation of such deformations, several attempts have been made to unfold the same. A work done by Manko et al. [37] used the Dirac quantization method to study the classical and quantum q -deformed oscillators and thereby constructed the classical oscillator from its quantum q -deformed counterpart. Their results conclude that the quantum q -deformed oscillator is a classical oscillator with a special type of nonlinearity. Another study was done by Gruver [38] on the dynamical properties of a q -deformed oscillator showed that a q -deformed oscillator is equivalent to an anharmonic oscillator, and the deformation parameter q is a measure of its anharmonicity. Another special case of f -deformation, the physics-type q -deformation is also has some interesting research outcomes. It is reported in the literature that quantum logic gates have been constructed using physics-type q -deformed harmonic oscillator algebras [39]. It has been shown that physics-type q -deformed bosonic exciton gas constitutes the high-density limit of Frenkel excitons which may provide valuable insight into Frenkel excitons inside nanomaterials [40]. The (p, q) -deformed bosons, another particular case of f -deformed states, have been used to study deformed Bose gases with critical temperature ratio $T_c^{p,q}/T_c$, which explicitly depends on the deformation parameters p and q [41]. The solutions of deformed Einstein equations and quantum black holes which use q and (p, q) -deformed algebras, have been obtained recently [42]. The low-temperature behavior of deformed fermion gas models has been used to find interactions of quasiparticles that have applications in nanomaterials [43].

We begin the second part of our work by studying the nonclassical properties of the math-type q -deformed states. The generalized squeezed states [44] are interesting and re-

cently gained importance as they provide additional degrees of freedom in a system [45]. The generalized states can be constructed by replacing the ordinary ladder operators with the generalized ones [46]. Generalized photon-subtracted squeezed vacuum states are already studied, and their nonclassical properties are investigated [47]. As there exists a wide variety of nonclassical states of light, we aim to search for nonclassicality in the superposition of q -deformed states. The linear superposition principle is one of the fundamental concepts of quantum mechanics [48]. The study of the superposition of a variety of squeezed states is gaining importance in recent years. A study on the nonclassical properties of superposition of squeezed states in the non-deformed scenario was done recently [49]. Another study is about the dynamics and decoherence of the nonclassical properties of noncommutative deformed cat states [50]. The nonclassical properties of q -deformed noncommutative cat states are studied in another work [51]. In another work, the authors study the optical properties of the superposition of q -deformed coherent states [52]. A recent work [53] deals with a gravitational cat state (gravcat) where the authors explore the properties of the two-gravcat system for BECs. Also, the nonlinear dynamics of the superposition of quantum wavepackets are studied for various systems [54]. Our study is a generalization of the result obtained in the non-deformed scenario [49] to the q -deformed case. We can also find some other works in the literature which study the nonclassical properties of generalized squeezed states [55, 56], but they use non-deformed quadrature operators, which is conceptually wrong. Here, we focus on the superposition of two q -deformed squeezed vacuum states and the superposition of two q -deformed squeezed coherent states and study their squeezing and nonclassical properties in measures such as quadrature squeezing, higher-order squeezing, number squeezing, and deformed Husimi Q function.

Later, our study of the dynamical behavior of a math-type q -deformed harmonic oscillator ended up revealing the nonlinear behavior in the same system. A pure harmonic oscillator with energy eigenvalues E_n has a linear dependence on n . While in the deformed regime, we observed a nonlinear increase in its energy eigenvalues. It is already given in the literature that the linear dependence of energy eigenvalues in the case of a non-deformed oscillator leads to a periodic behavior of the dynamics of its expectation values. Thus we proceeded with a hint that this nonlinear behavior may show a chaotic nature in this system, which we have investigated thereafter. It is worth mentioning that some authors used the expectation values of dynamical variables to study the chaotic behavior of quantum systems [57, 58, 59]. Here, in the course of our study, we are advancing this analysis by extending it to the q -deformed systems. The deformation of the Lie algebra engenders unusual properties in these deformed quantum systems, thus deeming them potential candidates to search

for chaotic behavior in quantum mechanics. Various tools like the recurrence plots, first return time distributions, Lyapunov exponents and power spectra helped us in the proper analysis of the system.

After analyzing the expectation values of the dynamical variables and thereby showing the signatures of chaos in a math-type q -deformed quantum system, we have focused on a more detailed study of nonclassical properties of the same. In this part of the research, we analyze the entanglement dynamics of a q -deformed quantum system. The study of entanglement in deformed states is a promising and progressing area of research. The authors of [60] studied the entanglement of a deformed field interacting with a three-level atom and tested the observations with experimentally accessible parameters. Nonlinear optical tomography entangled pair coherent states in a q -deformed oscillator are studied and reported in another recent research [61]. Another recent research [62] reports the study of quantum scar states from q -deformed Lie algebras using entanglement entropy. Regarding the study of entanglement, the most important part is to test whether a given quantum state is entangled. There are different entanglement measures that are being used for the quantum states. They include von-Neumann entropy [63], concurrence [64], negativity [65] and quantum Fisher information [58]. In light of all the current research, we put forward the aim of the final part of our research to investigate the entanglement dynamics of the q -deformed states in the presence of a Kerr-like nonlinear medium. It is important to know the entanglement dynamics of a deformed system which plays a vital role in quantum information processing. As we stated earlier, the deformed systems are more favorable than the ideal non-deformed systems. Even though not yet been achieved experimentally, such an advantageous system will surely find applications in the near future.

A summary of the contents of the rest of this thesis is given below:

In **Chapter (2)**, we propose the study of the f -deformed quadrature operator and thereby obtain the energy eigenfunctions of the prominent f -oscillators. We plotted wavefunctions for three different types of deformations. Also, we made a comparison with the non-deformed oscillator's wavefunctions.

Chapter (3) reports the study of the squeezing and nonclassicality in the q -deformed squeezed vacuum states, the superposition of two q -deformed squeezed vacuum states, and the superposition of two q -deformed squeezed coherent states using deformed quadra-

ture operators. Despite the quadrature and number squeezing, the analysis of the Husimi Q-function reveals that these states are highly nonclassical.

In **Chapter (4)**, we report the study of the dynamical behavior of the math-type q -deformed harmonic oscillator system widely studied in quantum optics. The analysis of expectation values of dynamical variables carried out in this work clearly shows signatures of inherent quantum chaos in the system.

Chapter (5) is an extension of the analysis of nonclassical properties of deformed oscillators. Here we discussed the propagation of a single-mode math-type q -deformed field through a nonlinear medium and studied the entanglement dynamics of the system in terms of the von Neumann entropy. The system in different initial states is investigated.

Chapter (6) concludes the thesis with a discussion on possible interesting future works.

Chapter 2

Quadrature operator eigenstates and energy eigenfunctions of f -deformed oscillators

2.1 Introduction

“The career of a young theoretical physicist consists of treating the harmonic oscillator in ever-increasing levels of abstraction”

The quote by Sidney Richard Coleman, the famous American theoretical physicist, said during one of his lectures at Harvard University, refers to the key role that the harmonic oscillator plays in all fields of physics.

Using a simple harmonic oscillator to illustrate the basic concepts and methods makes it one of the most important systems in quantum mechanics. Such a system is important because it provides general solutions that contribute to the modeling and understanding of many oscillatory systems, for example, the vibrational motion between two atoms in a diatomic molecule. Quantum harmonic oscillator finds practical applications in various fields, such as quantum optics, quantum field theory, nuclear physics, etc.

A pure quantum harmonic oscillator is deformed, so a deformed commutation relation replaces the usual canonical commutation relation. Considering the importance and the recent research regarding deformed oscillators, as mentioned in Chapter(1), we propose the study of f -deformed quadrature operator in this chapter and thereby obtain the energy eigenfunctions of the prominent f -oscillators. Despite their importance in the literature, the fact that their wavefunctions remain unknown has become the basic motivation of our study. Our results will be helpful for quantum state reconstruction and quantum information

processing.

2.2 The non-deformed harmonic oscillator

The basic Hamiltonian for a pure quantum harmonic oscillator is given by

$$H = \frac{1}{2}(a^\dagger a + a a^\dagger), \quad (2.1)$$

with $\hbar\omega = 1$, a and a^\dagger are the annihilation and creation operators which obey the canonical commutation relation

$$[a, a^\dagger] = a a^\dagger - a^\dagger a = I, \quad [a, I] = [a^\dagger, I] = 0, \quad (2.2)$$

where I , is the identity operator.

The number operator N can be defined as $N = a^\dagger a$, where $N|n\rangle = n|n\rangle$ and $|n\rangle$ are the oscillator energy eigenstates with $n = 0, 1, 2, \dots$. In terms of N , the Hamiltonian (2.1) can be rewritten as

$$H = N + \frac{1}{2}, \quad (2.3)$$

which means the energy eigen values of the non-deformed harmonic oscillator are

$$E = n + \frac{1}{2} \quad (2.4)$$

with the smallest possible value $E_0 = \frac{1}{2}$ known as the zero-point energy. (2.4) gives the quantized energy levels in the system with a difference of E_0 from the lower one. The corresponding energy eigen functions in the position representation are

$$\psi_n(x) = \frac{H_n(x)}{\pi^{\frac{1}{4}} 2^{\frac{n}{2}} \sqrt{n!}} e^{-in\theta} e^{-\frac{x^2}{2}}, \quad (2.5)$$

with $H_n(x)$ being the Hermite polynomial and $\frac{e^{-\frac{x^2}{2}}}{\pi^{\frac{1}{4}}}$ being the ground state wavefunction $\psi_0(x)$. Also, the position and momentum operators satisfy the commutation relation $[x, p] = i$. The position probability distributions $P_n(x) = |\psi_n(x)|^2$ corresponding to different energy values is shown in figure (2.1).

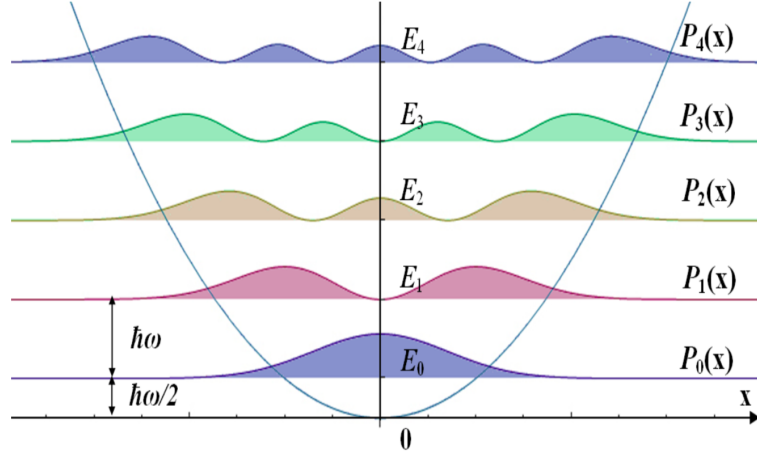


Figure 2.1: Position probability distributions of a non-deformed harmonic oscillator for different values of n , and corresponding energy eigen values.

2.3 Review of f -oscillators

The authors of [66] have defined the operator A_f and its adjoint A_f^\dagger as a nonlinear expansion of the usual harmonic oscillator operators a and a^\dagger :

$$A_f = af(n), \quad A_f^\dagger = f^\dagger(n)a^\dagger. \quad (2.6)$$

The operators A_f and A_f^\dagger in terms of a function $f(n)$ define a new class of oscillators called as f -oscillators which reduces to the usual harmonic oscillator operators a and a^\dagger when $f(n) = I$, where A_f and A_f^\dagger satisfy [67]:

$$[A_f, A_f^\dagger] = \phi(n), \quad (2.7)$$

where $\phi(n) = f(n+1)f^\dagger(n+1)(n+1) - f(n)f^\dagger(n)n$. They also obey the Q -commutation relation

$$\begin{aligned} [A_f, A_f^\dagger]_Q &= A_f A_f^\dagger - Q A_f^\dagger A_f \\ &= f(n+1)f^\dagger(n+1)(n+1) - Q f(n)f^\dagger(n)n, \end{aligned} \quad (2.8)$$

where Q is a general deformation parameter and different forms of Q provide different types of deformation; we will be considering a few specific types of deformations in this paper. The above relation reduces to the canonical commutation relation (2.2) when $Q \rightarrow 1$ and $f(n) = I$.

We can now define a new set of eigenstates $|n\rangle_f$ that form a complete orthonormal basis in the f -deformed Fock space provided that there exists a deformed number operator $N_f = A_f^\dagger A_f$ with eigenvalue $[n]_f$ having the form

$$[n]_f = |f(n)|^2 n, \quad (2.9)$$

such that,

$$N_f |n\rangle_f = A_f^\dagger A_f |n\rangle_f = [n]_f |n\rangle_f, \quad {}_f\langle m|n\rangle_f = \delta_{mn}. \quad (2.10)$$

The action of A_f and A_f^\dagger on the deformed Fock states $|n\rangle_f$ are given by

$$\begin{aligned} A_f |n\rangle_f &= \sqrt{[n]_f} |n-1\rangle_f, \quad A_f |0\rangle_f = 0 \text{ and} \\ A_f^\dagger |n\rangle_f &= \sqrt{[n+1]_f} |n+1\rangle_f. \end{aligned} \quad (2.11)$$

$|n\rangle_f$ is also the eigenstate of the Hamiltonian [67]

$$H_f = \frac{\omega}{2} \left(A_f^\dagger A_f + A_f A_f^\dagger \right) \quad (2.12)$$

with the eigenvalue

$$E_{n,f} = \frac{\omega}{2} [(n+1)f(n+1)f^*(n+1) + nf(n)f^*(n)]. \quad (2.13)$$

Now we review some special cases of f -oscillators which we will be considering in our study:

- The math-type q -deformation obeys the commutation relation [46]:

$$A_q^m A_q^{m\dagger} - q^2 A_q^{m\dagger} A_q^m = I, \quad (2.14)$$

where, $0 < q < 1$ with $Q = q^2$. Here,

$$[n]_q^m = \frac{1 - q^{2n}}{1 - q^2}, \quad (2.15)$$

where q is the deformation parameter and the superscript m stands for math-type q -deformation and we use the same in the rest of the work.

- The (p, q) -deformation follows the commutation relation [68]:

$$A_{(p,q)} A_{(p,q)}^\dagger - p A_{(p,q)}^\dagger A_{(p,q)} = q^{-n}. \quad (2.16)$$

Here, $Q = p$ and

$$[n]_{(p,q)} = \frac{q}{1-pq} (q^{-n} - p^n). \quad (2.17)$$

The subscript (p, q) represents the (p, q) -deformation, where p and q are the deformation parameters.

- The physics-type q -deformation [69] is actually a special case of (2.16) with $p = q$, giving us

$$A_q^p A_q^{p\dagger} - q A_q^{p\dagger} A_q^p = q^{-n}, \quad (2.18)$$

where $q > 1$. Here, $Q = q$ and putting $p = q$ in (2.17), we get

$$[n]_q^p = \frac{q}{1-q^2} (q^{-n} - q^n), \quad (2.19)$$

where the superscript p denotes the physics-type q deformation with the deformation parameter q .

Similar relations can be obtained for other maths-type [70, 71] and physics-type [72] deformed oscillators.

2.4 Deformed position and momentum operators

In quantum mechanics, the position and momentum operators \hat{x} and \hat{p} are the operators corresponding to the position and momentum observables of a particle. They are known to satisfy the canonical commutation relation

$$[x, p] = i, \quad (2.20)$$

which forms one of the cornerstones of quantum mechanics. The commutation relation leads to the position-momentum uncertainty relation of W. Heisenberg,

$$\langle (\Delta x)^2 \rangle \langle (\Delta p)^2 \rangle \geq \frac{1}{4}, \quad (2.21)$$

It is a key principle in quantum mechanics which states that if we know exactly where the particle is placed, we know nothing about its momentum and vice versa.

As we said earlier, the deformations are imposed in such a way that the usual commutation relation is replaced by the deformed one. Consider the position operator X_f and momentum operator P_f for the f -oscillator in terms of the f -deformed ladder operators [73, 74]

$$X_f = \alpha(A_f^\dagger + A_f), \quad P_f = i\beta(A_f^\dagger - A_f), \quad (2.22)$$

where $\alpha, \beta \in \mathfrak{R}$. In the non-deformed limit, (2.22) reduces to

$$x = \frac{1}{\sqrt{2}}(a^\dagger + a), \quad p = \frac{i}{\sqrt{2}}(a^\dagger - a), \quad (2.23)$$

which are the non-deformed position and momentum operators respectively. Rearranging (2.22), we obtain the expressions for A_f and A_f^\dagger in terms of X_f and P_f . Substituting these expressions for A_f and A_f^\dagger into (2.8), for $\alpha = \beta = \frac{\sqrt{1+Q}}{2}$, we obtain the following commutation relation for the deformed operators X_f and P_f :

$$[X_f, P_f] = i[f(n+1)f^\dagger(n+1)(n+1) - Qf(n)f^\dagger(n)n - \frac{1-Q}{1+Q}(X_f^2 + P_f^2)]. \quad (2.24)$$

We can see that the above relation gives distinct deformed algebras for the examples mentioned in the previous section when their respective functions $|f(n)|^2$ and respective deformation parameters Q are substituted. Also, the deformed commutation relation (2.4) reduces to the non-deformed case (2.4) as $q \rightarrow 1$.

2.5 The f -deformed quadrature operator and wavefunctions of the f -deformed oscillator

A quadrature operator, also known as a quadrature variable, serves a vital role in quantum optical systems. The quadrature operator is a function of a phase factor, and it becomes the position or momentum operator when the phase factor acquires a value 0 or π , respectively. One can use the homodyne detection method to observe the quadrature operator associated with a field.

The detection setup is briefly discussed here: The figure (2.2) depicts the basic experi-

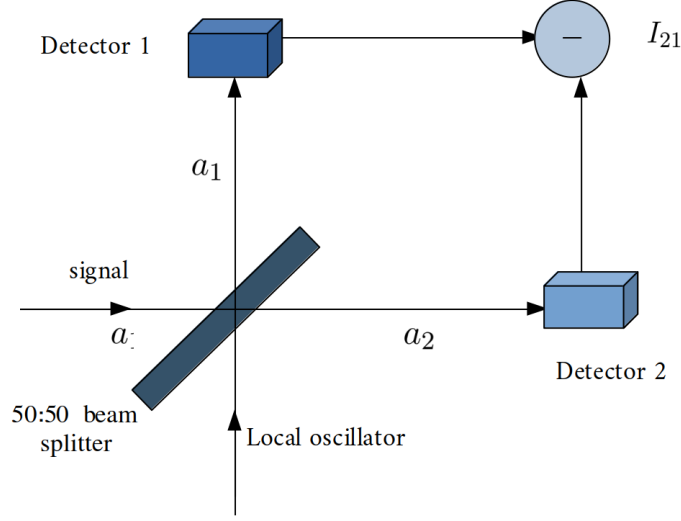


Figure 2.2: A schematic representation of the balanced homodyne detection setup.

mental setup for the balanced homodyne detection setup. We send a signal (for which the quadrature is to be measured) that interferes with a local oscillator using a balanced 50:50 beam splitter. The local oscillator provides the phase difference ‘ θ ’ which can be varied by adjusting the local oscillator during the measurement. The local oscillator is chosen to behave classically (which means we can neglect the quantum fluctuations in it); hence we choose a coherent laser beam for it. After the optical mixing, the split beams are directed towards two photodetectors. The photocurrents I_1 and I_2 , thus detected, are measured and subtracted from each other. The resulting quantity contains the interference term of the signal and the local oscillator, from which the quadrature component can be extracted. The detector also serves as an amplifier that amplifies the signal above the electronic noises of the photodiodes, thereby increasing its efficiency to a nearly perfect technical solution.

Quadrature variables such as position and momentum play an important role in the phase-space representation of quantum mechanics. Wigner function and Husimi Q function are frequently used quasi-probability distributions which are functions of quadrature variables. Also, the quadrature wavefunctions of quantum systems are essential for better understanding physical systems and reconstruction of quantum systems from experiments.

The homodyne quadrature operator corresponds to the non-deformed canonical commutation relation given in (2.2) is [75, 76, 77, 78]

$$x_\theta = \frac{1}{\sqrt{2}}(ae^{-i\theta} + a^\dagger e^{i\theta}). \quad (2.25)$$

where θ is the phase of the local oscillator, such that $0 \leq \theta \leq 2\pi$. It is easy to see that we obtain the canonical position and momentum operators x and p when $\theta = 0$ and $\theta = \pi/2$, respectively.

The q -deformed homodyne quadrature operator $X_{\theta,q}$ is defined in [31] that reports the study of optical tomogram of q -deformed coherent states. In a similar way, it can be easily verified using the photon-number difference in the two output channels of the beam splitter in homodyne detection setup that the f -deformed homodyne quadrature operator takes the form

$$X_{\theta,f} = \frac{\sqrt{1+Q}}{2}(A_f e^{-i\theta} + A_f^\dagger e^{i\theta}), \quad (2.26)$$

and it becomes deformed position and momentum operators X_f and P_f when $\theta = 0$ and $\theta = \pi/2$, respectively. In the limit, $f(n) = I$ and $Q \rightarrow 1$, the deformed quadrature operator $X_{\theta,f}$ reduces to the non-deformed quadrature operator given in (2.25). Using the definition of the deformed quadrature given above, we find the quadrature wavefunction of f -oscillator in the following part of the paper.

The eigenstate of the deformed quadrature operator is represented by $|X_\theta\rangle_f$ and it has an eigenvalue $X_{\theta,f}$ given by

$$\hat{X}_{\theta,f}|X_\theta\rangle_f = X_{\theta,f}|X_\theta\rangle_f. \quad (2.27)$$

These eigenstates can be represented in the deformed Fock state basis of the f -deformed oscillator as:

$$|X_\theta\rangle_f = \sum_{n=0}^{\infty} |n\rangle_{ff} \langle n|X_\theta\rangle_f, \quad (2.28)$$

where,

$${}_f\langle X_\theta|n\rangle_f = \Psi_{n,f}(X_{\theta,f}) \quad (2.29)$$

is the energy eigenfunction of the f -oscillator for a given deformed eigenstate $|n\rangle_f$ in the quadrature representation. We obtain the excited state wavefunctions in terms of the ground state wavefunction in what follows. It will simplify the problem by reducing the unknowns to just the ground state wavefunction.

The eigenvalue equation (2.27) of the operator $X_{\theta,f}$ allows us to derive a recurrence relation obeyed by the wavefunctions $\Psi_{n,f}(X_{\theta,f})$. Using (2.3), (2.26) and (2.27) we get,

$${}_f\langle n|X_{\theta,f}|X_{\theta}\rangle_f = X_{\theta,f}\bar{\Psi}_{n,f}(X_{\theta,f}) \quad (2.30)$$

$$= \frac{\sqrt{1+Q}}{2} {}_f\langle n|(A_f e^{-i\theta} + A_f^\dagger e^{i\theta})|X_{\theta}\rangle_f \quad (2.31)$$

Solving the above equation, we get

$${}_f\langle n|X_{\theta,f}|X_{\theta}\rangle_f = \frac{\sqrt{1+Q}}{2} \left(\sqrt{[n+1]_f} e^{-i\theta} \bar{\Psi}_{n+1,f}(X_{\theta,f}) + \sqrt{[n]_f} e^{i\theta} \bar{\Psi}_{n-1,f}(X_{\theta,f}) \right) \quad (2.32)$$

for $n = 1, 2, 3, \dots$, and

$$X_{\theta,f} \bar{\Psi}_{0,f}(X_{\theta,f}) = \frac{\sqrt{1+Q}}{2} \left(\sqrt{[1]_f} e^{-i\theta} \bar{\Psi}_{1,f}(X_{\theta,f}) \right), \quad (2.33)$$

where $\bar{\Psi}_{n,f}(X_{\theta,f})$ is the complex conjugate of the wavefunction corresponding to the deformed state $|n\rangle_f$. The complex conjugate of (2.32) gives us a two term recurrence relation for $\Psi_{n+1}(X_{\theta,f})$ in the quadrature representation:

$$\Psi_{n+1,f}(X_{\theta,f}) = \frac{e^{-i\theta}}{\sqrt{[n+1]_f}} \left[\frac{2}{\sqrt{1+Q}} X_{\theta,f} \Psi_{n,f}(X_{\theta,f}) - \sqrt{[n]_f} \Psi_{n-1,f}(X_{\theta,f}) e^{-i\theta} \right] \quad (2.34)$$

for $n = 1, 2, 3, \dots$, with

$$\Psi_{1,f}(X_{\theta,f}) = \frac{e^{-i\theta}}{\sqrt{[1]_f}} \frac{2X_{\theta,f}}{\sqrt{1+Q}} \Psi_{0,f}(X_{\theta,f}). \quad (2.35)$$

Using (2.34) and (2.35), we obtain some of the excited state wavefunctions in the quadrature representation:

$$\Psi_{2,f}(X_{\theta,f}) = \frac{e^{-2i\theta}}{\sqrt{[2]_f}} \left[\frac{2X_{\theta,f}}{\sqrt{1+Q}} \left(\frac{2X_{\theta,f}}{\sqrt{[1]_f(1+Q)}} \right) - \sqrt{[1]_f} \right] \Psi_{0,f}(X_{\theta,f}), \quad (2.36)$$

$$\Psi_{3,f}(X_{\theta,f}) = \frac{e^{-3i\theta}}{\sqrt{[3]_f}} \left[\frac{2X_{\theta,f}}{\sqrt{1+Q}} \frac{1}{\sqrt{[2]_f}} \left(\frac{2X_{\theta,f}}{\sqrt{1+Q}} \frac{2X_{\theta,f}}{\sqrt{[1]_f(1+Q)}} - \sqrt{[1]_f} \right) - \sqrt{[2]_f} \frac{2X_{\theta,f}}{\sqrt{[1]_f(1+Q)}} \right] \Psi_{0,f}(X_{\theta,f}). \quad (2.37)$$

Similarly, we can obtain any other excited state using the recurrence relation. We observe that form of the solutions is similar to the solutions obtained for the q -deformed state [31] with the following changes: q^2 has been replaced by a general deformation parameter Q and $[n]_f$ has the value $|f(n)|^2 n$.

Now, we can write the analytical expression for the f -deformed Fock state $|n\rangle_f$ in the quadrature basis as

$$\Psi_{n,f}(X_{\theta,f}) = e^{-in\theta} J_{n,f}(X_{\theta,f}) \Psi_{0,f}(X_{\theta,f}), \quad (2.38)$$

where $\Psi_{0,f}(X_{\theta,f})$ is the ground state wavefunction and the new polynomial $J_{n,f}(X_{\theta,f})$ is defined by the following recurrence relation:

$$J_{n+1,f}(X_{\theta,f}) = \frac{1}{\sqrt{[n+1]_f}} \left[\frac{2X_{\theta,f}}{\sqrt{1+Q}} J_{n,f}(X_{\theta,f}) - \sqrt{[n]_f} J_{n-1,f}(X_{\theta,f}) \right]. \quad (2.39)$$

It is very clear from the above expression that $J_{n,f}(X_{\theta,f})$ is dependent on Q and therefore, varies for each case that is being studied. The initial two terms of $J_{n,f}(X_{\theta,f})$ are:

$$J_{0,f}(X_{\theta,f}) = 1, \quad (2.40)$$

$$J_{1,f}(X_{\theta,f}) = \frac{2X_{\theta,f}}{\sqrt{[1]_f(1+Q)}}. \quad (2.41)$$

Since we have the three-term recurrence relation (2.39), which connects the polynomials, the polynomials are orthogonal according to Favard's theorem [79]. Also, because of the relation between the polynomial $J_{n,f}(X_{\theta,f})$ and the orthogonal energy eigenfunctions $\Psi_{n,f}(X_{\theta,f})$ in equation (2.38), we can easily see that the polynomials are orthogonal. From

(2.39), we find the second and third terms of $J_{n,f}(X_{\theta,f})$, as representative examples, to be

$$J_{2,f}(X_{\theta,f}) = \frac{4X_{\theta,f}^2 - (1+Q)[1]_f}{\sqrt{[2]_f!(1+Q)^2}}, \quad (2.42)$$

$$J_{3,f}(X_{\theta,f}) = \frac{8X_{\theta,f}^3 - 2(1+Q)([1]_f + [2]_f)X_{\theta,f}}{\sqrt{[3]_f!(1+Q)^3}}, \quad (2.43)$$

where, $[n]_f! = [n]_f[n-1]_f \dots [1]_f$. Notice the similarity of the numerators with the Hermite polynomials. In the limit $|f(n)|^2 = 1$ and $Q \rightarrow 1$, the recurrence relation

(2.39) reduces to the recurrence relation of the Hermite polynomial:

$$H_{n+1}(x_\theta) = 2x_\theta H_n(x_\theta) - 2n H_{n-1}(x_\theta). \quad (2.44)$$

In the above limit, (2.38) also reduces to the quadrature representation of the non-deformed Fock state $|n\rangle$:

$$\Psi_n(X_{\theta,f} \rightarrow x_\theta) = \frac{H_n(x_\theta)}{\pi^{1/4} 2^{n/2} \sqrt{n!}} e^{-in\theta} e^{-x_\theta^2/2}, \quad (2.45)$$

where $H_n(x_\theta)$ is the Hermite polynomial of order n . The ground state in the above limit is given by:

$$\Psi_0(X_{\theta,f} \rightarrow x_\theta) = \frac{e^{-x_\theta^2/2}}{\pi^{1/4}}. \quad (2.46)$$

Now, we can obtain an explicit representation for quadrature operator eigenstates $|X_\theta\rangle_f$ in (2.27), in terms of the orthogonal polynomials $J_{n,f}(X_{\theta,f})$:

$$|X_\theta\rangle_f = \sum_{n=0}^{\infty} |n\rangle_f \langle n|X_\theta\rangle_f = \bar{\Psi}_{0,f}(X_{\theta,f}) \sum_{n=0}^{\infty} J_{n,f}(X_{\theta,f}) e^{in\theta} |n\rangle_f, \quad (2.47)$$

where the expression

$${}_f \langle X'_\theta | X_\theta \rangle_f = \delta(X_{\theta,f} - X'_{\theta,f}) = \bar{\Psi}_{0,f}(X_{\theta,f}) \Psi_{0,f}(X'_{\theta,f}) \sum_{n=0}^{\infty} J_{n,f}(X_{\theta,f}) J_{n,f}(X'_{\theta,f}) \quad (2.48)$$

is used to find $\Psi_{0,f}(X_{\theta,f})$ numerically. Afterwards, all the higher-order wavefunctions can be calculated using the equation (2.38) and normalized the wavefunctions numerically.

Using the general expressions derived above, we obtain the polynomials $J_n(X_{\theta,f})$ and wavefunctions $\Psi_{n,f}(X_{\theta,f})$ for different types of deformations in the next Section.

2.5.1 Math-type q -deformed oscillator wavefunctions

The math-type q -deformation is introduced in [46]. The deformation is named as ‘math-type’ because this algebra was used in the mathematical literature over 150 years [80]. For the math-type q -deformation described by the deformed algebra (2.14), we had seen that $Q = q^2$ and $[n]_q^m = (1 - q^{2n})/(1 - q^2)$. Therefore in this case, the q -deformed Fock state in the quadrature basis becomes

$$\Psi_{n,q}^m(X_{\theta,q}^m) = e^{-in\theta} J_{n,q}^m(X_{\theta,q}^m) \Psi_{0,q}^m(X_{\theta,q}^m), \quad (2.49)$$

where, the polynomial $J_n^m(X_{\theta,q}^m)$ has reduced to

$$J_{n+1,q}^m(X_{\theta,q}^m) = \frac{1}{\sqrt{[n+1]_q^m}} \left[\frac{2X_{\theta,q}^m}{\sqrt{1+q^2}} J_{n,q}^m(X_{\theta,q}^m) - \sqrt{[n]_q^m} J_{n-1,q}^m(X_{\theta,q}^m) \right]. \quad (2.50)$$

From the above equation, an explicit expression for the deformed Fock state in the position representation ($\theta = 0$) is given by

$$\Psi_{n,q}^m(X_q^m) = J_{n,q}^m(X_q^m) \Psi_{0,q}^m(X_q^m). \quad (2.51)$$

In the limit $q \rightarrow 1$, $\Psi_{n,q}^m(X_q^m)$ reduces to the non-deformed harmonic oscillator position wavefunction

$$\frac{H_n(x)}{\pi^{1/4} 2^{n/2} \sqrt{n!}} e^{-x^2/2}. \quad (2.52)$$

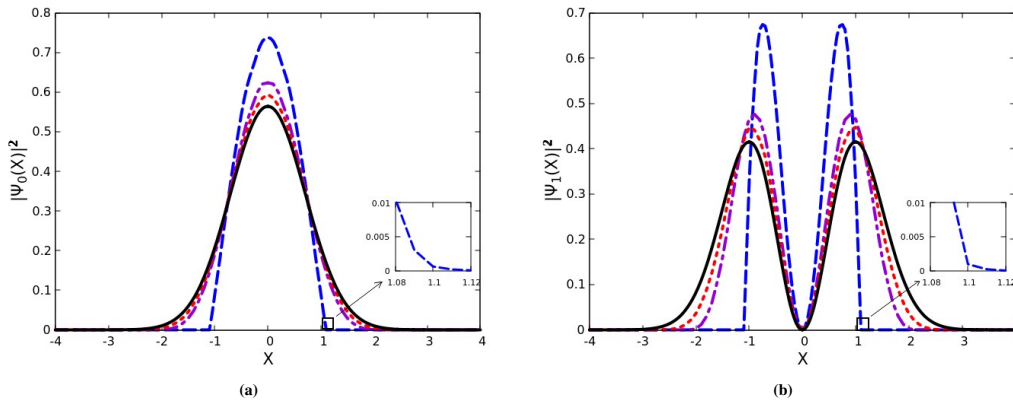


Figure 2.3: (a) ground state and (b) first excited state probability distribution functions for the harmonic oscillator (solid), a deformed oscillator with $q = 0.90$ (dotted), $q = 0.80$ (dash-dotted), and $q = 0.30$ (dashed) in the case of math type q -deformation. For $q = 0.3$, we have included insets in Figures 1(a) and 1(b) to show that wavefunctions go to zero moderately.

Figures 2.3.(a) and 2.3.(b) show the deformed normalized ground state and first excited

state position probability densities, respectively, for different deformation values. It can be seen that as the q value decreases (deformation increases), the peak of the probability curve increases in both figures. Moreover, in each case as $q \rightarrow 1$, the probability curve is seen to become the non-deformed harmonic oscillator probability distribution function.

2.5.2 Physics-type q -deformed oscillator wavefunctions

[28] introduced the physics-type q -deformation, which was used to study quantum groups[81], lattice models[82], etc. In the physics-type q -deformation described by the algebra (2.18) with $Q = q$ and $[n]_q^p = q(q^{-n} - q^n)/(1 - q^2)$, the q -deformed Fock state in the quadrature basis is given by

$$\Psi_{n,q}^p(X_{\theta,q}^p) = e^{-in\theta} J_{n,q}^p(X_{\theta,q}^p) \Psi_{0,q}^p(X_{\theta,q}^p), \quad (2.53)$$

where the polynomial $J_{n_f}(X_{\theta,q}^p)$ has reduced to

$$J_{n+1,q}^p(X_{\theta,q}^p) = \frac{1}{\sqrt{[n+1]_q^p}} \left[\frac{2X_{\theta,q}^p}{\sqrt{1+q}} J_{n,q}^p(X_{\theta,q}^p) - \sqrt{[n]_q^p} J_{n-1,q}^p(X_{\theta,q}^p) \right]. \quad (2.54)$$

In the position representation the deformed Fock state has the form,

$$\Psi_{n,q}^p(X_q^p) = J_{n,q}^p(X_q^p) \Psi_{0,q}^p(X_q^p), \quad (2.55)$$

which reduces to (2.52) when $q \rightarrow 1$.

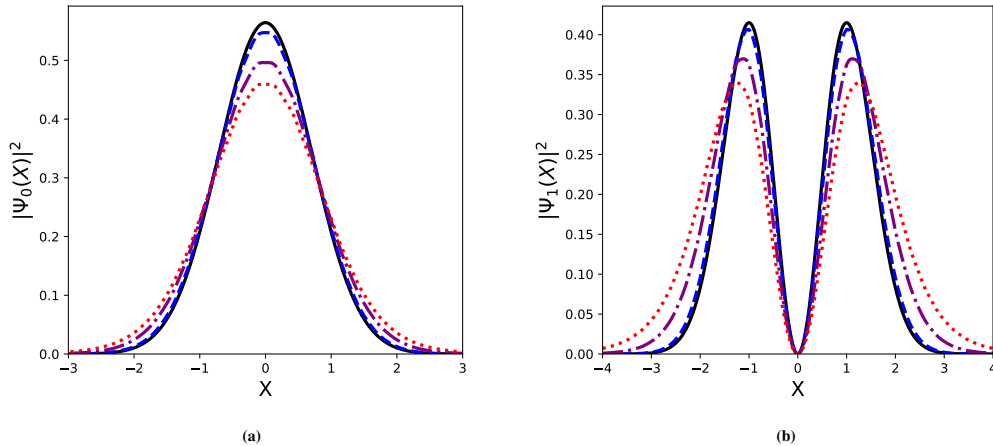


Figure 2.4: (a) ground state and (b) first excited state probability distribution functions for the harmonic oscillator (solid), deformed oscillator with $q=1.1$ (dashed), $q=1.5$ (dash-dotted) and $q=1.9$ (dotted) in the case of physics type q -deformation.

The plots of the normalized position probability densities of the ground state and first

excited state for different q values are shown in figures 2.4. (a) and 2.4. (b), respectively. We find that the probability density for the harmonic oscillator displays the highest peak. In this case, as the q value increases (deformation increases), the height of the peak is seen to decrease in contrast to the math-type q -deformation studied in the previous subsection. Moreover, the curve approaches the distribution function corresponding to the harmonic oscillator wavefunction as $q \rightarrow 1$ in both figures.

2.5.3 (p,q) -deformed oscillator wavefunctions

In the case of (p,q) -deformation described by the algebra (2.16) with $Q = p$ and $[n]_{(p,q)} = \frac{q(q^{-n}-p^n)}{(1-pq)}$, the (p,q) -deformed Fock state in the quadrature representation is given by,

$$\Psi_{n,(p,q)}(X_{\theta,(p,q)}) = e^{-in\theta} J_{n,(p,q)}(X_{\theta,(p,q)}) \Psi_{0,(p,q)}(X_{\theta,(p,q)}), \quad (2.56)$$

where, the polynomial $J_{n_f}(X_{\theta,(p,q)})$ has reduced to

$$J_{n+1,(p,q)}(X_{\theta,(p,q)}) = \frac{1}{\sqrt{[n+1]_{(p,q)}}} \left[\frac{2X_{\theta,(p,q)}}{\sqrt{1+p}} J_{n,(p,q)}(X_{\theta,(p,q)}) - \sqrt{[n]_{(p,q)}} J_{n-1,(p,q)}(X_{\theta,(p,q)}) \right]. \quad (2.57)$$

In the position representation, the deformed Fock state is given by,

$$\Psi_{n,(p,q)}(X_{p,q}) = J_{n,(p,q)}(X_{p,q}) \Psi_{0,(p,q)}(X_{p,q}), \quad (2.58)$$

which reduces to (2.52) when $(p,q) \rightarrow 1$.

The normalized ground state and first excited state position probability densities for (p,q) -deformation are plotted for the same q value and different p values in figures 2.5.(a) and 2.5.(b), respectively. We observe that for the same q value, as p increases (deformation increases), the height of the peak decreases. Further, the densities tend to the harmonic oscillator probability distribution when $(p,q) \rightarrow 1$.

2.6 Conclusion

We have defined the f -deformed quadrature operator with the help of the homodyne detection method and represented its eigenstates in the f -deformed Fock state basis. The quadrature operator allowed us to produce a recurrence relation for the wavefunctions, which allowed us to discover a new class of orthogonal polynomials $J_{n,f}(X_{\theta,f})$. These new

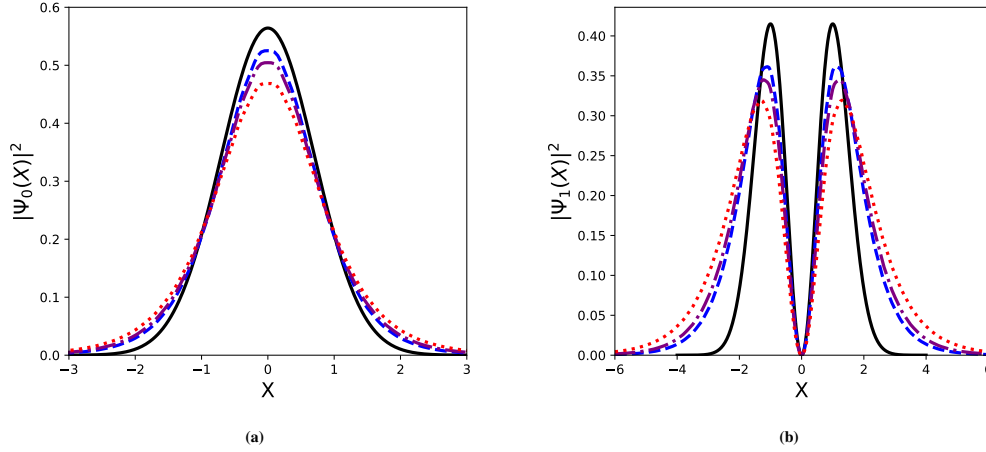


Figure 2.5: (a) ground state and (b) first excited state probability distribution functions for harmonic oscillator(solid), deformed oscillator with $p=1.3$ $q=0.5$ (dashed), $p=1.5$ $q=0.5$ (dash-dotted) and $p=1.9$ $q=0.5$ (dotted) in the case of (p,q) -deformation.

polynomials enabled us to represent the excited state wavefunctions of the f -oscillators in terms of the ground state wavefunction $\Psi_{0,f}(X_{\theta,f})$. The polynomials $J_{n,f}(X_{\theta,f})$ were found to be similar in properties of the Hermite polynomials $H_n(x)$.

We then considered different types of deformation and studied how the form of the polynomial $J_{n,f}(X_{\theta,f})$ (and thus the form of the deformed wavefunction $\Psi_{n,f}(X_{\theta,f})$) varies with the nature of deformation. Three types of deformed systems, namely math-type q -deformation, physics-type q -deformation and (p, q) -deformation, were studied by appropriate substitution for $|f(n)|^2$ and Q in the expressions for the general f -oscillator. We also plotted the position probability distributions for the deformed ground state and the first excited state for each type of deformation studied. By comparing the probability curves for different values of the deformation parameter in each case, we demonstrated the difference between the deformed and the non-deformed harmonic oscillator wavefunctions. Quadrature operator eigenstates are required to reconstruct quantum states and process quantum information using optical tomograms [83, 84, 85, 86]. So our calculation will be useful for the state reconstruction and quantum information processing of f -deformed quantum states. Also, we propose a further study of the f -oscillators using the factorization method discussed in [87].

Chapter 3

Squeezing and nonclassicality of q -deformed superposition states

3.1 Introduction

The term ‘*nonclassical states of light*’ started to appear in physics in the early 1960s. The name was roughly coined for those states of light which need sophisticated setups for their production. Some of the best-known examples of nonclassical states are squeezed states, Schrodinger cat states, entangled states, etc. The most nonclassical of all nonclassical states of light is the single-photon state. Of course, a criterion determines the nonclassicality of a state, called the Klauder-Glauber-Sudarsan P -function. If P is positive, the state is a classical one. On the other hand, the states for which P is negative are nonclassical. There exists different types of nonclassical behavior exhibited by quantum systems. Squeezing is an important one among them, which finds applications in fields where low-noise applications are needed. Quantum entanglement falls in the same category, mainly for quantum teleportation, quantum communication, etc.

In optical communication systems, there is a standard quantum limit to the possible reduction of noise in a coherent signal called ‘the zero point fluctuations’, because of which even an ideal laser would still possess quantum noise. Squeezed states have less fluctuations in one quadrature than a coherent state, which is a significant feature. The squeezed states have a non-positive non-singular Glauber-Sudarshan P -function so that their statistical properties cannot be determined using the techniques analogous to the classical probability theory, which makes the squeezed states ‘nonclassical’. The low-noise behavior of squeezed states make them find applications in fields such as gravitational wave detection [88], in LIGO [89] and VIRGO [4] projects, etc. The field of optical communications is also greatly benefited from squeezed states [90]. All these applications make their study,

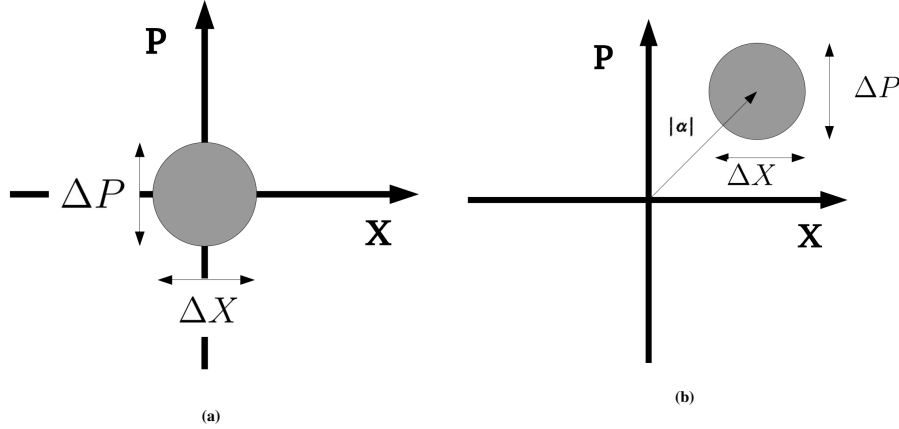


Figure 3.1: (a) Vacuum state and (b) the coherent state in the phase space representation.

generation and detection inevitably important in quantum physics.

Nonclassicality, especially squeezing in deformed states, is a prominent area of research. A deformed system being more generalized than the ideal non-deformed systems, the study of squeezing in such states will be far more advantageous in relevant fields. Since we have an additional degree of freedom in the deformed systems (i.e., the deformation parameter q), we can desirably control the squeezing using q . Here we deal with the math-type q -deformation, which follows the q -deformed commutation relation (2.14) and we specifically consider the superposition of two q -deformed squeezed vacuum states, and the superposition of two q -deformed squeezed coherent states. Among different measures of nonclassicality, such as squeezing, Husimi Q function, quantum entanglement, etc., we pay attention to squeezing and Husimi Q function in this chapter. Quantum entanglement of a math-type q -deformed system will be discussed in one of the forthcoming chapters.

3.2 Squeezing and Husimi Q function

There are different kinds of squeezing that can be observed in quantum systems. They are quadrature squeezing, higher-order squeezing, and photon number squeezing. All these serve as measures of nonclassicality. Apart from squeezing, the Husimi Q function is another measure of nonclassicality in a given system. Each of them is discussed below in detail:

(i) Quadrature squeezing and higher-order squeezing

Two operators A_1 and A_2 (deformed or non-deformed) obeying the commutation relation $[A_1, A_2] = iA_3$ will satisfy the uncertainty relation

$$\langle(\Delta A_1)^2\rangle\langle(\Delta A_2)^2\rangle \geq \frac{1}{4}|\langle A_3\rangle|^2. \quad (3.1)$$

A state of the system is squeezed if either $\langle(\Delta A_1)^2\rangle \leq \frac{1}{2}|\langle A_3\rangle|$ or $\langle(\Delta A_2)^2\rangle \leq \frac{1}{2}|\langle A_3\rangle|$ is true. The conjunction ‘either-or’ is used just because it is not possible to have both the variances less than $\frac{1}{2}|\langle A_3\rangle|$, as it would be a violation of the uncertainty relation.

While considering the quadrature squeezing, the operators A_1 and A_2 are replaced by the quadratures x and p , in the case of non-deformed oscillators which satisfy the commutation relation

$$[x, p] = \frac{i}{2}. \quad (3.2)$$

It implies that the quadrature squeezing exists only if either $\langle(\Delta x)^2\rangle \leq \frac{1}{4}$ or $\langle(\Delta p)^2\rangle \leq \frac{1}{4}$ is satisfied. The state for which one of these conditions holds is said to have ‘less noise’ in the corresponding quadrature. At the same time, the fluctuations in the other quadrature will be larger so that the uncertainty relation is not violated.

For an example, let us consider the non-deformed squeezed vacuum state. Squeezed vacuum states find applications in fields like quantum fluctuations, quantum teleportation [91, 92] etc. A squeezed vacuum state in the non-deformed algebra can be generated mathematically by the action of squeezing operator $S(\xi)$ on the vacuum state:

$$S(\xi) = \exp\left(\frac{\xi^* a^2 - \xi a^{\dagger 2}}{2}\right), \quad |\xi\rangle = S(\xi)|0\rangle, \quad (3.3)$$

where the squeezing parameter $\xi = r e^{i\theta}$, $0 \leq r < \infty$ and $0 \leq \theta \leq 2\pi$. The operator $S(\xi)$ is also known as ‘a two-photon generalization of the displacement operator’ since its action on vacuum state generates a kind of two-photon coherent state.

The squeezed vacuum state can also be represented as [93]:

$$|\xi\rangle = \sqrt{\operatorname{sech}(r)} \sum_{n=0}^{\infty} \frac{\sqrt{(2n)!}}{2^n n!} (-e^{i\theta} \tanh(r))^n |2n\rangle. \quad (3.4)$$

When $\theta = 0$, the variances in the quadratures turn out to be,

$$\langle(\Delta x)^2\rangle = \frac{1}{4}e^{-2r}, \quad \langle(\Delta p)^2\rangle = \frac{1}{4}e^{2r}. \quad (3.5)$$

The squeezing shifts to the p -quadrature when $\theta = \pi$. It is to be noted that the state yields minimum uncertainty, i.e., $\frac{1}{16}$ when $\theta = 0$. To grab the idea of squeezing more quickly, it is more convenient to use their graphical representation. For a vacuum state and a coherent state, fluctuations in both the quadratures are equal, i.e., $\Delta x = \Delta p = \frac{1}{2}$. It is depicted in figure (3.1). A representation of squeezed vacuum state for $\theta = 0$ and $\theta = \pi$ is shown in figure (3.2). A more convenient way to characterize the squeezing is to calculate the squeezing coefficient S_x :

$$S_x = \frac{\langle(\Delta x)^2\rangle - \frac{1}{2}|\langle[x, p]\rangle|}{\frac{1}{2}|\langle[x, p]\rangle|}. \quad (3.6)$$

Squeezing exists in x -quadrature if $-1 < S_x < 0$ and $-1 < S_p < 0$ indicates that the p -quadrature is squeezed.

Hong and Mandel [94] introduced the generalization for the concept of quadrature squeezing, called ‘higher-order squeezing’, which refers to the squeezing in higher-order moments of a quadrature operator. The parameter given in (3.6) is extended to the general case of N^{th} order squeezing as

$$S_x^N = \frac{\langle(\Delta x)^N\rangle - \frac{(N-1)!!}{2^{\frac{N}{2}}}|\langle([x, p])^{\frac{N}{2}}\rangle|}{\frac{(N-1)!!}{2^{\frac{N}{2}}}|\langle([x, p])^{\frac{N}{2}}\rangle|}. \quad (3.7)$$

Same as in the second-order case, $-1 \leq S_x^N \leq 0$ indicates N^{th} order squeezing.

The f -deformed quadrature operators and their commutation relation are already discussed in Chapter (2). In the case of math-type q -deformation which we are interested in, the position and momentum operators become [74, 31]

$$X_q^m = \frac{\sqrt{1+q^2}}{2}(A_q^{m\dagger} + A_q^m), \quad P_q^m = \frac{i\sqrt{1+q^2}}{2}(A_q^{m\dagger} - A_q^m), \quad (3.8)$$

which reduced to (2.4) when $q \rightarrow 1$. Also, A_q^m and $A_q^{m\dagger}$ are the q -deformed ladder operators given by

$$A_q^m |n\rangle_q^m = \sqrt{[n]_q^m} |n-1\rangle_q^m, \quad A_q^{m\dagger} |n\rangle_q^m = \sqrt{[n+1]_q^m} |n+1\rangle_q^m \quad (3.9)$$

and obeys the commutation relation (2.14).

A deformed system is said to be quadrature squeezed if either $\langle(\Delta X_q^m)^2\rangle \leq \frac{1}{2}|\langle[X_q^m, P_q^m]\rangle|$

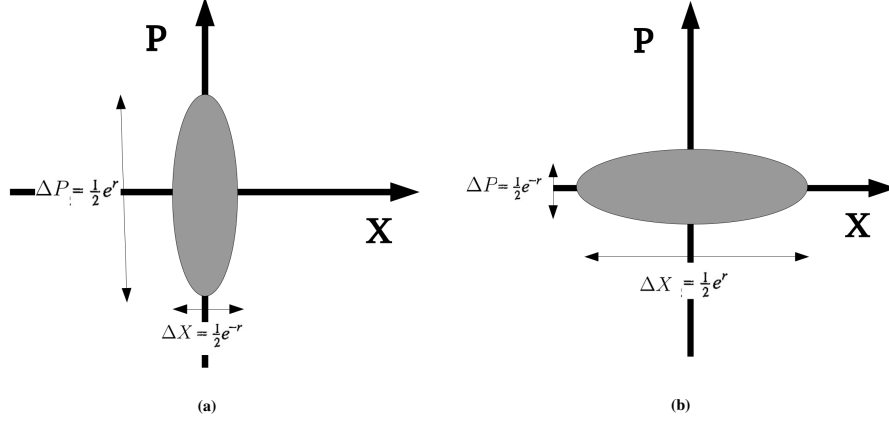


Figure 3.2: (a) Squeezed vacuum state with $\theta = 0$ and (b) Squeezed vacuum state with $\theta = \pi$ showing squeezing in different quadratures.

or $\langle(\Delta P_q^m)^2\rangle \leq \frac{1}{2}|\langle[X_q^m, P_q^m]\rangle|$ holds. The deformed squeezing coefficient S_X :

$$S_X = \frac{\langle(\Delta X_q^m)^2\rangle - \frac{1}{2}|\langle[X_q^m, P_q^m]\rangle|}{\frac{1}{2}|\langle[X_q^m, P_q^m]\rangle|} \quad (3.10)$$

If $-1 < S_X < 0$, then there exists squeezing in the X_q^m -quadrature. Similar definition can be used for the P_q^m -quadrature also. Also, when $q \rightarrow 1$, (3.10) reduces to the non-deformed squeezing coefficient 3.6.

As stated in the non-deformed case, the second-order squeezing coefficient (3.10) can be extended to the general case of N^{th} order squeezing as

$$S_X^N = \frac{\langle(\Delta X_q^m)^N\rangle - \frac{(N-1)!!}{2^{\frac{N}{2}}}|\langle([X_q^m, P_q^m])^{\frac{N}{2}}\rangle|}{\frac{(N-1)!!}{2^{\frac{N}{2}}}|\langle([X_q^m, P_q^m])^{\frac{N}{2}}\rangle|}, \quad (3.11)$$

which reduces to the corresponding non-deformed counterpart (3.7) in the appropriate limits.

Same as in the second-order case, $-1 \leq S \leq 0$ indicates N^{th} order squeezing.

(ii) Number squeezing

The photon number distribution of a coherent state is always Gaussian. A state having number squeezing is said to exhibit sub-Poissonian statistics, that is, the distribution will be narrower than that for a coherent state. In other words, the photon number distribution of the state is narrower than the average number of photons. A more simple way to find the

nature of photon statistics is to find the Mandel Q -parameter:

$$Q = \frac{\langle(\Delta n)^2\rangle - \langle n\rangle}{\langle n\rangle}, \quad (3.12)$$

where $\langle n\rangle = \langle a^\dagger a\rangle$ and $\langle(\Delta n)^2\rangle = \langle n^2\rangle - \langle n\rangle^2$. The expression for Q is taken from a study [95] of photon statistics in the resonance fluorescence. For the Q value in the range $-1 \leq Q < 0$ implies that the statistics of the state are sub-Poissonian. If the value falls in the range $Q > 0$, the statistics is super-Poissonian. Also, $Q = 0$ for a coherent state which will be Poissonian statistics.

In the case of the math-type q -deformation, the Mandel parameter (3.12) becomes

$$Q = \frac{\langle(\Delta N_q^m)^2\rangle - \langle N_q^m\rangle}{\langle N_q^m\rangle}, \quad (3.13)$$

where $\langle N_q^m\rangle = \langle A_q^{m\dagger} A_q^m\rangle$. Here also Q value in the range $-1 \leq Q < 0$ indicates number squeezing.

(iii) Husimi Q function

Husimi function, or Q function [96, 97] is a phase-space probability distribution which can be defined as the expectation value of the density operator with respect to the coherent state and is having a positive value for all quantum states. It is a measure of the nonclassicality of a given state irrespective of squeezing. Husimi function Q can be expressed as:

$$Q(\alpha) = \frac{1}{\pi} \langle \alpha | \rho | \alpha \rangle, \quad (3.14)$$

where $|\alpha\rangle$ is the coherent state.

Also, the Q function of the non-deformed coherent state is just a Gaussian, while the distribution other than a Gaussian-type indicates the nonclassical behaviour of the corresponding state.

The math-type q -deformed Husimi Q function is written as

$$Q(\alpha) = \frac{1}{\pi^q} \langle \alpha | \rho | \alpha \rangle_q^m, \quad (3.15)$$

where $|\alpha\rangle_q^m$ is the math-type q -deformed coherent state is given by [70]

$$|\alpha\rangle_q^m = e_q^{-\frac{|\alpha|^2}{2}} \sum_{n=0}^{\infty} \frac{(\alpha)^n}{\sqrt{[n]_q^m!}} |n\rangle_q^m, \quad (3.16)$$

where, $e_q^{(\bullet)} = \sum_{n=0}^{\infty} \frac{(\bullet)^n}{[n]_q^m!}$, is the q -deformed exponential function.

As we have discussed the measures of nonclassicality, let us now move on to the states we are interested in. In the upcoming section, we will be discussing the q -deformed squeezed states and their superpositions, followed by the results where we analyze the effect of q -deformation on the nonclassicality of each state.

3.3 q -deformed squeezed states and their superpositions

3.3.1 q -deformed squeezed vacuum state and its superposition

A squeezed vacuum state is generated by the action of the squeeze operator (3.2) on the vacuum $|0\rangle$. The action of squeeze operator is in such a way that the photons are created or destroyed in pairs; hence the resulting squeezed vacuum is called a ‘two-photon coherent state’. The analytical expression for a non-deformed squeezed vacuum is given in (3.4). Such a state was experimentally realized in the early 1980s [98]. The schemes employed for the generation of squeezed states are mainly degenerate parametric down-conversion and degenerate four-wave mixing [93]. A non-deformed squeezed vacuum state exhibits quadrature squeezing [93]. The superposition of squeezed vacuum states is discussed in [49], which shows that squeezing vanishes when we go for their superposition.

When we move on to the deformed regime, f -deformed squeezed state are discussed in [56]. Now, we can express the math-type q -deformed squeezed vacuum state in the deformed Fock basis as

$$|\xi\rangle_q^m = N_q^m \sum_{n=0}^{\infty} (-e^{i\theta} \tanh(r))^n \sqrt{\frac{[2n-1]_q^m!!}{[2n]_q^m!!}} |2n\rangle_q^m, \quad (3.17)$$

where

$$N_q^m = \left(\sum_{n=0}^{\infty} (\tanh(r))^{2n} \frac{[2n-1]_q^m!!}{[2n]_q^m!!} \right)^{-1/2}. \quad (3.18)$$

Generalized squeezed vacuum states are already known to be nonclassical [99, 44]. While dealing with the superposition, we focus on both the quadrature squeezing and photon

number squeezing. Note that in the generalized case, all the operators are replaced by their deformed counterpart. In the non-deformed limit, Eq. (3.17) reduces to the non-deformed squeezed vacuum state 3.4.

Now, let us look at the superposition of two q -deformed squeezed vacuum states given by,

$$\begin{aligned} |\xi\rangle_{s,q}^m &= N_{s,q}^m (|\xi\rangle_q^m + |-\xi\rangle_q^m) \\ &= N_{s,q}^m \sum_{n=0}^{\infty} (e^{i\theta} \tanh(r))^{2n} \sqrt{\frac{[4n-1]_q^{m!!}}{[4n]_q^{m!!}}} |4n\rangle_q^m, \end{aligned} \quad (3.19)$$

where the normalization constant

$$N_{s,q}^m = \left(\sum_{n=0}^{\infty} (\tanh(r))^{4n} \frac{[4n-1]_q^{m!!}}{[4n]_q^{m!!}} \right)^{-1/2}. \quad (3.20)$$

When there's no deformation ($q = 1$), (3.19) reduces to the corresponding non-deformed superposition state.

3.3.2 q -deformed squeezed coherent states and its superposition

Squeezed coherent state is another important class of squeezed state with important applications in quantum information processing, quantum sensing etc [100, 101]. The non-deformed squeezed coherent states $|\alpha, \xi\rangle$ can be obtained by the action of the displacement operator $D(\alpha)$ on the squeezed vacuum state:

$$|\alpha, \xi\rangle = D(\alpha)S(\xi)|0\rangle, \quad (3.21)$$

where

$$D(\alpha) = \exp(\alpha a^\dagger - \alpha^* a), \quad (3.22)$$

and α is the displacement parameter which is a complex number. The squeezed coherent states and their squeezing properties are studied in [93], which explicitly shows the existence of quadrature squeezing and photon number squeezing. The superposition of two squeezed coherent states, their generation, and squeezing properties are discussed in [102]. We use these results as references to compare our results in the following section.

The non-deformed definitions are directly generalized for the math-type q -deformed ladder operators A_q^m and $A_q^{m\dagger}$. An explicit expression for the q -deformed squeezed coherent

states is given in [103] in which the authors construct the entangled squeezed states in a noncommutative space. Thus we have,

$$|\alpha, \xi\rangle_q^m = N_q^m(\alpha, \xi) \sum_{n=0}^{\infty} \frac{I(\alpha, \xi, n)}{\sqrt{[n]_q^m!}} |n\rangle_q^m, \quad (3.23)$$

where

$$N_q^{m^2}(\alpha, \xi) = \left(\sum_{n=0}^{\infty} \frac{|I(\alpha, \xi, n)|^2}{[n]_q^m!} \right)^{-1}, \quad (3.24)$$

and the function $I(\alpha, \xi, n)$ is defined by the three-term recurrence relation

$$I(\alpha, \xi, n+1) = \alpha I(\alpha, \xi, n) - \xi [n] I(\alpha, \xi, n-1), \quad (3.25)$$

with $I(\alpha, \xi, 0) = 1$ and $I(\alpha, \xi, 1) = \alpha$.

Squeezing properties of the q -deformed squeezed coherent states have already studied in the literature [99]. Similar to the superposition of q -deformed squeezed vacuum states, we can define the superposition of two q -deformed squeezed coherent states with different squeezing parameters. The superposition state will be,

$$|\alpha, \xi\rangle_{s,q}^m = N_{s,q}^m(\alpha, \xi) (|\alpha, \xi\rangle_q^m + |\alpha, -\xi\rangle_q^m), \quad (3.26)$$

where

$$N_{s,q}^{m^2}(\alpha, \xi) = \left(2 + 2N_q^m(\alpha, \xi)N_q^m(\alpha, -\xi) \times \sum_{n=0}^{\infty} \frac{I(\alpha, \xi, n)I(\alpha, -\xi, n)}{[n!]_q^m} \right)^{-1}. \quad (3.27)$$

When there's no deformation, (3.26) reduces to the corresponding non-deformed superposition state

$$|\alpha, \xi\rangle_s = N_s(\alpha, \xi) (|\alpha, \xi\rangle + |\alpha, -\xi\rangle). \quad (3.28)$$

3.4 Results and discussion

Now, let us look into the squeezing and nonclassical behavior of different types of math-type q -deformed squeezed states and their superpositions and how the nonclassicality of a

given state depends on the amount of deformation.

3.4.1 q -deformed squeezed vacuum state

3.4.1.1 *Quadrature squeezing and higher-order squeezing*

The second-order squeezing coefficient can be evaluated as (3.10). For the q -deformed squeezed vacuum states,

$$\begin{aligned} \langle (\Delta X_q^m)^2 \rangle &= \langle X_q^{m^2} \rangle \\ &= \frac{(1+q^2)}{4} N_q^{m^2} \left(1 + \tanh(r)^2 - 2 \cos \theta \tanh(r) \right) \\ &\quad \times \sum_{n=0}^{\infty} (\tanh(r))^{2n} \frac{[2n+1]_q^{m!!}}{[2n]_q^{m!!}}, \end{aligned} \quad (3.29)$$

and

$$\begin{aligned} \langle \frac{1}{i} [X_q^m, P_q^m] \rangle &= \frac{(1+q^2)}{2} N_q^{m^2} (1 - \tanh(r)^2) \\ &\quad \times \sum_{n=0}^{\infty} (\tanh(r))^{2n} \frac{[2n+1]_q^{m!!}}{[2n]_q^{m!!}}. \end{aligned} \quad (3.30)$$

$\langle X_q^{m^2} \rangle$ is calculated using

$$X_q^{m^2} = \left(\frac{1+q^2}{4} \right) \left(A_q^{m^2} + A_q^{m^{\dagger 2}} + (1+q^2) A_q^{m\dagger} A_q^m + 1 \right). \quad (3.31)$$

Now, substituting in (3.10), we get S_X ,

$$S_X = 2 \sinh(r) (\sinh(r) - \cos \theta \cosh(r)). \quad (3.32)$$

The squeezing coefficient is independent of q because the variance and the uncertainty limit have the same functional dependence on the q value. They are evident from the definition of S_X ((3.10)), (3.29), and (3.30). Following a similar procedure, we can find out S_P also. S_X and S_P values are then plotted for a range of r values and are depicted in figure 3.3 and figure 3.4. When $\theta = 0^\circ$, there is squeezing in the X_q^m -quadrature for all r values. The squeezing shifts to the P_q^m -quadrature when $\theta = 180^\circ$. For all the values

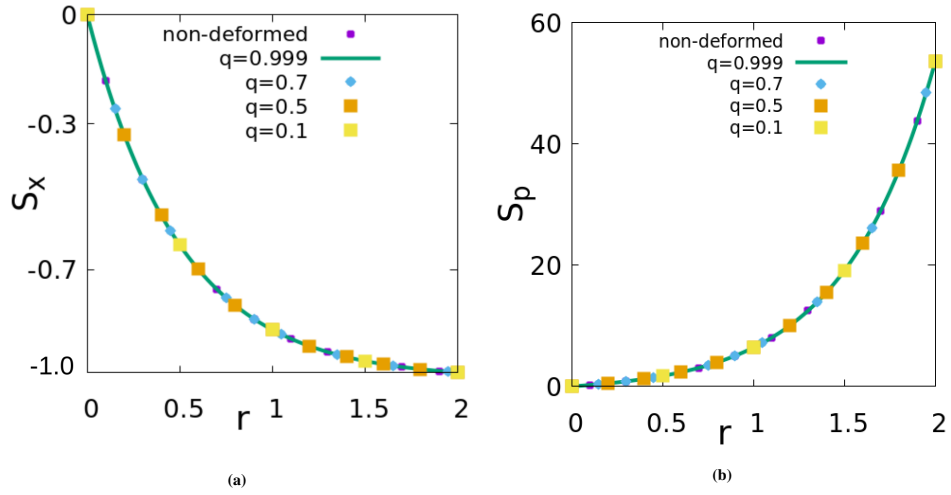


Figure 3.3: (a) Variation of the squeezing coefficient S_X and (b) the variation of S_P when $\theta = 0^\circ$ for the state $|\xi\rangle_q$. It shows that squeezing coefficient is the same for all q values.

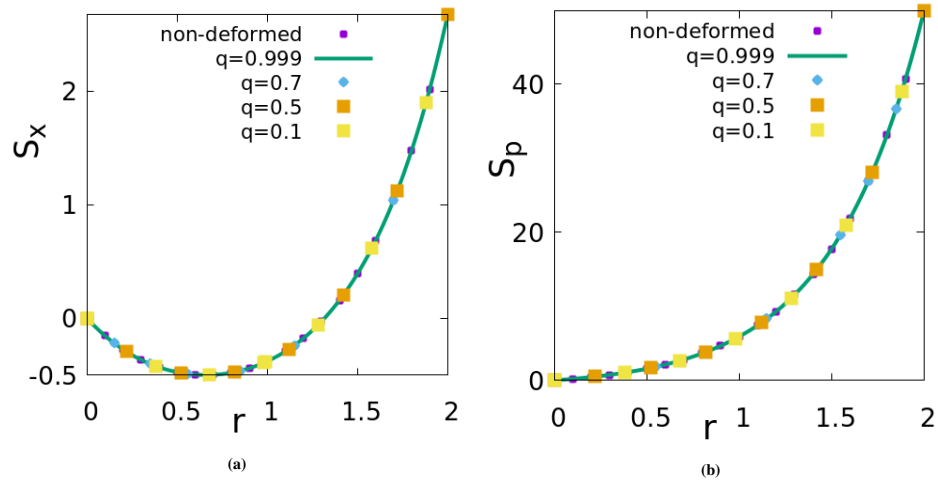


Figure 3.4: (a) Variation of the squeezing coefficient S_X and (b) the variation of S_P when $\theta = 30^\circ$, for the state $|\xi\rangle_q$. Squeezing coefficient is same for any value of q .

of θ between 0° and 180° , the squeezing in the X_q^m -quadrature gradually vanishes and the squeezing disappears when $\theta = 90^\circ$ for both the quadratures. This transition is evident from the figures, figure 3.3 (a) and figure 3.4 (a). In figure 3.4 (a), there is squeezing in the X_q^m -quadrature only for a certain range of r values. It is important to note that the squeezing becomes maximum in the X_q^m -quadrature for $\theta = 0^\circ$ (and in the P_q^m -quadrature for $\theta = 180^\circ$) as the deformation and squeezing parameter are increased. Also, it is interesting that both S_X and S_P values are found to be independent of the deformation (q value) for a given θ .

Now, let us move on to the higher order squeezing of the same state. The 4^{th} order squeezing coefficient in X_q^m -quadrature is given by,

$$S_X^4 = \frac{\langle(\Delta X_q^m)^4\rangle - \frac{3}{4}|\langle[X_q^m, P_q^m]^2\rangle|}{\frac{3}{4}|\langle[X_q^m, P_q^m]^2\rangle|}, \quad (3.33)$$

where

$$\langle(\Delta X_q^m)^4\rangle = \langle X_q^{m4}\rangle - 4\langle X_q^{m3}\rangle\langle X_q^m\rangle + 6\langle X_q^{m2}\rangle\langle X_q^m\rangle^2 - 3\langle X_q^m\rangle^4 \quad (3.34)$$

and the expectation values are taken with respect to $|\xi\rangle_q^m$ (Eq. 3.17). Since $\langle X_q^m\rangle = 0$, $\langle(\Delta X_q^m)^4\rangle = \langle X_q^{m4}\rangle$. Now substituting for X_q^m on terms of A_q^m and $A_q^{m\dagger}$, we get

$$\begin{aligned} \langle(\Delta X_q^m)^4\rangle &= \left(\frac{1+q^2}{4}\right)^2 \left[\langle(A_q^{m2} + A_q^{m\dagger 2})\rangle + 2(1+q^2)\langle A_q^{m\dagger} A_q^m\rangle \right. \\ &\quad + 1 + (1+q^2)^2 \langle(A_q^{m\dagger} A_q^m)^2\rangle + \langle(A_q^{m4} + A_q^{m\dagger 4})\rangle \\ &\quad + \langle A_q^{m2} A_q^{m\dagger 2}\rangle + \langle A_q^{m\dagger 2} A_q^{m2}\rangle \\ &\quad + (1+q^2)\langle(A_q^{m2} A_q^{m\dagger} A_q^m + A_q^{m\dagger} A_q^m A_q^{m\dagger 2})\rangle \\ &\quad \left. + (1+q^2)\langle(A_q^{m\dagger 3} A_q^m + A_q^{m\dagger} A_q^{m3})\rangle \right]. \end{aligned} \quad (3.35)$$

We can calculate each term separately and substitute it in (3.35) to obtain $\langle(\Delta X_q^m)^4\rangle$. Similarly, we can find $\langle(\Delta P_q^m)^4\rangle$. Also,

$$[X_q^m, P_q^m] = 1 + \frac{q^2 - 1}{q^2 + 1}(X_q^{m2} + P_q^{m2}) = 1 + \frac{q^2 - 1}{2} A_q^{m\dagger} A_q^m, \quad (3.36)$$

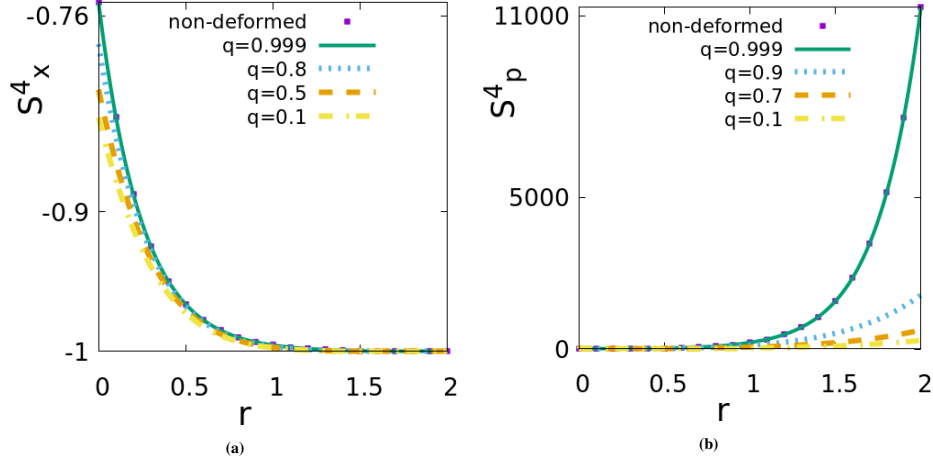


Figure 3.5: (a) Variation of the squeezing coefficient S_X^4 when $\theta = 0^\circ$ ($= S_P^4$ when $\theta = 180^\circ$) and (b) shows the variation of S_P^4 when $\theta = 0^\circ$ ($= S_X^4$ when $\theta = 180^\circ$) with r , for the state $|\xi_q^m$. In contrast to squeezing, the higher order squeezing is different for different q values.

and

$$\begin{aligned} \langle [X_q^m, P_q^m]^2 \rangle &= \frac{(q^2 + 1)^2}{4} + (q^4 - 1) \frac{q^2 + 1}{2} \langle A_q^{m\dagger} A_q^m \rangle \\ &+ \frac{(q^4 - 1)^2}{4} \langle (A_q^{m\dagger} A_q^m)^2 \rangle. \end{aligned} \quad (3.37)$$

Substitution of (3.37) and (3.34) in (3.33) gives us the 4th order squeezing coefficient in the X_q^m -quadrature, and it is plotted for different r values. The same can be performed for the P_q^m -quadrature.

Figure 3.5 shows the variation of the squeezing coefficients with respect to r . As in the case of the second order squeezing, here also squeezing exists in the X_q^m -quadrature when $\theta = 0^\circ$ and shifts to the P_q^m -quadrature when $\theta = 180^\circ$ and it can be seen that both these values are the same. The S_X^4 values fall in the range $-1 \leq S^4 \leq 0$ which means there is squeezing in X_q^m -quadrature and the positive S_P^4 values show that there is no squeezing in the P_q^m -quadrature. It is found that the higher order squeezing coefficient is different for different q values in contrast to second-order squeezing coefficient. This is due to the different functional dependence of fourth-order central moment and the uncertainty limit on q . It is manifested in figure 3.5 as S_X^4 attains its extreme possible value -1 when we increase the deformation and squeezing parameter. From the equations it is evident that $\langle (\Delta X_q^m)^4 \rangle = \langle (\Delta P_q^m)^4 \rangle$ when $\theta = 90^\circ$ and hence no squeezing. Following the same procedure, the squeezing for squeezed vacuum state is also calculated. It is observed that the squeezing in the deformed case reduces to that in the non-deformed one when $q \rightarrow 1$,

as shown in figure 3.5.

3.4.1.2 Number squeezing

The Mandel Q -parameter for the q -deformed squeezed vacuum states can be calculated using (3.13), where

$$\langle N_q^m \rangle = N_q^{m^2} \sum_{n=0}^{\infty} (\tanh(r))^{2n+2} \frac{[2n+1]_q^{m!!}}{[2n]_q^{m!!}} \quad (3.38)$$

and

$$\langle N_q^{m^2} \rangle = N_q^{m^2} \sum_{n=0}^{\infty} (\tanh(r))^{2n} \frac{[2n-1]_q^{m!!} [2n]_q^m}{[2n-2]_q^{m!!}}. \quad (3.39)$$

The result is plotted for different values of q and r , shown in figure 3.6. Number squeezing exists when Q lies between -1 and 0 . When a state shows number squeezing, the photon number distribution becomes sub-Poissonian. Here we can see that there is number squeezing only for specific q and r . From the plot, it is clear that the number squeezing becomes more prominent with an increase in the squeezing parameter r and a decrease in the q value. In other words, number squeezing is significant for a highly deformed state with a large squeezing parameter. It implies that the state becomes more nonclassical with an increase in deformation. The number squeezing vanishes completely with $q \rightarrow 1$ and $r \rightarrow 0$, when the state approaches a classical state. The Mandel parameter Q is also calculated for the non-deformed state (3.4) and is found to be coinciding with the deformed case for $q \rightarrow 1$.

3.4.1.3 q -deformed Husimi Q function

The Q function is calculated for the state $|\xi\rangle_q^m$ (Eq. (3.17)) using Eq. (3.15):

$$\begin{aligned} Q &= \frac{1}{\pi e_q} \left| N_q^m \sum_{n=0}^{\infty} (-1)^n (e^{i\theta} \tanh(r))^n \sqrt{\frac{[2n-1]_q^{m!!}}{[2n]_q^{m!!}}} \right. \\ &\quad \left. \times \frac{(\alpha^*)^{2n}}{\sqrt{[2n]_q^{m!}}} \right|^2, \end{aligned} \quad (3.40)$$

where e_q is the q -deformed exponential and N_q^m is given in (3.18). The results are shown in the figure (3.7). ‘x’ and ‘y’ are the real and imaginary parts of α respectively. It is obvious that Q is having a non-Gaussian behavior, showing the nonclassical nature of the state $|\xi\rangle_q^m$.

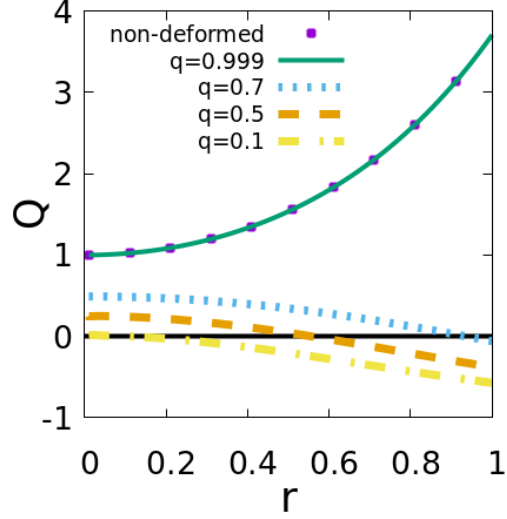


Figure 3.6: The variation of Q with r for the state $|\xi\rangle_q^m$. Q is different for different q values. The black horizontal line ($Q = 0$) shows Poisson statistics. Number squeezing is shown below this line.

The Q is different for different q and r values.

Next, we find the squeezing properties of the superposition of two math-type q -deformed squeezed vacuum states.

3.4.2 Superposition of two q -deformed squeezed vacuum states

3.4.2.1 Quadrature squeezing and higher-order squeezing

The variance in X_q^m -quadrature is given by

$$\langle(\Delta X_q^m)^2\rangle = \langle X_q^{m^2}\rangle - \langle X_q^m\rangle^2, \quad (3.41)$$

where $\langle X_q^m\rangle$ is calculated to be zero and $\langle X_q^{m^2}\rangle$ is calculated using (3.31). Calculating expectation values of each term, we get

$$\langle A_q^{m^2}\rangle = \langle (A_q^{m^\dagger})^2\rangle = 0 \quad (3.42)$$

and

$$\langle A_q^{m^\dagger} A_q^m\rangle = |N_{s,q}^m|^2 \sum_{n=0}^{\infty} (\tanh(r))^{4n} \frac{[4n-1]_q^{m!!}}{[4n-2]_q^{m!!}}. \quad (3.43)$$

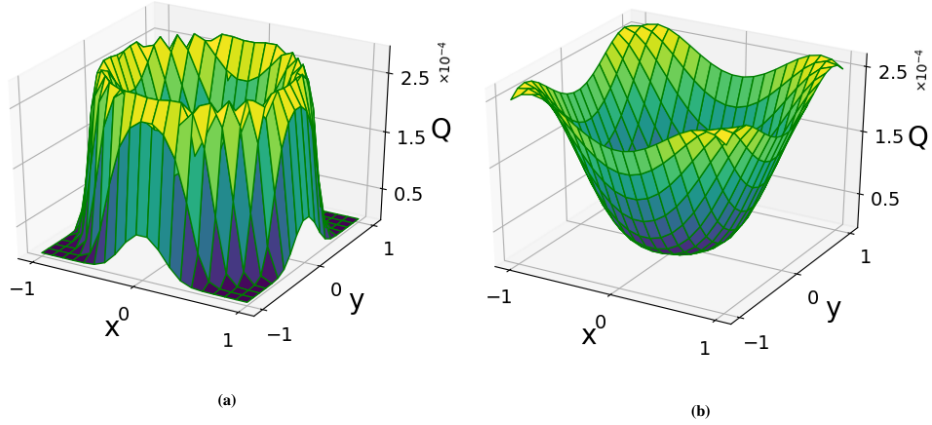


Figure 3.7: (a) Q function for $q = 0.1$ and (b) Q function for $q = 0.9$ for the state $|\xi\rangle_q^m$, with $r = 0.1$.

Then the variances in X_q^m and P_q^m quadratures of the state $|\xi\rangle_{s,q}^m$ are calculated and they are turned out to be the same:

$$\begin{aligned} \langle(\Delta X_q^m)^2\rangle &= \langle(\Delta P_q^m)^2\rangle = \\ &= \left(\frac{1+q^2}{4}\right) \left(1 + (1+q^2)|N_{s,q}^m|^2 \sum_{n=0}^{\infty} (\tanh(r))^{4n} \frac{[4n-1]_q^{m!!}}{[4n-2]_q^{m!!}}\right). \end{aligned} \quad (3.44)$$

This implies that there is no quadrature squeezing. Also, it is obvious that there is no dependence on θ . These observations imply that the nonclassical behavior in the q -deformed squeezed vacuum states vanishes when we go for their superposition, same as observed in the non-deformed scenario [49].

Now let us have a look into the corresponding higher-order squeezing. We have the 4th order squeezing coefficient in X_q^m -quadrature (3.33), and $\langle(\Delta X_q^m)^4\rangle$ given in (3.34). In the case of superposition of two q -deformed squeezed vacuum states (3.19),

$$\begin{aligned} \langle(\Delta X_q^m)^4\rangle &= \langle(\Delta P_q^m)^4\rangle \\ &= \left(\frac{1+q^2}{4}\right)^2 \left(2(1+q^2)\langle A_q^{m\dagger} A_q^m\rangle \right. \\ &\quad \left. + (1+q^2)^2 \langle (A_q^{m\dagger} A_q^m)^2 \rangle + 1 \right. \\ &\quad \left. + \langle (A_q^{m^4} + A_q^{m\dagger 4}) \rangle + \langle A_q^{m^2} A_q^{m\dagger 2} \rangle + \langle A_q^{m\dagger 2} A_q^{m^2} \rangle\right). \end{aligned} \quad (3.45)$$

The (3.45) implies that there is no squeezing in both the quadratures. Therefore as in the case of second-order squeezing, the superposition states are found to have no quadrature

squeezing in the fourth-order case.

3.4.2.2 Number squeezing

The Mandel parameter Q is plotted for different values of r , which is shown in figure 3.8. It can be seen that there is no number squeezing for any values of r , when $q \geq 0.9$. As the q value decreases from 0.9 to 0.1, the state begins to show number squeezing for some values of r . When $q = 0.1$, there is number squeezing for all values of r . When $q \rightarrow 1$, Q reduces to the non-deformed case which can be determined following the same procedure and the results are also included in Fig. 3.8. The behavior of the system is thus differs from that of the non-deformed case which has no number squeezing for any value of r [102]. As in the earlier case, the state becomes more nonclassical with an increase in q deformation.

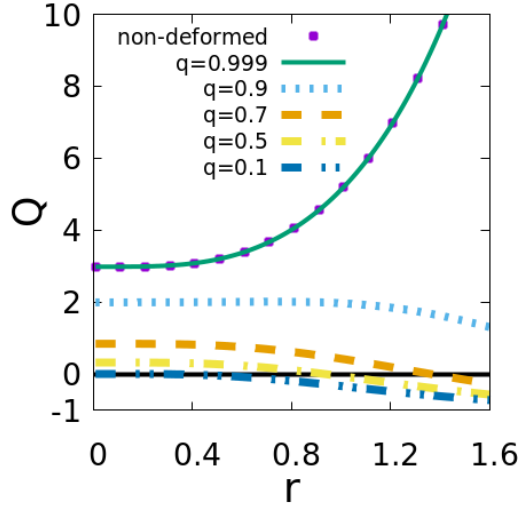


Figure 3.8: The variation of Q with r for the superposition state $|\xi\rangle_{s,q}^m$. Q is different for different q values. Number squeezing is shown below the black horizontal line ($Q = 0$).

3.4.2.3 q -deformed Husimi Q function

The Q function for the state $|\xi\rangle_{s,q}^m$ is calculated using Eq. (3.15) and is given by,

$$Q = \frac{1}{\pi e_q} \left| N_{s,q}^m \sum_{n=0}^{\infty} (e^{i\theta} \tanh(r))^{2n} \sqrt{\frac{[4n-1]_q^{m!!}}{[4n]_q^{m!!}}} \frac{(\alpha^*)^{4n}}{\sqrt{[4n]_q^{m!}}} \right|^2, \quad (3.46)$$

where e_q is the q -deformed exponential and $N_{s,q}^m$ is given in (3.20).

The results are shown in figure (3.9). It can be seen that Q is a non-Gaussian distribution, showing the nonclassical behavior of the state $|\xi\rangle_{s,q}^m$. The Q values differ for different

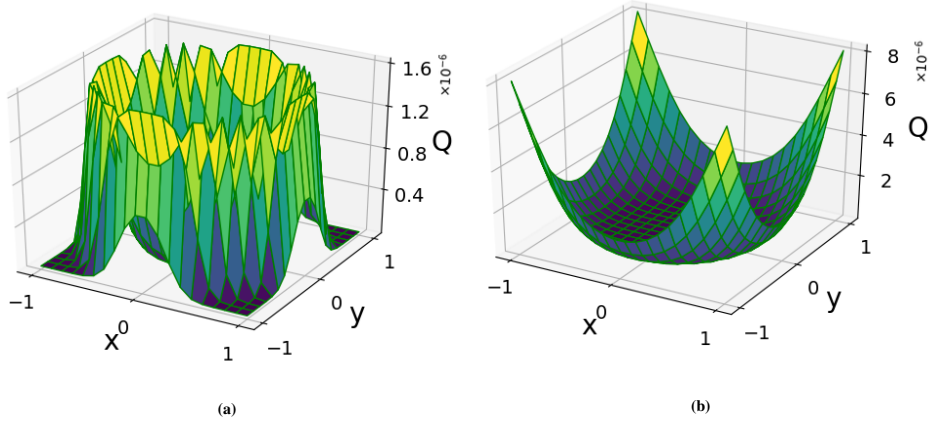


Figure 3.9: (a) Q function for $q = 0.1$ and (b) Q function for $q = 0.9$ for the state $|\xi\rangle_{s,q}^m$, with $r = 0.1$.

q and r .

3.4.3 Superposition of two q -deformed squeezed coherent states

3.4.3.1 Quadrature squeezing and higher-order squeezing

We calculate the squeezing coefficient in the X_q^m -quadrature using (3.10) for the state $|\alpha, \xi\rangle_{s,q}^m$. In general α is a complex number but for simplicity we have taken it as a real one in the calculations. The expectation value of X_q^m is given by

$$\begin{aligned}
\langle X_q^m \rangle &= \sqrt{1+q^2} N_{s,q}^{m^2} \left(N_q^{m^2}(\alpha, \xi) \sum_{n=0}^{\infty} \frac{I(\alpha, \xi, n) I(\alpha, \xi, n+1)}{[n]_q^{m!}} \right. \\
&\quad + N_q^{m^2}(\alpha, -\xi) \sum_{n=0}^{\infty} \frac{I(\alpha, -\xi, n) I(\alpha, -\xi, n+1)}{[n]_q^{m!}} \\
&\quad + N_q^m(\alpha, \xi) N_q^m(\alpha, -\xi) \left(\sum_{n=0}^{\infty} \frac{I(\alpha, \xi, n) I(\alpha, -\xi, n+1)}{[n]_q^{m!}} \right. \\
&\quad \left. \left. + \sum_{n=0}^{\infty} \frac{I(\alpha, \xi, n) I(\alpha, -\xi, n+1)}{[n]_q^{m!}} \right) \right). \tag{3.47}
\end{aligned}$$

We also find out $\langle X_q^{m^2} \rangle$ to calculate the X_q^m -variance, which is included in the Appendix (B). In a similar way, we can also find out the variance of P_q^m . The calculation of

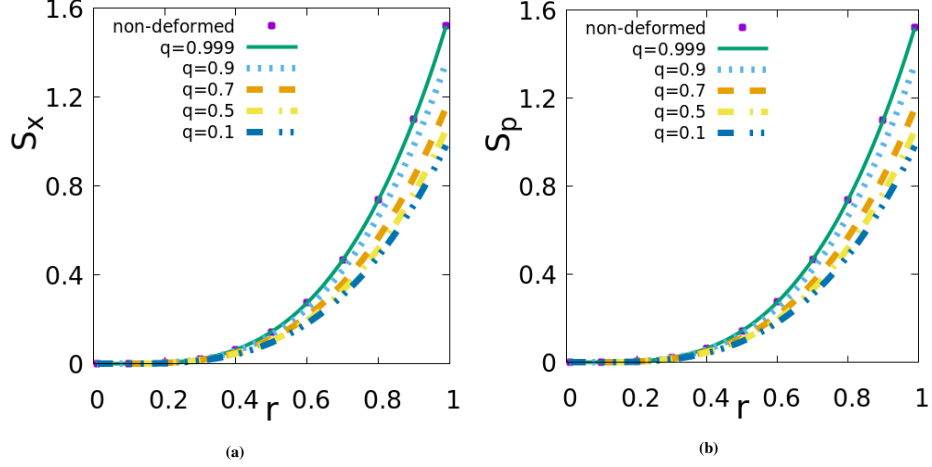


Figure 3.10: (a) Variation of the squeezing coefficient S_X and (b) shows the variation of S_P with r for the state $|\alpha, \xi\rangle_{s,q}^m$. Squeezing coefficient is different for different q values and we have taken $\alpha = 1$.

squeezing coefficient demands the term $\langle [X_q^m, P_q^m] \rangle$. $\langle [X_q^m, P_q^m] \rangle$ can be obtained using

$$\begin{aligned}
\langle A_q^{m\dagger} A_q^m \rangle &= N_{s,q}^{m^2} \left(N_q^{m^2}(\alpha, \xi) \sum_{n=0}^{\infty} \frac{I^2(\alpha, \xi, n)}{[n-1]_q^{m!}} \right. \\
&\quad + N_q^{m^2}(\alpha, -\xi) \sum_{n=0}^{\infty} \frac{I^2(\alpha, -\xi, n)}{[n-1]_q^{m!}} \\
&\quad \left. + 2N_{m_q}(\alpha, \xi) N_q^m(\alpha, -\xi) \sum_{n=0}^{\infty} \frac{I(\alpha, \xi, n) I(\alpha, -\xi, n)}{[n-1]_q^{m!}} \right). \tag{3.48}
\end{aligned}$$

Then the squeezing coefficients S_X and S_P are calculated for different values of r . The recurrence relation given in (3.25) is not easy to solve analytically, so we worked it out using numerical methods. As we stated earlier, α values are taken to be real. Also we choose $\theta = 0^\circ$. S_X and S_P values are plotted for $\alpha = 1$ and are shown in Fig. 3.10. The results reveal that $S_X = S_P$ for all r and α values, and hence there's no squeezing. Moreover, the squeezing coefficient value approaches the squeezing coefficient in the non-deformed regime [102] for the state $|\alpha, \xi\rangle_s^m$ as $q \rightarrow 1$, for any value of α .

The higher-order squeezing in generalized squeezed coherent states is analyzed in [104]. We now focus on the higher-order squeezing of their superposition. The 4th order squeezing coefficient in the X_q^m -quadrature is calculated using (3.33) and (3.34). For the superposition of two q -deformed squeezed coherent states (3.26), $\langle X_q^m \rangle$ and $\langle X_q^{m^2} \rangle$ are already

calculated. Also,

$$\begin{aligned} \langle X_q^{m^3} \rangle = & \frac{(1+q^2)^{\frac{3}{2}}}{8} \left(2\langle A_q^{m^3} \rangle + 2\langle A_q^m A_q^{m\dagger} A_q^m \rangle \right. \\ & \left. + 2\langle A_q^{m^2} A_q^{m\dagger} \rangle + 2\langle A_q^{m\dagger} A_q^{m^2} \rangle \right). \end{aligned} \quad (3.49)$$

Now we can get

$$\begin{aligned} \langle A_q^{m^3} \rangle = & \sqrt{1+q^2} N_{s,q}^{m^2} \left(N_q^{m^2}(\alpha, \xi) \sum_{n=0}^{\infty} \frac{I(\alpha, \xi, n) I(\alpha, \xi, n+3)}{[n]_q^{m!}} \right. \\ & + N_q^{m^2}(\alpha, -\xi) \sum_{n=0}^{\infty} \frac{I(\alpha, -\xi, n) I(\alpha, -\xi, n+3)}{[n]_q^{m!}} + \\ & N_q^m(\alpha, \xi) N_q^m(\alpha, -\xi) \left(\sum_{n=0}^{\infty} \frac{I(\alpha, \xi, n) I(\alpha, -\xi, n+3)}{[n]_q^{m!}} \right. \\ & \left. \left. + \sum_{n=0}^{\infty} \frac{I(\alpha, \xi, n) I(\alpha, -\xi, n+3)}{[n]_q^{m!}} \right) \right). \end{aligned} \quad (3.50)$$

Similarly, other terms in (3.49) are also calculated, and we obtain $\langle X_q^{m^3} \rangle$. In a similar way, we can find out $\langle X_q^{m^4} \rangle$ also to get the corresponding squeezing coefficient in the X_q^m -quadrature. Following a similar procedure, we can generate the squeezing coefficient in the P_q^m -quadrature also. The plots are given in figure 3.11. There is squeezing in the P_q^m -quadrature for all values of q below 0.999, but for a certain range of r values. The squeezing extends to more r values as the q value decreases. $S_P \rightarrow -1$ as the deformation increases show the superposition state has maximum squeezing. Higher-order squeezing shows that the state is nonclassical even though there is no quadrature squeezing. Since quadrature and higher-order squeezing are different manifestations of nonclassical states, they can appear in quantum states independently. The vanishing of second-order squeezing is already observed in the literature for the states like photon-added coherent states [105], even and odd coherent states [93], etc., even though an explicit higher-order squeezing exists. Also, the analysis of quadrature squeezing for the non-deformed superposition state given in (3.28) shows that the results coincide with that of the deformed case when $q \rightarrow 1$, as shown in figure 3.11.

3.4.3.2 Number squeezing

The Mandel Q -parameter is calculated using (3.13).

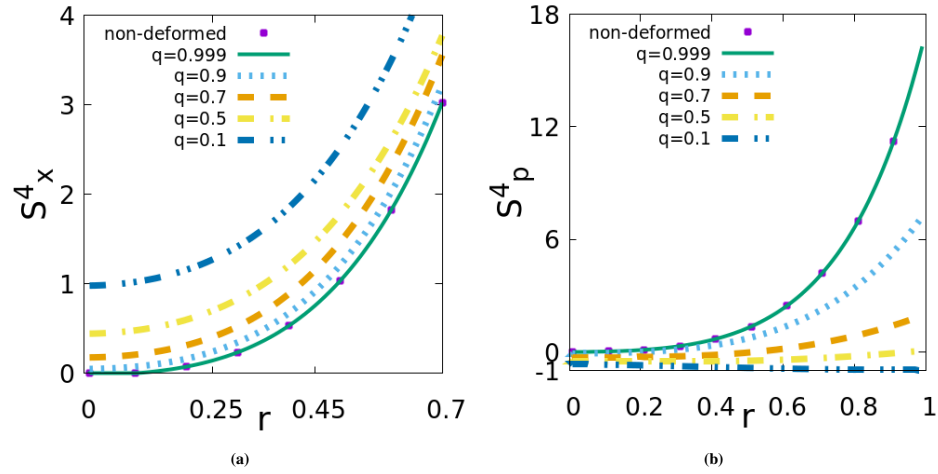


Figure 3.11: (a) The variation of the squeezing coefficient S_X^4 and (b) shows the variation of S_P^4 with r , for the state $|\alpha, \xi\rangle_{s,q}^m$ with $\alpha = 1$.

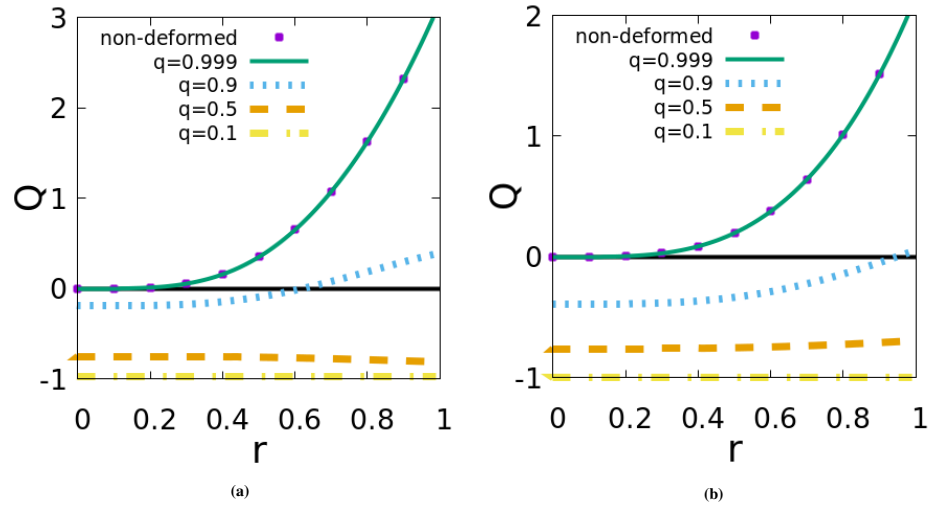


Figure 3.12: Variation of the Mandel Q -parameter for (a) $\alpha = 1$ and (b) $\alpha = 2$, for the state $|\alpha, \xi\rangle_{s,q}^m$. Q is different for different q values. The sub-Poissonian behavior is shown below $Q = 0$ (black horizontal line).

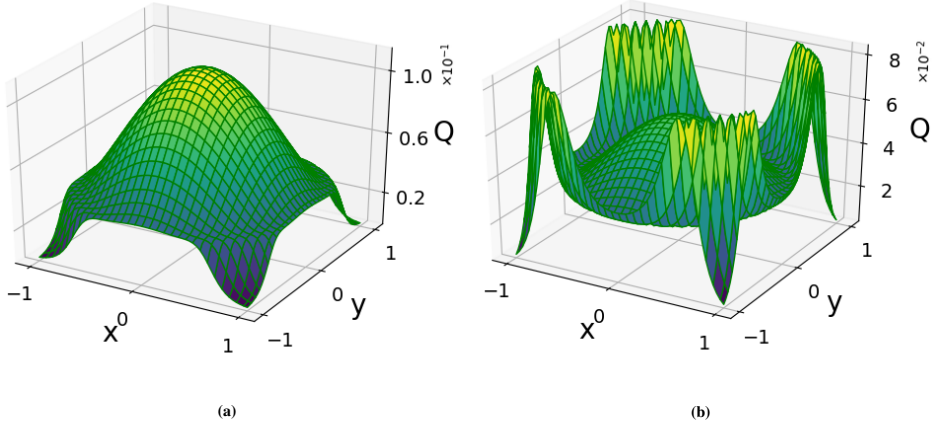


Figure 3.13: Q function for $q = 0.5$ with (a) $r = 0.8$, $\alpha = 0.3$ and (b) $r = 1.2$, $\alpha = 0.5$ for the state $|\alpha, \xi\rangle_{s,q}^m$.

For the state $|\alpha, \xi\rangle_{s,q}^m$, $\langle A_q^{m\dagger} A_q^m \rangle$ is given by (Eq. (3.48)) and

$$\begin{aligned}
\langle (A_q^{m\dagger} A_q^m)^2 \rangle &= N_{s,q}^{m^2} \left(N_q^{m^2}(\alpha, \xi) \sum_{n=0}^{\infty} \frac{I^2(\alpha, \xi, n) [n]_q^m}{[n-1]_q^{m!}} \right. \\
&\quad + N_q^{m^2}(\alpha, -\xi) \sum_{n=0}^{\infty} \frac{I^2(\alpha, -\xi, n) [n]_q^m}{[n-1]_q^{m!}} \\
&\quad + 2N_q^m(\alpha, \xi) N_q^m(\alpha, -\xi) \\
&\quad \left. \times \sum_{n=0}^{\infty} \frac{I(\alpha, \xi, n) I(\alpha, -\xi, n) [n]_q^m}{[n-1]_q^{m!}} \right). \tag{3.51}
\end{aligned}$$

Now Q is plotted for various values of r and q , the result is shown in figure 3.12. It is clear that the Mandel parameter is negative, which means the state $|\alpha, \xi\rangle_{s,q}^m$ has number squeezing. Also, as the deformation increases, $Q \rightarrow -1$, means the state achieves maximum squeezing. When $q = 0.999$ and any r value, there is no number squeezing. The Mandel parameter for the corresponding non-deformed case can be determined using (3.28) and it is matching with that of the deformed one when $q \rightarrow 1$. As in the previous cases, the state shows more sub-Poissonian features with more significant deformation.

3.4.3.3 q -deformed Husimi Q function

The Q function is calculated for the state $|\alpha, \xi\rangle_{s,q}^m$ using (3.15) and is given by

$$Q = \frac{1}{\pi e_q} \left| N_{s,q}^m(\alpha, \xi) \sum_{n=0}^{\infty} \frac{[I(\alpha, \xi, n) + I(\alpha, -\xi, n)] (\alpha^*)^n}{\sqrt{[n]_q^m!}} \right|^2, \quad (3.52)$$

where $N_{s,q}^m(\alpha, \xi)$ is given in (3.27).

As shown in figure 3.13, Q is varying in a non-Gaussian pattern, thus the state is nonclassical in nature. The Q values are different for different q , α and r values.

3.5 Conclusion

This chapter has studied the nonclassicality of q -deformed squeezed states: the deformed squeezed vacuum states, the superposition of two deformed squeezed vacuum states, and the superposition of two deformed squeezed coherent states. By analyzing the quadrature squeezing, higher-order squeezing, number squeezing, and the deformed Husimi Q function, we have arrived at the following results.

We have shown that the quadrature squeezing coefficients in the q -deformed squeezed vacuum states are independent of the deformation parameter q . In contrast, the dependence on q is apparent in the case of their superposition. In contrast to the deformed squeezed vacuum states, their superposition lacks quadrature squeezing for any value of the squeezing parameter r and the deformation parameter q . While analyzing the higher-order squeezing, we found that the higher squeezing present in the deformed squeezed vacuum states also vanishes as we go for their superposition. The q -deformed squeezed vacuum states exhibit maximum squeezing for $\theta = 0$ and $\theta = 180$ as the deformation and squeezing parameters are increased. Attaining maximum squeezing becomes prominent in its higher-order for almost all values of q . However, when we look into the superposition of two deformed squeezed coherent states, it is interesting that there is a fourth-order quadrature squeezing, whereas there is absolutely no second-order squeezing for any values of q , r , and α . Moreover, the Mandel Q parameter calculation reveals the number squeezing in all the deformed squeezed states considered in this paper, but only for a specific range of q , r , and α values. Also, for the superposition of two q -deformed squeezed coherent states, the higher-order squeezing attains its maximum value as $q \rightarrow 0$ and $r \rightarrow 1$. A similar trend is observed for the Mandel parameter also. All the results mentioned above in the deformed scenario are found to be coinciding with the non-deformed case when $q \rightarrow 1$, as required.

We have also studied the q -deformed Husimi Q function for the q -deformed states. The deviation from the Gaussian shape is evident in all the Q function plots and is a clear indicator of its nonclassicality. We found that the Q function depends on the values of q , r , and α . As q decreases (i.e., more deformation), the Q function becomes closer to an annular-shaped distribution. It is worth mentioning that the Q function of the most nonclassical state $|n\rangle$, the number state, is annular in shape [93]. Thus, we conclude that the states are still highly nonclassical despite quadrature squeezing vanishing. In the deformed states, we have an additional degree of freedom to produce the required nonclassicality in terms of the deformation parameter q . We can even attain the maximum nonclassicality possible by adjusting the value of q .

Chapter 4

Dynamics of observables in a q -deformed harmonic oscillator

4.1 Introduction

In this chapter, we report the study of the dynamical behavior of math-type q -deformed harmonic oscillator system which is widely studied in quantum optics [74, 106, 107, 31]. The study of the dynamics of a quantum system plays a crucial role in several fields like quantum computing, quantum optics, etc. In the study of dynamics of a system, we investigate how quantum mechanical variables change over time. We are all familiar with the classical and quantum mechanical harmonic oscillators, which will be reviewed in detail in the upcoming sections. A quantum mechanical harmonic oscillator possesses discrete energy levels with energy values E_n linearly dependent on n , which is observed to be the reason for its periodic dynamical behavior.

In previous chapters, we have already familiarized ourselves with the idea of math-type q -deformed oscillators and their algebra. In a preliminary analysis, we observed that the deformation of the Lie algebra causes the energy eigenvalues of the q -deformed harmonic oscillator to deviate from the linearly increasing energy eigenvalues of the non-deformed harmonic oscillator. This hints at the possibility of chaotic behavior in the system, which we will investigate in this study. As already mentioned in Chapter (1), even though Bohr's correspondence principle points at the possibility of the existence of chaos in quantum systems, inherent quantum chaos is not yet observed, which points to the relevance of the work included in this chapter.

4.2 Harmonic oscillator and energy eigenvalues

In classical physics, a simple harmonic oscillator is an object that performs harmonic motion about an equilibrium position, such as an object with mass vibrating on a spring. The total energy of such an oscillator is the sum of its kinetic energy $K = \frac{mv^2}{2}$ and potential energy $U = \frac{kx^2}{2}$, where k is the spring constant in the system. The motion of the oscillator is constrained between the turning points, and the lowest energy it may have is zero when the object is at rest at its equilibrium position, as illustrated in the figure (4.1). The energy of a classical oscillator thus changes continuously.

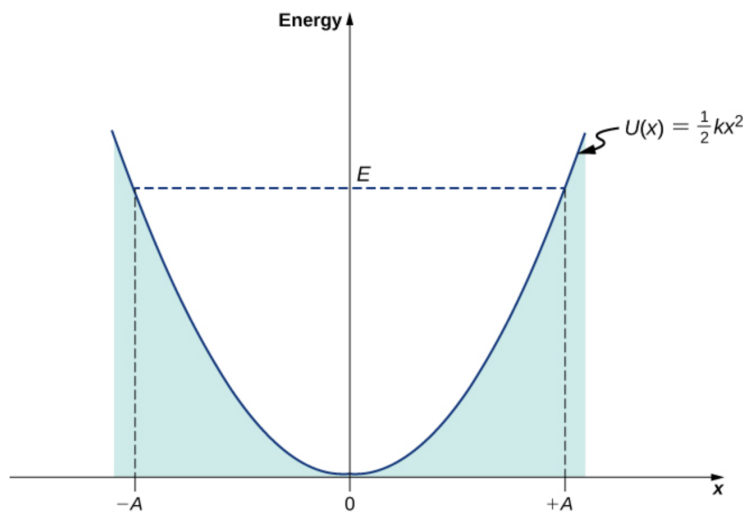


Figure 4.1: The energy of a classical harmonic oscillator against its position. The total energy E is the sum of potential and kinetic energies. A and $-A$ are the turning points at which the kinetic energy of the oscillator is zero.

While moving into the area of quantum physics, the potential energy function acquires a more general form, $U = \frac{m\omega^2 x^2}{2}$.

The pure quantum harmonic oscillator can be described by the Hamiltonian

$$H = (1/2)(aa^\dagger + a^\dagger a), \quad (4.1)$$

where a, a^\dagger correspond to the non-deformed annihilation and creation operators, respectively. In this chapter, we work with the units $\hbar = \omega = 1$. It is to be noted that the scaling of these terms does not affect the results of this study in anyway. Apart from the classical oscillator, the quantum harmonic oscillator possess discrete energy levels with values $E_n = (n + \frac{1}{2})$, which is depicted in figure (2.1) in Chapter 2. It is to be noted that the energy values have a linear dependence on n . It has been already reported in literature that

this linear dependence of energy eigenvalues in n gives periodic behaviour in the dynamics of its expectation values [108].

4.2.1 Energy eigen values of the q -deformed Harmonic Oscillator

The Hamiltonian for a math-type q -deformed harmonic oscillator is given in [109] where the q -deformed harmonic oscillator and its coherent states are studied. The Hamiltonian

$$H_q^m = \frac{1}{2}(A_q^m A_q^{m\dagger} + A_q^{m\dagger} A_q^m), \quad (4.2)$$

where A_q^m and its adjoint $A_q^{m\dagger}$ are the math-type q -deformed annihilation and creation operators, respectively. The oscillator described by the Hamiltonian H_q^m is called the q -deformed harmonic oscillator. The operators A_q^m and $A_q^{m\dagger}$ obey the deformed commutation relation,

$$A_q^m A_q^{m\dagger} - q^2 A_q^{m\dagger} A_q^m = I, \quad (4.3)$$

where, I is the identity matrix and $0 < q < 1$. The Hamiltonian (4.2) has an eigenvalue

$$E_{q,n}^m = \left([n]_q^m + \frac{q^{2n}}{2} \right). \quad (4.4)$$

In the limit of $q \rightarrow 1$, $[n]_q^m \rightarrow n$ and $E_{q,n}^m$ reduces to E_n of the non-deformed quantum harmonic oscillator. In figure (4.2), we can clearly see that the energy values of the q -deformed harmonic oscillator departs significantly from the linear energy curve of the non-deformed harmonic oscillator, as the deformation increases. Thus, the nonlinear variation of the energy eigenvalues with n for q -deformed harmonic oscillator may give rise to other dynamical properties such as quasi-periodicity and chaos, which is the prime motivation for this study.

4.3 Time evolution with q -deformation

The canonical position and momentum operators X_q^m and P_q^m for the deformed harmonic oscillator are given in (3.8), which reduces to the non-deformed x and p when $q \rightarrow 1$. Further, the action of A and A^\dagger on the deformed Fock state $|n\rangle_q$ is already described in Chapter 2. Now, in the next section, we describe the dynamical evolution of the q -deformed observables X_q^m and P_q^m . To proceed further, let us first analyze how the autocorrelation function of the system has changed due to the q -deformation.

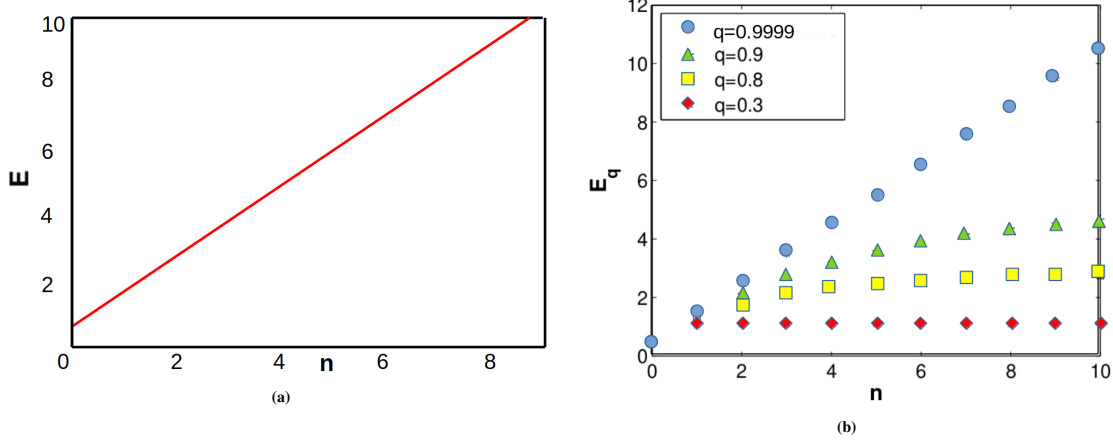


Figure 4.2: Plot of energy vs n for a (a) non-deformed oscillator and a (b) deformed oscillator with different q values. (b) shows that the energy eigenvalues are distributed in a nonlinear fashion for the q -deformed oscillator which is in contrast to (a) the linearly distributed energy eigenvalues of the non-deformed harmonic oscillator.

4.3.1 Time evolved deformed coherent state

The q -deformed coherent state for the deformed harmonic oscillator is already discussed in (3.16).

Expression for $[n]_q^m$ can be re-arranged to obtain

$$q^{2n} = 1 + (q^2 - 1) [n]_q^m . \quad (4.5)$$

Using equations (3.16) and (4.5), the time evolved deformed coherent state $|\alpha(t)\rangle_q^m$ is derived as,

$$\begin{aligned} |\alpha(t)\rangle_q^m &= e^{-iH_q^m t} |\alpha(0)\rangle_q^m , \\ &= e_q^{-\frac{|\alpha|^2}{2}} \sum_{n=0}^{\infty} \frac{(\alpha(0))^n}{\sqrt{[n]_q^m!}} e^{-it\left([n]_q^m + \frac{q^{2n}}{2}\right)} |n\rangle_q^m , \\ &= e^{-\frac{it}{2}} e_q^{-\frac{|\alpha|^2}{2}} \sum_{n=0}^{\infty} \frac{(\alpha(0))^n}{\sqrt{[n]_q^m!}} e^{-\frac{it}{2}[n]_q^m (q^2+1)} |n\rangle_q^m . \end{aligned} \quad (4.6)$$

From (4.6), we obtain the autocorrelation function of the time evolved deformed coherent state:

$${}_q^m \langle \alpha(0) | \alpha(t) \rangle_q^m = e_q^{-|\alpha|^2} e^{-\frac{it}{2}} \sum_{n=0}^{\infty} \frac{|\alpha(0)|^{2n}}{[n]_q^m!} e^{-\frac{it}{2}[n]_q^m (q^2+1)} . \quad (4.7)$$

The corresponding plot is given in figure 4.3 and compared with the non-deformed one, from which it is evident that, upon time evolution, the deformed coherent state no longer retains its coherent form.

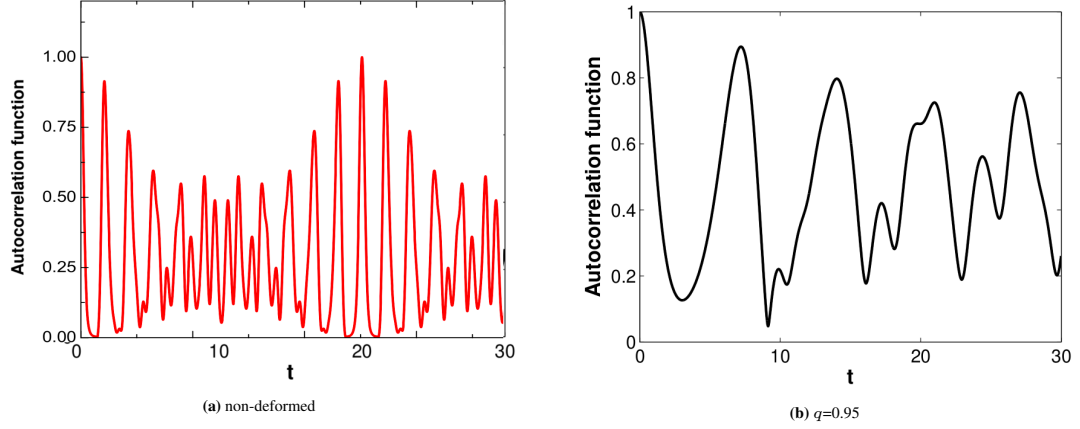


Figure 4.3: Plot of autocorrelation function as a function of time for (a) non-deformed harmonic oscillator and (b) deformed one with $|\alpha|^2 = 1$ and $q = 0.95$

The dynamical evolution of the expectation values of the deformed position operator X_q^m and the deformed momentum operator P_q^m are derived as:

$$\begin{aligned}
\langle X(t) \rangle_q^m &= {}^m \langle \alpha(t) | X_q^m(t) | \alpha(t) \rangle_q^m, \\
&= \frac{\sqrt{1+q^2}}{2} e_q^{-|\alpha|^2} \\
&\times \sum_{n=0}^{\infty} \left\{ \frac{|\alpha|^{2n}}{[n]_q^m!} \alpha e^{\frac{it}{2}(1+q^2)} ([n]_q^m - [n+1]_q^m) \right. \\
&\quad \left. + \frac{|\alpha|^{2n+1}}{[n]_q^m!} \alpha^{-1} e^{-\frac{it}{2}(1+q^2)} ([n]_q^m - [n+1]_q^m) \right\}. \tag{4.8}
\end{aligned}$$

$$\begin{aligned}
\langle P(t) \rangle_q^m &= {}^m \langle \alpha(t) | P_q^m(t) | \alpha(t) \rangle_q^m, \\
&= i \frac{\sqrt{1+q^2}}{2} e_q^{-|\alpha|^2} \\
&\times \sum_{n=0}^{\infty} \left\{ \frac{|\alpha|^{2n+1}}{[n]_q^m!} \alpha^{-1} e^{-\frac{it}{2}(1+q^2)} ([n]_q^m - [n+1]_q^m) \right. \\
&\quad \left. - \frac{|\alpha|^{2n}}{[n]_q^m!} \alpha e^{\frac{it}{2}(1+q^2)} ([n]_q^m - [n+1]_q^m) \right\}, \tag{4.9}
\end{aligned}$$

using the expressions of the action of operators A_q^m and $A_q^{m\dagger}$ on the Fock state and (4.6).

4.3.2 Nature of the time evolved observables

The time evolved observables, in this case, the expectation values of the deformed position and momentum, produce respective time series when computed numerically. One can perform a generic analysis of this series by applying the common procedures followed for a typical time series data. Here, the nature of these time evolved variables are studied using four complimentary analysis tools, namely, first-return-time distributions, recurrence plots, Lyapunov exponents and the power spectra.

4.3.2.1 Recurrence plots:

The analysis of complex systems using recurrence plots is studied in [110] by using the graphical representation of

$$R_{i,j} = \begin{cases} 1, & \text{if } \vec{x}_i \approx \vec{x}_j; \\ 0, & \text{otherwise.} \end{cases} \quad i, j = 1, 2, \dots, N, \quad (4.10)$$

where N is the number of data points under consideration and $\vec{x}_i \approx \vec{x}_j$ refers to its equivalence within a designated parameter ϵ . The simulation of this calculation produces an $N \times N$ matrix, whose elements are a series of ones and zeroes, with 1 representing points that lie close to each other. We can classify a given series as periodic, quasi-periodic or chaotic based on the particular features of its recurrence plots. As a general rule, we may establish that periodic trajectories are characterized by parallel, equidistant diagonal lines. Quasi-periodicity is characterised by two or more sets of parallel, diagonal lines. Chaos is characterized by a single *line of identity* which may or may not be surrounded by other short broken lines at random distances from the *line of identity*.

4.3.2.2 Power spectra

We also utilize the power spectrum of the time series to understand the nature of the non-linear system better. The power spectra are easily obtained by the technique of fast Fourier transform of the time series. It is to be noted that in case of a chaotic series, the power spectrum displays “grassiness” with the spectrum also showing a decreasing trend. Quasi-periodicity is indicated by peaks which may or may not exhibit splitting [57, 111].

4.3.2.3 First-return-time distributions:

First-return-time distribution encompasses information about the recurrence of a small range of values over a large series of datapoints [57, 58]. We construct computational cells of suitable sizes and determine the frequency of recurrence of datapoints within this cell. We compute the probability of recurrence and attempt to fit appropriate probability distributions. Based upon the requirement of ergodicity, from the Poincaré recurrence theorem [112], the recurrence time t is found to satisfy an exponential distribution of the form $F_1(\tau) = (1/\tau) e^{-t/\tau}$, where the mean μ is given by $\mu^{-1} = \langle \tau \rangle$ [57, 112]. This implies that the first-return-time distributions which satisfy this relation correspond to ergodic behaviour. In the present study, we obtain the first-return-time distribution for cell sizes less than or equal to 10^{-3} .

4.3.2.4 Lyapunov exponent

The next parameter analysed in this study is the Lyapunov exponent. The Lyapunov exponent (λ) describes the divergence from an initial trajectory, of an almost identical trajectory produced by an infinitesimal perturbation in the initial conditions. A positive Lyapunov exponent is indicative of chaos in the system, in which case the trajectories diverge at an exponential rate defined by the largest Lyapunov exponent λ_{max} of the system as described in [113] where the method of calculation of Lyapunov exponent is discussed in detail. In particular, the slope of the graph of $\ln(d(j))$ vs $j \Delta t$, where, $d(j)$ stands for the divergence of the trajectory and $j \Delta t$ denotes the time, gives us an idea of the sign of the Lyapunov exponent and its magnitude. In this study, we use the Rosenstein algorithm [113] to determine the greatest Lyapunov exponent λ_{max} . We also cross verify our calculation of the Lyapunov exponent using another conventional algorithm called the Wolf algorithm [114]. The results were found to be in agreement with each other.

It must be noted that all these analysis methods ideally complement each others findings and none of them can be utilized as a confirmation for a system property, on its own. The results thus we obtained are listed below:

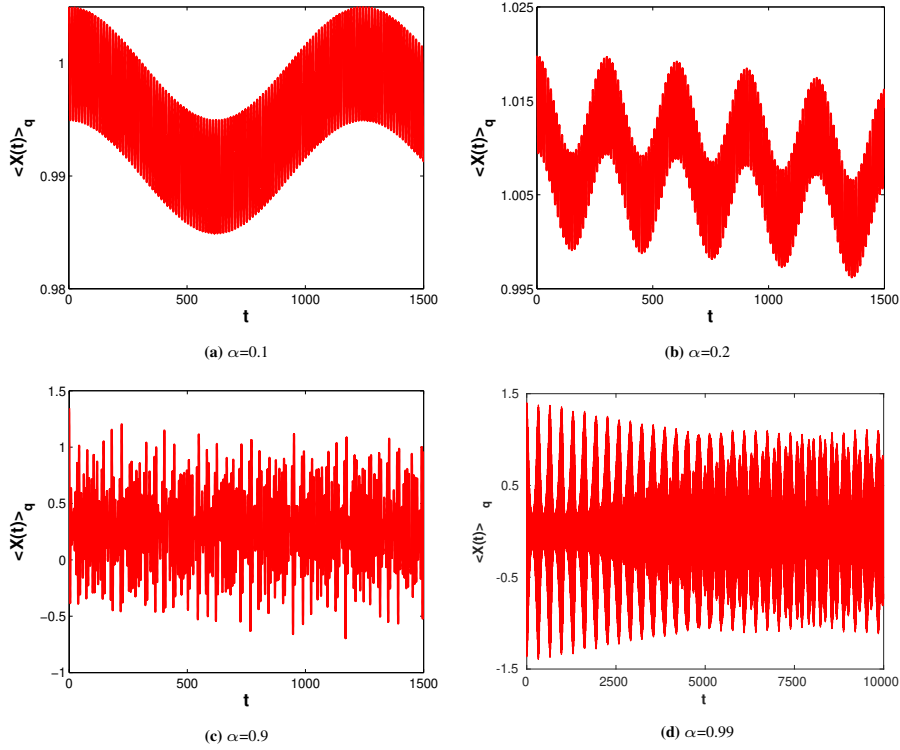


Figure 4.4: Time evolution of $\langle X(t) \rangle_q^m$ for different q values and $\alpha = 1$.

4.4 Results and Discussion

4.4.1 Analysis of dynamical variations

As a preliminary step, we analyse the autocorrelation function in Fig. 4.3. Here we present the results obtained for real values of α but our result holds true for any general complex value of α . If a system is periodic, the respective autocorrelation function is bound to be periodic. For $\alpha = 1$ and $q = 0.9$, the autocorrelation function appears to peak at random intervals, hinting at the probable chaotic nature of the system for the chosen set of parameters. Based on this observation, we proceed to investigate further into the properties of the system.

A qualitative reasoning for the system at hand can be obtained from the plots of its dynamic evolution and phase space diagrams.

These results, shown in figures (4.4) and (4.5), reinforce our guesses regarding the chaotic nature of the expectation values. Similar plots have been obtained previously for physics-type q -deformation in [115], but an analysis in terms of chaos was not performed on the data in their study. Now, in the present case, an interesting trend is observed when

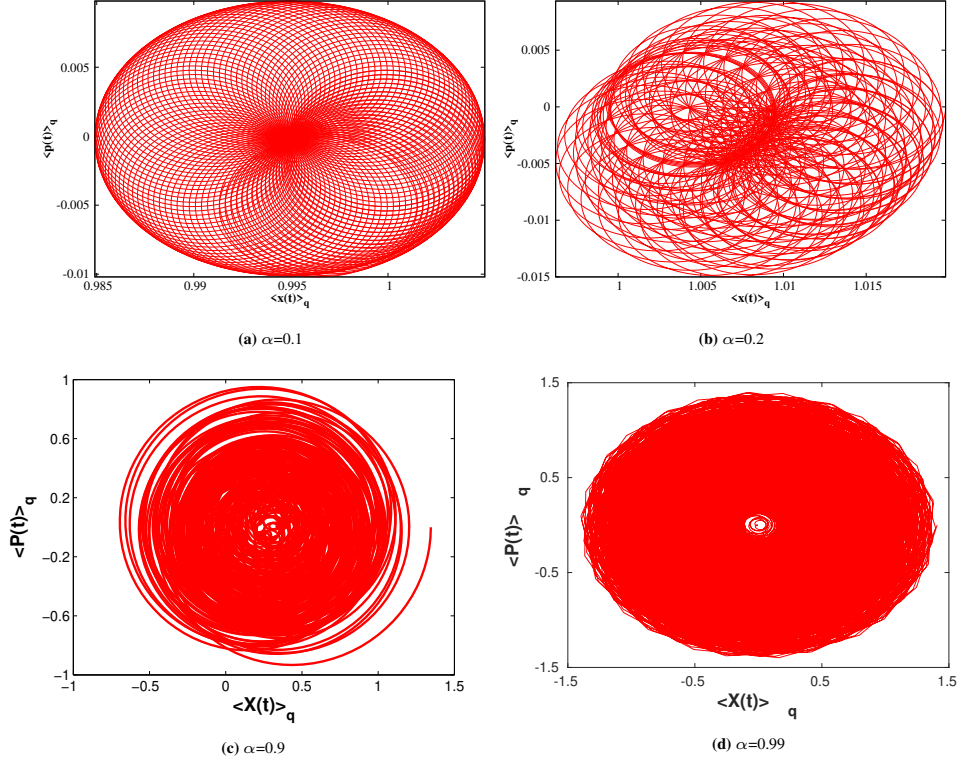


Figure 4.5: Phase space diagrams $\langle X(t) \rangle_q^m$ vs $\langle P(t) \rangle_q^m$ for different q values and $\alpha = 1$.

the values of α and q are varied. In figure 4.4, we summarize how the dynamic behavior of the expectation values vary gradually with q for $\alpha = 1$. In figure 4.4(d) we plot the data for a longer time (10^4) to make its nature more clear. All other plots in Fig. 4.4 have been made for $t = 1500$ as the nature of the system in these cases is clearly evident with this data set. On the higher extreme (as q increases/ as deformation decreases), we see that the behaviour gradually approaches that of a harmonic oscillator, while on the lower end (as q decreases/ as deformation increases), the behavior first appears chaotic, turns quasi-periodic and finally progresses towards periodicity. Specifically, this new found periodicity seems to emerge for values of $q \leq 0.1$. As q increases for the same α , the plot of expectation values vs t appears to get constricted between the given pair of points. This constriction increases relatively with every step rise in q .

This gradual change appears to be taking the system from periodic to aperiodic behavior. The corresponding behavior is reflected in the phase space diagram by the effective “order” or “disorder” of the data points. However, the system does not continue to be aperiodic, rather as $q \rightarrow 1$, its behavior rapidly approaches that of the non-deformed harmonic oscillator. We study these characteristics of the expectation values in detail in the following sections quantitatively.

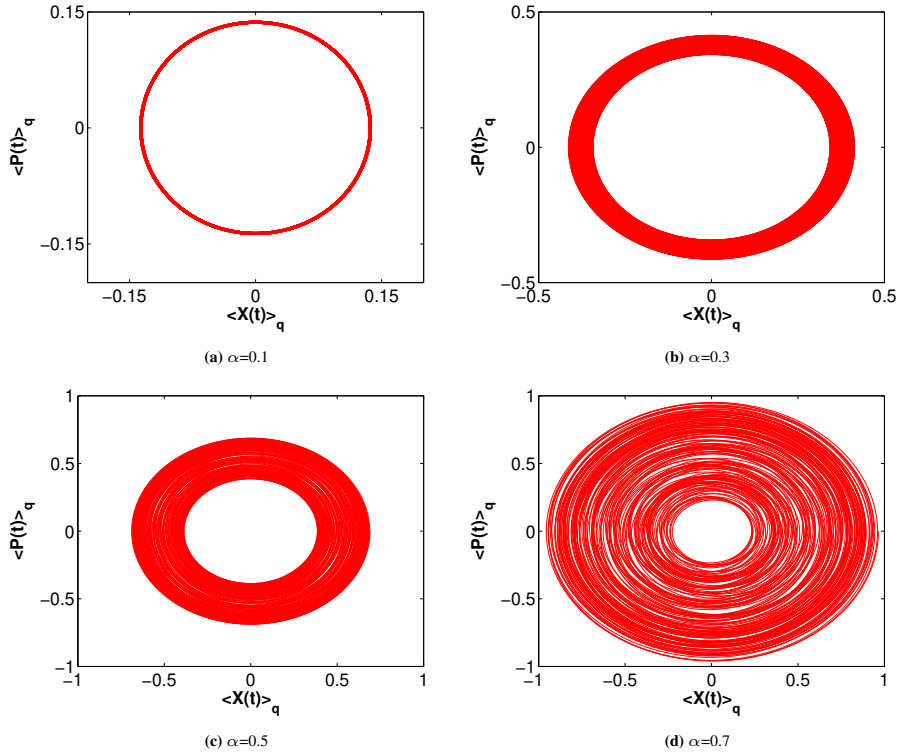


Figure 4.6: Phase space diagrams for different values of α and $q=0.95$.

Another interesting dependence of the system dynamics is on the parameter α . In figure 4.6, the phase space plots show specific behaviour depending on α value. We identify that the typical chaotic behaviour exists only for $\alpha > 0.5$ when $q = 0.95$. Below this value of α , the phase space plot takes on a band-like structure. In the later sections, we will explain how these band-structures conform to quasi-periodic behaviour. The width of the band is seen to decrease with α . For lower values of α (typically for $|\alpha|^2 \leq 0.1$), the behaviour approaches periodicity. It should be noted that there exists a restriction on α values for a given value of q [109]:

$$|\alpha|^2 \leq \frac{1}{1-q}. \quad (4.11)$$

When $\alpha = 2$, due to the limit in equation (4.11), the values of q below 0.75 are not allowed. For $\alpha = 1$, (4.11) permits all q values in the range $0 \leq q \leq 1$. Now let us look at some more features of the system which will help us to get a better qualitative understanding of the properties stated above.

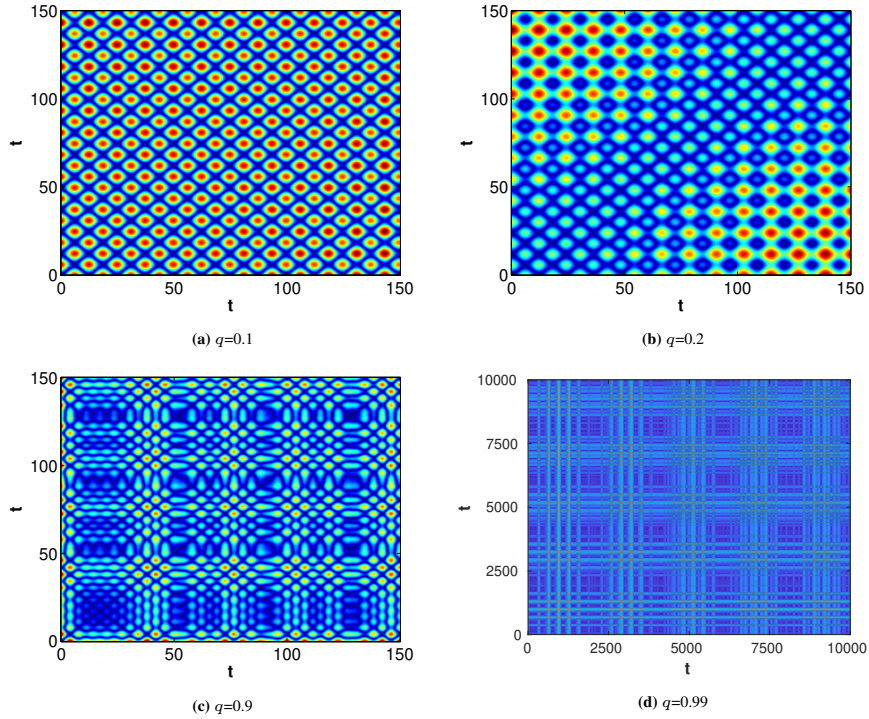


Figure 4.7: Recurrence plots for different q values when $\alpha = 1$. (a) corresponds to periodic data, (b), (d) correspond to quasi-periodic data and (c) corresponds to chaotic data.

4.4.2 Recurrence plots

The recurrence plots in figure 4.7, underscores our observations regarding the time series. Through careful observation, we identify the defining features in the recurrence plots that classify its behaviour as periodic or aperiodic.

In the figure 4.7, when $\alpha = 1$ for $q = 0.1$, the recurrence plot is characterised by equidistant, parallel diagonals, which is an attribute of periodic systems. For $q = 0.2$, we can roughly identify two sets of parallel lines, each set composed of respective equidistant lines. This denotes the presence of two periods for the corresponding time series, thus implying a quasi-periodic behaviour. In figure 4.7(c), we can clearly distinguish a *line of identity* (as described in the previous section), combined with symmetrically distributed short broken lines at random distances on both of its sides. At $q = 0.99$, the system displays a quasi-periodic behaviour and progresses towards periodicity as $q \rightarrow 1$. Thus, we are able to mark out a clear chaotic regime with the help of these recurrence plots.

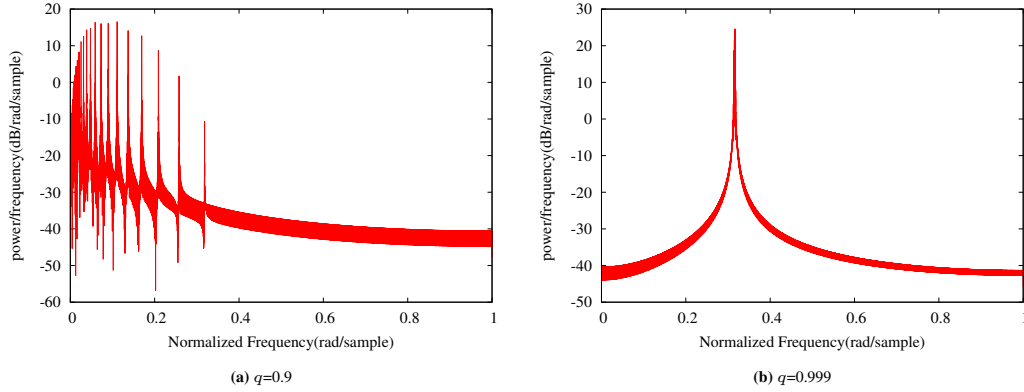


Figure 4.8: Power spectra for $\alpha = 2$ showing (a) chaotic nature ($q = 0.9$), and (b) periodic nature ($q = 0.999$).

4.4.3 Power Spectrum

The power spectrum for the system, in the range of $0.2 < q < 0.99$ for $\alpha = 1$, shows grassiness and decreasing trend, which is a typical feature of a chaotic power spectrum. An example of such a spectrum is given in figure 4.8(a). The decreasing trend is in such a way that initially there is an exponential decay which is followed by a much slower algebraic decay. The grassiness is more if $\alpha = 2$ than if $\alpha = 1$. One expects multiple (and/or split) peaks in a quasi-periodic power spectrum. As such, we observe, two distinct split peaks near zero for $q = 0.2$ when $\alpha = 1$, thus re-affirming our observations regarding its quasi-periodic behaviour. Our analysis also shows quasi-periodic behaviour in the range $0.1 < q \leq 0.2$ when $\alpha = 1$. The resurgence of an exact periodic behaviour is observed when $q \leq 0.1$ for $\alpha = 1$. For the quasi periodic behaviour arising when $\alpha \leq 0.5$ at $q = 0.95$, we observe two peaks, affirming the presence of two distinct periods.

Based on the qualitative understanding of the system from the previous sections, we now move onto the quantitative analysis of the system.

4.4.4 First-return-time distributions

Figure 4.9 presents the first-return-time distributions. The first-return-time plots for those time series that were observed to produce chaotic behaviour earlier are seen to fit the exponential probability density function explained in [58]. This points to their ergodic dynamical behaviour. When $\alpha = 1$, traces of chaotic behaviour is observed around $q = 0.3$ and becomes more evident as q increases. Around this initial chaotic region, although the distribution resembles an exponential decay, it fits only approximately to the said distribution. The expectation values for $\alpha = 1$ in the range $0.1 < q \leq 0.2$ seems to exhibit

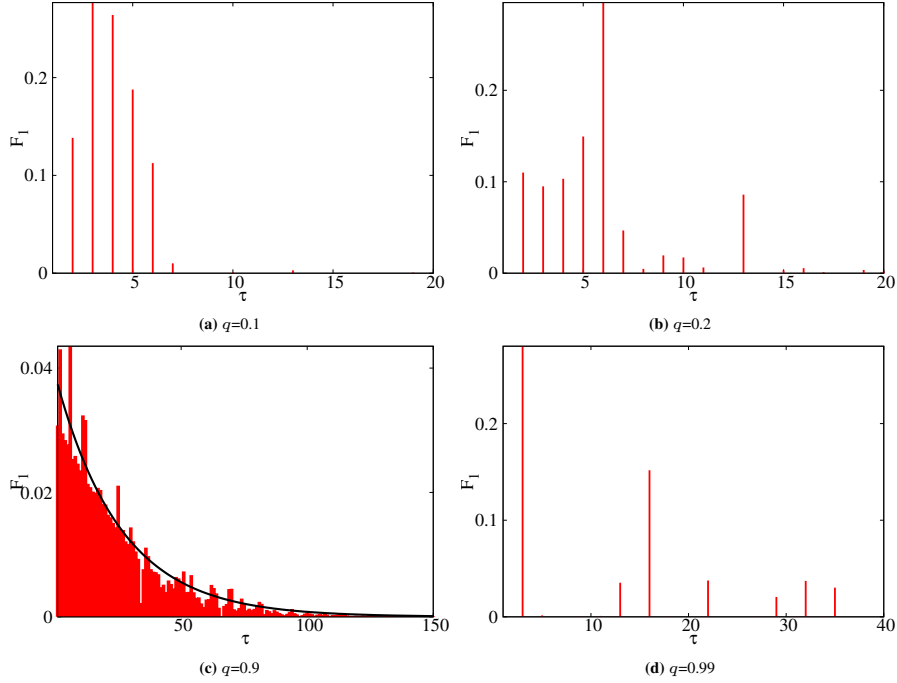


Figure 4.9: First-return-time distributions for different values of q and $\alpha = 1$. (a) corresponds to periodic data, (b), (d) corresponds to quasi-periodic data and (c) corresponds to chaotic data. The solid black line in the first-return-plot represents the fitted exponential curve mentioned in section 4.3.2.

a quasi-periodic behaviour, characterised by the distribution of the type shown in figure 4.9(b). In the case of exponential fitting, the mean recurrence time, μ , is found to be large, thus indicating large time variation before recurrence. For $q \leq 0.1$, the behaviour strictly adheres to periodicity, thus not fitting any special distributions.

Similarly, for low α featuring a band-like phase space structure, the first-return-time analysis revealed quasi-periodic behaviour. Higher α values produce chaotic behaviour for a larger range of the allowed q values, while lower α values show more quasi-periodic and periodic properties for a larger range of q values. Comparing the dynamical behaviour for $\alpha = 1$ and $\alpha = 2$, we find that chaotic behaviour is prevalent for nearly all allowed q values for $\alpha = 2$ while it is seen only for $0.2 < q < 0.99$ when $\alpha = 1$. For lower values of α , the system is periodic for all values of q .

4.4.5 Lyapunov exponent of the time series

The maximum Lyapunov exponents of the time series evaluated for different combinations of α and q values were found to be positive for those ranges that were deduced to be chaotic in the previous section. The plot of the logarithm of distance between two closely spaced trajectories versus time is of particular importance. This curve is ideally expected to be a

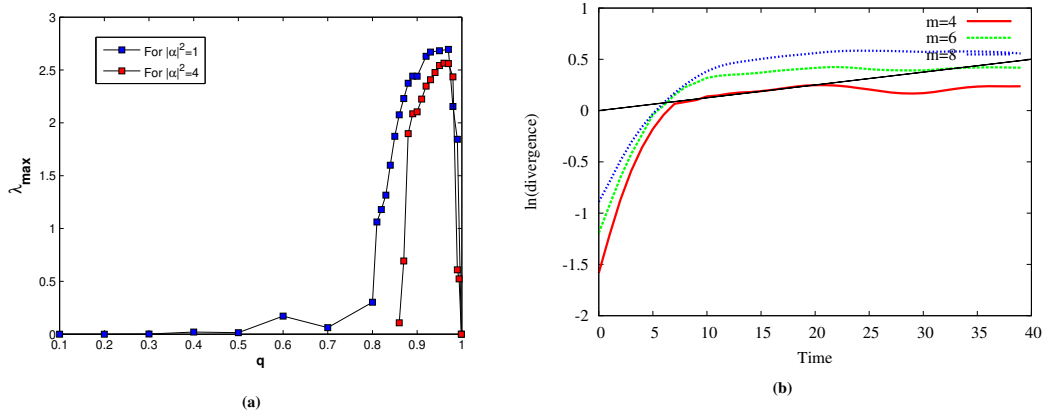


Figure 4.10: Plots showing (a) variation of largest Lyapunov exponent with q value, and (b) the Lyapunov exponent plot for $\alpha = 1$ and $q = 0.9$ showing the chaotic nature of the system.

straight line, whose slope gives the magnitude and sign of the Lyapunov exponent. The plot for different q values and different α values were determined and plotted, with the results in agreement with our findings in the previous sections.

The sign of the Lyapunov exponent is unambiguously confirmed to be positive for $0.2 < q < 0.99$ when $\alpha = 1$, which is a signature of chaos. Further, the slope of the curve for the periodic and quasi-periodic regime is found to be 0, thus re-affirming our conclusions regarding their behaviour as well. Figure (4.10a) shows the variation of λ_{max} with q . For a given value of α , the transition to periodicity is faster in the region of $q \rightarrow 1$ than when $q \rightarrow 0$. We also include figure (4.10b) to portray the nature of the curves used to determine the largest Lyapunov exponents [113]. Here, the linear region is used for the calculation of the exponent.

As we come to the conclusion, with all the proven results, we provide an approximate demarcation of the various dynamical regimes in the $q - \alpha$ plane using figure 4.11.

4.5 Conclusion

In this chapter, we attempted to understand how the q -deformation of an ordinary Hamiltonian changes the behavior of the system. We find that the q -deformation confers non-linear properties to the ordinary quantum harmonic oscillator. By studying the dynamics of the resultant time series obtained for the expectation values of the dynamical variables X_q^m and P_q^m , we conclude that the system studied exhibits periodic, quasi-periodic and chaotic behaviour depending on the deformation parameter q and the deformed coherent amplitude

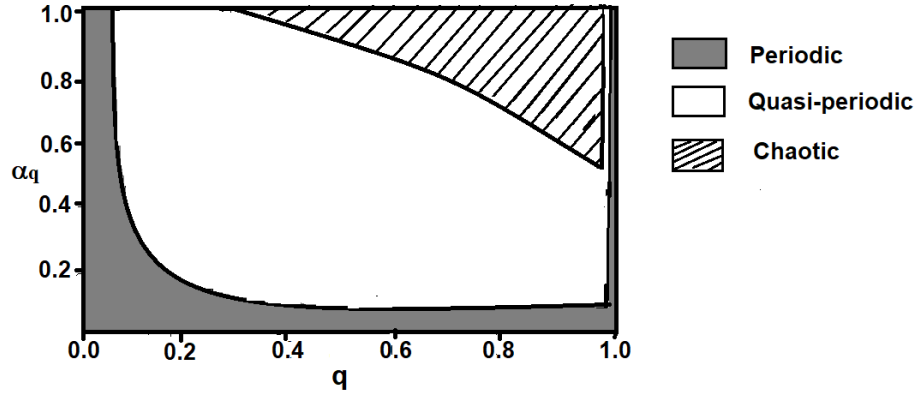


Figure 4.11: Behaviour of a q -deformed oscillator with respect to α and q values.

α . As the value of α increases, we observe that chaotic nature is the more prominent dynamical behaviour. For lower values of α , the dynamical behavior is mostly quasi-periodic or periodic.

The qualitative verification of the dynamical properties of this system was performed through recurrence plots and power spectra of the time series. First-return-time distributions were used to verify the ergodic behavior of the system in the chaotic regimes obtained from the qualitative analysis. The quantitative verification of the above conclusions using Lyapunov exponents revealed that the exponents are positive in the estimated chaotic regime and zero in the periodic and quasi-periodic regimes. The magnitude of the Lyapunov exponents and, thus, the magnitude of the exponential divergence of trajectories is dependent on the magnitude of the deformation.

Thus, the analysis of expectation values of dynamical variables carried out here clearly shows signatures of chaos in another quantum system.

Chapter 5

Entanglement dynamics in q -deformed states

5.1 Introduction

Chapter 3 has already discussed the squeezing properties and Husimi Q function of the math-type q -deformed oscillators. Another important nonclassical feature of quantum states is quantum entanglement. It is a physical phenomenon in which two or more particles interact so that their quantum states cannot be described independently. Even though quantum entanglement continues to puzzle researchers around the world, it serves as a key resource for quantum information processing and hence finds applications in fields like quantum teleportation [116], quantum cryptography [117], superdense coding [118], quantum metrology [11], etc. The study of entanglement in deformed states is a progressing area of research [60, 61]. Regarding the study of entanglement, the essential part is to test whether a given quantum state is entangled. There are different entanglement measures that are being used for the quantum states. They include von-Neumann entropy [63], concurrence [64], negativity [65], and quantum Fisher information [119]. Among them, concurrence and negativity are used to analyze mixed states, whereas the von Neumann entropy has been proposed for the study of pure state entanglement. Regarding a non-deformed system, the study of entanglement dynamics pertaining in the interaction of a single mode field with atoms of a nonlinear medium is reported in [120], in which entropy of entanglement indicates the existence of revivals and fractional revivals. [120] also reports the study of entanglement dynamics for different initial states, using the entanglement measures like subsystem von Neumann entropy, linear entropy, and overlap fidelity. The results show that entanglement measures significantly depend on the nature of the initial state. Apart from an ideal non-deformed system, the deformed ones are more advantageous as they consider the possible deformations in the system. It is really important to know the entanglement dynamics of a deformed system which plays a vital role in quantum optics and quantum

information processing.

5.2 Light propagating through a Kerr medium

A linear medium is the one with its refractive index independent of the field transmitting through it. The medium becomes birefringent when strong laser light is propagated through a nonlinear isotropic medium. Birefringence is the optical property of a material having a refractive index that depends on the polarization and propagation direction of light. For example, the elliptical polarization of a light will get rotated as it passes through a nonlinear medium. The phenomenon by which the refractive index of a medium depends on the intensity of light passing through it is called the *optical Kerr effect* (also called “quadratic electro-optic effect”), and such a medium is called a *Kerr medium*. It is a nonlinear polarization developed in a medium, which causes a change in its refractive index. The dependence of refractive index on field intensity is given by [121] in which the authors study the quantum propagation in a Kerr medium,

$$n = n_0 + n_1 I \quad (5.1)$$

which is the so-called *Kerr law*. n_0 is the linear index of refraction, n_1 is the nonlinear refractive index and I is the field intensity. Kerr effect exists in crystals, glasses and many other materials, sometimes in isotropic materials also. In this study, we analyze the propagation of a field through a Kerr-like medium, which is described in the model given below.

5.3 The model

Consider the propagation of a single-mode math-type q -deformed field through a Kerr-like nonlinear medium. We assume a beam splitter kind of interaction between the field modes and atomic modes of the system. The total Hamiltonian representing the interaction is taken from [120] dealing with the entanglement dynamics of two-mode states,

$$H_{tot} = H_q^m + H_{atom} + H_{int}, \quad (5.2)$$

where H_q^m represents the Hamiltonian of the math-type q -deformed field, H_{atom} represents the Hamiltonian of the atomic nonlinear medium, and H_{int} is the Hamiltonian representing the interaction between the deformed field and the atoms of the nonlinear medium. The

math-type q -deformation of the field is governed by the Hamiltonian discussed in equation (4.2). The Hamiltonian of the nonlinear atomic medium is taken as

$$H_{atom} = \omega (b^\dagger b + 1/2) + \chi b^{\dagger 2} b^2, \quad (5.3)$$

where b and b^\dagger are the atomic ladder operators, ω is the natural frequency of the atomic field, and χ is the nonlinearity parameter. The interaction between the deformed field and the atomic medium is represented by the interaction Hamiltonian

$$H_{int} = \gamma (A_q^{m\dagger} b + A_q^m b^\dagger) \quad (5.4)$$

where γ is the parameter characterizing the strength of coupling between the field and the atoms. In this paper, we study the time evolution of the above given system governed by the equation

$$|\psi(t)\rangle = e^{-iH_{tot}t} |\psi(0)\rangle \quad (5.5)$$

for different types of initial states. The system dynamics explicitly depend on the initial states of the system. Thus we assume the deformed field to be initially in the Fock state $|N\rangle_q^m$ and also in the coherent state $|\alpha\rangle_q^m$. Throughout the study, the atom is taken to be in the ground state $|0\rangle$. Also, as a field propagates through a nonlinear medium, the revivals appear if the nonlinearity of the field is weak. As the nonlinearity increases, the revival phenomena becomes less noticeable [122]. Hence in the following calculations, we keep the nonlinearity of the medium to be of a lower value. We are interested in studying the entanglement dynamics of the system described above in detail. Further analysis is included in the upcoming sections.

5.4 Entanglement measures and von Neumann entropy

The entanglement measures are used to quantify the amount of entanglement contained in a given state. There exists a variety of entanglement measures, such as entanglement cost, distillable entanglement, distance-based measures (for example, relative entropy of entanglement), robustness measures, entanglement of assistance, etc. von Neumann entropy is one of them, and here we are trying to figure out the entanglement in the system in terms of the von Neumann entropy.

The term von Neumann entropy named after John von Neumann is actually a quantum mechanical counterpart of the Gibbs entropy of classical statistical mechanics. In general,

for a quantum system described by a density matrix ρ , the von Neumann entropy S is given by [63],

$$S = -\text{Tr}(\rho \ln(\rho)). \quad (5.6)$$

It can be used to measure the entanglement between two subsystems, provided that the total system is in a pure state. This entropy has become fundamental as it has applications in areas such as data compression, measures of entanglement, etc. The Von Neumann entropy of the reduced density matrix for any subsystems is also called ‘the entropy of entanglement’, which is zero for a pure state and a non-zero value indicates that the subsystem is in a mixed state, and hence the two subsystems are entangled.

We use the von Neumann entropy of the subsystem S_k as the measure of entanglement, given by

$$S_k = -\text{Tr}_k [\rho_k(t) \ln \rho_k(t)]. \quad (5.7)$$

where the suffix k stands for the either q or b , depending upon the subsystem considered. Also, ρ_k represents the time-dependent reduced density matrix for the subsystem.

5.5 Entanglement dynamics

As the total particle number $\mathcal{N}_{tot} = A_q^{m\dagger} A_q^m + b^\dagger b$, is conserved during the interaction (One can show that $[\mathcal{N}_{tot}, H_{tot}] = 0$), we choose the basis states as $|N - n\rangle \otimes |n\rangle \equiv |(N - n)_q^m; n\rangle$, where N is the eigenvalue of \mathcal{N}_{tot} . Here N runs from 0 to ∞ and n runs from 0 to N . One can see that $\langle (N - n)_q^m; n | H_{tot} | (N' - n')_q^m; n' \rangle = 0$ for $N \neq N'$. Hence for a particular N , the total Hamiltonian H_{tot} can be diagonalized in the space of $\{|(N - n)_q^m; n\rangle\}$ with $n = 0, 1, 2, \dots, N$. Let the eigenvalues and eigenvectors of H_{tot} be λ_{Ns} and $|\psi_{Ns}\rangle$, respectively. Here the index s designate the eigenvectors in each block of the Hamiltonian H_{tot} for a particular N , that is, $s = 0, 1, 2, \dots, N$. The eigenvectors $|\psi_{Ns}\rangle$ can be expanded in the basis $\{|(N - n)_q^m; n\rangle\}$ as

$$|\psi_{Ns}\rangle_q^m = \sum_{n=0}^N C_n^{Ns} |(N - n)_q^m; n\rangle, \quad (5.8)$$

with $C_n^{Ns} = \langle (N-n)_q^m ; n | \psi_{Ns} \rangle$. An initial state of the system evolves in time as

$$|\psi(t)\rangle = \exp[-i H_{tot} t] |\psi(0)\rangle \quad (5.9)$$

$$= \sum_{N=0}^{\infty} \sum_{s=0}^N e^{-i\lambda_{Ns} t} \langle \psi_{Ns} | \psi(0) \rangle | \psi_{Ns} \rangle. \quad (5.10)$$

The time-evolved density matrix of the total system is calculated as

$$\begin{aligned} \rho_{tot}(t) = & \sum_{N=0}^{\infty} \sum_{s=0}^N \sum_{N'=0}^{\infty} \sum_{s'=0}^{N'} e^{-i(\lambda_{Ns} - \lambda_{N's'}) t} \\ & \langle \psi_{Ns} | \psi(0) \rangle \langle \psi(0) | \psi_{N's'} \rangle | \psi_{Ns} \rangle \langle \psi_{N's'} |. \end{aligned} \quad (5.11)$$

5.5.1 Field initially in the deformed Fock state $|N\rangle_q^m$

Let the field be initially in the Fock state $|N\rangle_q^m$ and the atom be in the ground state $|0\rangle$. The corresponding time-evolved reduced density matrix $\rho_q^m(t)$ of the total system can be written as

$$\begin{aligned} \rho_q^m(t) = & \sum_{n=0}^N \sum_{s=0}^N \sum_{s'=0}^N C_0^{Ns} C_0^{Ns'} C_n^{Ns} C_n^{Ns'} \\ & |N-n\rangle_q^{mm} \langle N-n|, \end{aligned} \quad (5.12)$$

where $C_0^{Ns} = \langle N_q^m ; 0 | \psi_{Ns} \rangle$, where the detailed calculation of $\rho_q^m(t)$ is given in the Appendix (C).

Also,

$$\begin{aligned} \rho_a(t) = & \sum_{m=0}^N \sum_{j=0}^N \sum_{s'=0}^N C_0^{Nj} C_0^{Nj'} C_{N-m}^{Nj} C_{N-m}^{Ns'} \\ & |N-m\rangle_{aa} \langle N-m|, \end{aligned} \quad (5.13)$$

where $C_0^{Nj} = \langle N_q^m ; 0 | \psi_{Nj} \rangle$.

The variation of von Neumann entropy with the deformation parameter q is depicted in figure(5.1) for different values of N . The initial state chosen is $|5\rangle_q^m \otimes |0\rangle \equiv |5, 0\rangle$. We have taken the other parameter values as $\omega = 1, \chi = 0, \gamma = -\pi/4, t = 1$. The interaction

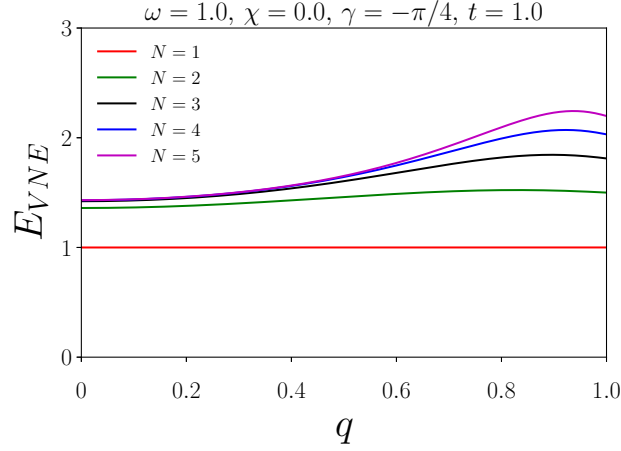


Figure 5.1: The variation of von Neumann entropy with q for different values of N , with the values of system parameters representing the action of a beam splitter.

Hamiltonian (5.4) when $\gamma = -\pi/4$ becomes the unitary operator representing the beam splitter in the deformed case. The von Neumann entropy for $N = 1, 2, 3, 4, 5$ are shown in figure (5.1) for the entire range of possible q values. A considerable variation can be seen for $N = 1$ from the other N values. For the lowest $N = 1$, entropy of the system stays a constant value equal to 1 for the entire range of possible q values. As $q \rightarrow 1$, the entropy becomes that of corresponding non-deformed cases.

A comparison of entanglement entropy of the system for an initial state $|5, 0\rangle$ for different deformations is shown in the figure(5.2). Figure(5.2a) represents the non-deformed case where the entropy returns to values close to zero at regular intervals of time, which clearly shows that there exists near revivals exhibited by the entangled states. The values of parameters are chosen to be $\omega = 1.0, \gamma = 1.0, \chi = 0.01$. In figure (5.2a), it can be noted that the revival time is approximately 2π . Fractional revivals can be observed around the times $\pi, \frac{2\pi}{3}$ and $\frac{\pi}{2}$. We can still observe the near revivals and fractional revivals for $q = 9.99$, but not much as pronounced in the case of the non-deformed system. Figure (5.2b) illustrates the entropy measured in the system for a very small deformation, say $q = 0.9$, even then the revivals have almost disappeared. The near revivals and fractional revivals have completely gone while moving to figure (5.2c) where the deformation parameter is having value $q = 0.7$. There are no revivals for $q = 0.5$. So for a given initial Fock state, even though the nonlinearity is minimum, the near revivals and fractional revivals gradually decay as the deformation in the field increases. The revival phenomena disappear even for a very small deformation.

Also, figure (5.3) outline the entropy of a different initial Fock state $|10, 0\rangle$. Here

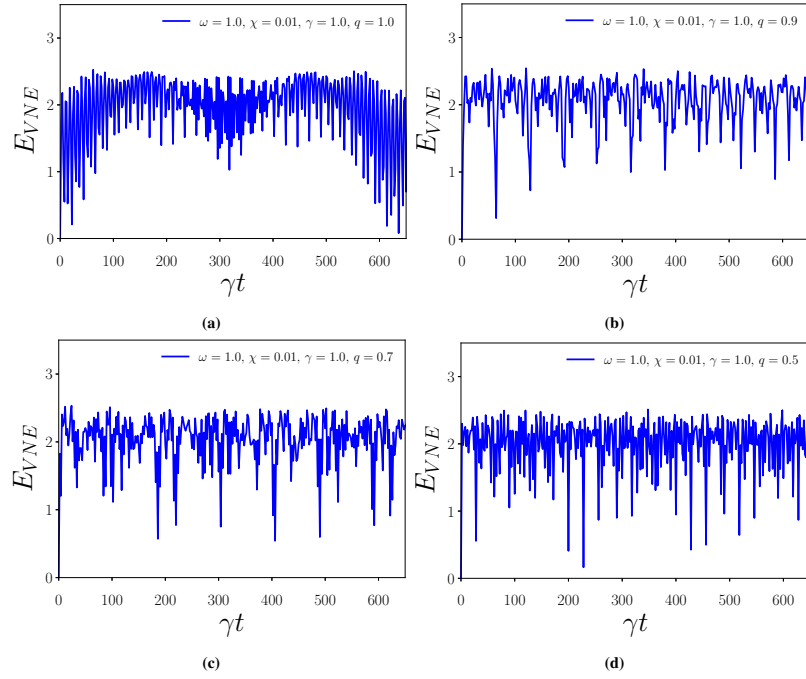


Figure 5.2: The variation of von Neumann entropy with γt for (a) non-deformed, (b) $q = 0.9$, (c) $q = 0.7$, (d) $q = 0.5$ for the initial state $|5, 0\rangle$.

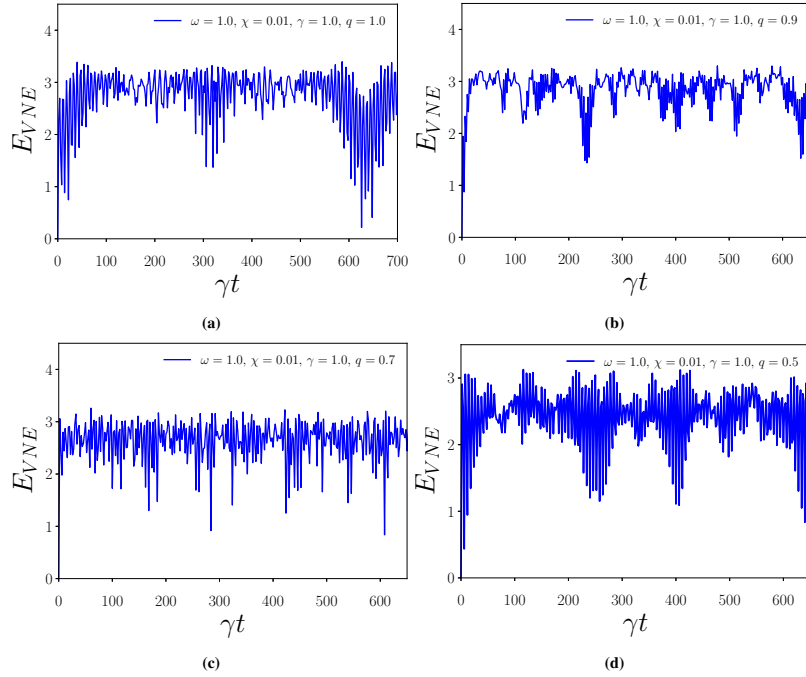


Figure 5.3: The variation of von Neumann entropy with γt for (a) non-deformed, (b) $q = 0.9$, (c) $q = 0.7$, (d) $q = 0.5$ for the initial state $|10, 0\rangle$.

also we choose weak nonlinearity ($\chi = 0.01$). Figure (5.3a) depicts the entropy of non-deformed $|10, 0\rangle$ state. It can be seen that here also the entropy regularly comes to minimum values indicating the existence of near revivals. Local minima repeating at regular intervals of time indicates fractional revivals. Even for very small deviation from the non-deformed case (i.e., for $q = 0.99$), the near revivals and fractional revivals start to disappear. The figure (5.3b) shows a further reduction in revivals as the deformation increased to $q = 0.9$. As the deformation increases, revivals gradually die out, quiet faster than for the state $|5, 0\rangle$ as the figure (5.3c) indicates. Again, the figure (5.3d) illustrates the entropy for $q = 0.5$ where the revivals have almost disappeared. Also, The entanglement entropy in the system varies for different defomation as indicated by figures (5.2) and (5.3).

5.5.2 Field initially in the deformed coherent state $|\alpha\rangle_q$

Another initial states under our consideration are, the atom in the ground state $|0\rangle$ and the field in the deformed coherent state $|\alpha\rangle_q^m$. The corresponding density matrix can be obtained through the steps described above. The reduced density matrix ρ_k in this case is given by,

$$\rho_q^m(t) = \sum_{N=0}^{\infty} \sum_{s=0}^N \sum_{N'=0}^{\infty} \sum_{s'=0}^{N'} \frac{\alpha^N (\alpha^*)^{N'}}{\sqrt{[N]![N']!}} C_0^{Ns} C_0^{N's'} C_n^{Ns} C_n^{N's'} |N-n\rangle_q^{mm} \langle N'-n| \quad (5.14)$$

and

$$\rho_a(t) = \sum_{N=0}^{\infty} \sum_{j=0}^N \sum_{N'=0}^{\infty} \sum_{j'=0}^{N'} \frac{\alpha^N (\alpha^*)^{N'}}{\sqrt{[N]![N']!}} C_0^{Nj} C_0^{N'j'} C_{N-m}^{Nj} C_{N-m}^{N'j'} |N-m\rangle_{aa} \langle N'-m|. \quad (5.15)$$

Figure (5.4) depicts the von Neumann entropy for the initial state $|\alpha\rangle_q^m \otimes |0\rangle \equiv |\alpha; 0\rangle$ for $|\alpha|^2 = 0.5$ and different deformation parameter q . Similar to a Fock state, for the non-

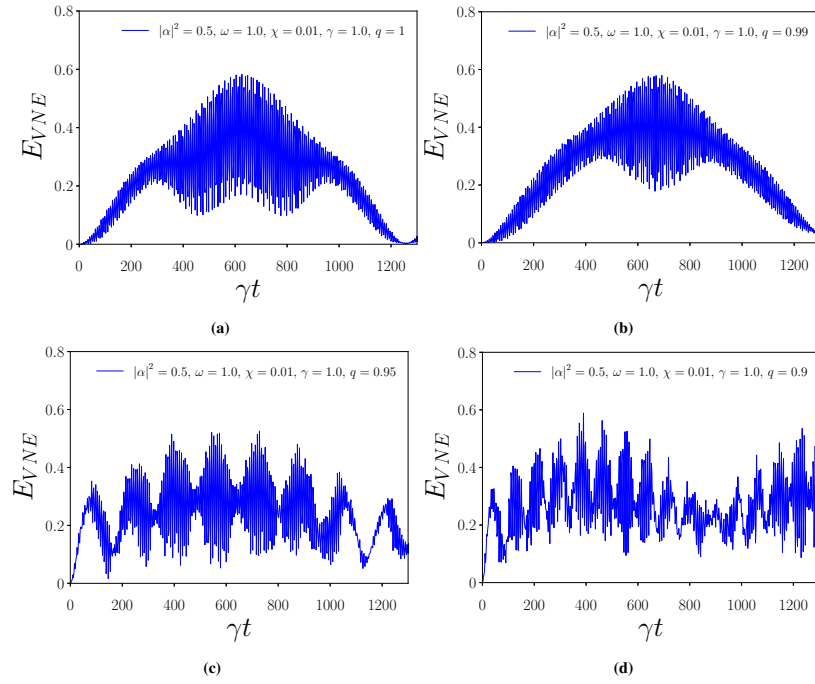


Figure 5.4: The variation of von Neumann entropy with γt for (a) non-deformed, (b) $q = 0.99$, (c) $q = 0.95$, (d) $q = 0.90$ for the initial state $|\alpha, 0\rangle$ for $|\alpha|^2 = 0.5$.

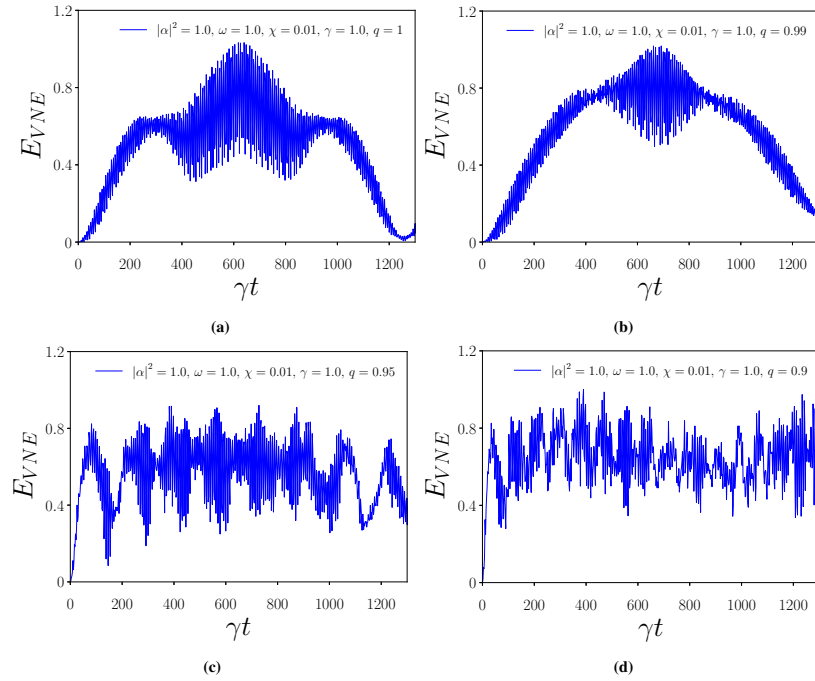


Figure 5.5: The variation of von-Neumann entropy with γt for (a) non-deformed, (b) $q = 0.99$, (c) $q = 0.95$, (d) $q = 0.90$ for the initial state $|\alpha, 0\rangle$ for $|\alpha|^2 = 1$.

deformed case given in figure (5.4a), we can observe that von Neumann entropy returns to values close to zero which happens at regular intervals of time, showing the near revivals. Again, we do the calculations for a low value of nonlinearity parameter ($\chi = 0.01$). As the deformation increases, the observed near revivals and fractional revivals die out even for a small increase in the deformation, as indicated by the figures (5.4b), (5.4c) and (5.4d) for q values $q = 0.99$, $q = 0.95$ and $q = 0.90$ respectively. Also it is clear that the entropy depends on the value of coherent parameter α . Again, the entropy values are plotted for $|\alpha|^2 = 1$ in figure (5.5) for different deformation, which also shows a similar trend. It is interesting to see that the entanglement entropy increases as the $|\alpha|^2$ value is increased.

5.6 Conclusion

In summary, we examined the interaction of a math-type q -deformed field with the atoms of a nonlinear medium through which the field propagates. The entanglement dynamics in the system is studied in terms of von Neumann entropy. The system in two different initial states are investigated: the deformed Fock state and the deformed coherent state. For the initial deformed Fock state, the variation of entropy with deformation for different values of N is studied, with the system parameters equivalent to the action of a beam splitter. As the deformation in the system decreases, the entropy gradually tends to the corresponding non-deformed cases. A more detailed analysis of the entanglement entropy for different deformation reveals that there exist revivals and fractional revivals in the non-deformed system. The entropy attains a maximum value which is a constant in each case, irrespective of the deformation present in the system. But as the deformation increases, even for a slight rise in deformation, the revivals and fractional revivals decay rapidly. The analysis is done for smaller values of the nonlinearity parameter where the revivals and fractional revivals are more visible. A similar effect is observed for the initial deformed coherent state also, with a dependence on the coherent parameter α . There is a rise in the amount of entanglement present in the system as the $|\alpha|^2$ value is increased. All the results clearly show that the entanglement in the system distinctly depends on the deformation. So, the deformation provides an additional degree of freedom, q , to control the entanglement dynamics.

Chapter 6

Conclusion

The non-deformed harmonic oscillator being ideal, the deformed oscillators are advantageous over the non-deformed one. We have included a detailed discussion of our results in the preceding chapters, each with an all-inclusive summary. Furthermore, our results lead us to propose some exciting and essential future research.

Our work begins with the discovery of the wavefunctions of the most general f -oscillators, which includes a newly obtained class of orthogonal polynomials $J_n(X_\theta)$, which is included in Chapter (2) in detail. The wavefunctions of different types of deformations (physics-type, math-type, and (p,q) -deformations) are also analyzed, and the position probability distributions for the ground and first excited state are plotted in each case. The effect of deformation on the wavefunction is studied. Even though $J_n(X_\theta)$ was found to have similar properties of Hermite polynomials $H_n(x)$, the salient features of $J_n(X_\theta)$ are not known. So, it would be interesting to investigate the properties of $J_n(X_\theta)$ in detail, to have in-depth knowledge of the f -oscillators. The study of the optical tomogram of f -oscillators will be another fascinating area of research.

Later on, in Chapter (3), we focussed on the math-type q -deformation, and the study of squeezing revealed the nonclassical behavior of the deformed superposition states in terms of quadrature squeezing, higher-order squeezing, and photon number squeezing. The quadrature squeezing independent of the deformation parameter q for deformed squeezed vacuum states and the vanishing of quadrature squeezing in the superposition states while having a higher-order squeezing were all interesting results. Also, the number squeezing persists in all the states considered. The non-Gaussian Husimi Q function reveals that the states are highly nonclassical irrespective of squeezing. The nonclassicality of the system is found to be highly dependent on q , α , and r . As the deformation increases, the system is

observed to be more nonclassical.

Further, the study of dynamics of expectation values of deformed position and momentum operators in a q -deformed harmonic oscillator included in Chapter (4) ended up in a conclusion that the system exhibits periodic, quasi-periodic, and chaotic behavior according to the values of q and α . We thus discovered a quantum system that is a source of inherent quantum chaos, with an additional degree of freedom q to control the system properties. The effects and control of decoherence on such a system will be an exciting area of future investigation.

The study of the nonclassicality of q -deformed states is extended to quantum entanglement in Chapter (5). The interaction of a math-type q -deformed field with the atoms of a nonlinear medium is analyzed in detail, for two different initial states. The entanglement exhibited by the system is measured in terms of von Neumann entropy. The revivals observed in the system are found to be highly dependent on the deformation parameter q . The study can be extended to the system with different initial states, like the deformed photon-added coherent states.

The deformed quadrature operator eigenstates that we obtained will be helpful for the quantum state reconstruction and quantum information processing of deformed states. It is very important to note that the deformation provides an additional degree of freedom to the system, i.e., the deformation parameter q , using which we can adjust the nonlinear and nonclassical properties of the system to achieve the desired results. All the analysis done for a q -deformed system can also be generalized for the f -deformed one.

Bibliography

- [1] C. M. Caves, “Quantum-mechanical noise in an interferometer,” *Phys. Rev. D*, vol. 23, p. 1693, 1981.
- [2] H. Vahlbruch, S. Chelkowski, B. Hage, A. Franzen, K. Danzmann, and R. Schnabel, “Coherent control of vacuum squeezing in the gravitational-wave detection band,” *Phys. Rev. Lett.*, vol. 97, p. 011101, 2006.
- [3] J. Aasi and et.al, “Enhanced sensitivity of the ligo gravitational wave detector by using squeezed states of light,” *Nature Photonics*, vol. 7, p. 613, 2013.
- [4] Y. Yamamoto and H. A. Haus, “Preparation, measurement and information capacity of optical quantum states,” *Rev. Mod. Phys.*, vol. 58, p. 1001, 1986.
- [5] M. F. Riedel, P. Böhi, and Y. Li, “Atom-chip-based generation of entanglement for quantum metrology,” *Nature*, vol. 464, p. 1170, 2010.
- [6] S. Roman, “Squeezed states of light and their applications in laser interferometers,” *Phys. Rep.*, vol. 684, p. 1, 2017, squeezed states of light and their applications in laser interferometers.
- [7] N. Shukla, S. Nimmrichter, and B. C. Sanders, “Squeezed comb states,” *Phys. Rev. A*, vol. 103, p. 012408, 2021.
- [8] X. Chuan and et.al., “Sensing and tracking enhanced by quantum squeezing,” *Photon. Res.*, vol. 7, p. A14, 2019.
- [9] I. G. Irastorza, “Shedding squeezed light on dark matter,” *Nature*, vol. 590, no. 6, pp. 10.1038/d41586-021-00295-6, 2021.
- [10] G. A. Durkin, C. Simon, and D. Bouwmeester, “Multiphoton entanglement concentration and quantum cryptography,” *Phys. Rev. Lett.*, vol. 88, p. 187902, 2002.

- [11] Z. Huang, C. Macchiavello, and L. Maccone, “Usefulness of entanglement-assisted quantum metrology,” *Phys. Rev. A*, vol. 94, p. 012101, 2016.
- [12] G. Moreno, R. Nery, C. de Gois, R. Rabelo, and R. Chaves, “Semi-device-independent certification of entanglement in superdense coding,” *Phys. Rev. A*, vol. 103, p. 022426, 2021.
- [13] M. Zhao, S. Fei, and X. Li-Jost, “Complete entanglement witness for quantum teleportation,” *Phys. Rev. A*, vol. 85, p. 054301, 2012.
- [14] T. Liu, Q. Su, S. Xiong, J. Liu, C. Yang, and F. Nori, “Generation of a macroscopic entangled coherent state using quantum memories in circuit QED,” *Sci. Rep.*, vol. 6, p. 32004, 2016.
- [15] L. Kuang, Z. Chen, and J. Pan, “Generation of entangled coherent states for distant Bose-Einstein condensates via electromagnetically induced transparency,” *Phys. Rev. A*, vol. 76, p. 052324, 2007.
- [16] R. F. Werner and M. M. Wolf, “Bound entangled gaussian states,” *Phys. Rev. Lett.*, vol. 86, p. 3658, 2001.
- [17] A. Dumitru and E. Kolbusz, “Quark and gluon entanglement in the proton on the light cone at intermediate x ,” *Phys. Rev. D*, vol. 105, p. 074030, 2022.
- [18] D. Bluvstein and et. al., “A quantum processor based on coherent transport of entangled atom arrays,” *Nature*, vol. 604, p. 451, 2022.
- [19] R. V. Jensen, “Quantum chaos,” *Nature*, vol. 355, p. 311, 1992.
- [20] G. Casati, B. V. Chirikov, F. M. Izraelev, and J. Ford, “Stochastic behavior of a quantum pendulum under a periodic perturbation,” in *Stochastic Behavior in Classical and Quantum Hamiltonian Systems*, G. Casati and J. Ford, Eds. Berlin, Heidelberg: Springer Berlin Heidelberg, 1979, p. 334.
- [21] G. Casati and L. Molinari, ““Quantum Chaos” with Time-Periodic Hamiltonians,” *Prog. Theor. Phys. Supp.*, vol. 98, p. 287, 1989.
- [22] E. G. Vergini and G. G. Carlo, “Semiclassical quantization with short periodic orbits,” *J. Phys. A: Math. Gen.*, vol. 33, no. 25, p. 4717, 2000.

- [23] M. Wilkinson, “Random matrix theory in semiclassical quantum mechanics of chaotic systems,” *J. Phys. A: Math. Gen.*, vol. 21, p. 1173, 1999.
- [24] M. R. Setare and P. Majari, “(2 + 1) -dimensional f-deformed dirac oscillator as f-deformed ajc model,” *Eur. Phys. J. Plus*, vol. 132, p. 458, 2017.
- [25] M. R. Setare and P. Majari, “Nonlinearity of the zigzag graphene nanoribbons with antidots via the f-deformed dirac oscillator in (2+1)-dimensions,” *Phys. Lett. A*, vol. 382, p. 428, 2018.
- [26] M. A. Marchioli, “On the q-deformed coherent states of a generalized f-oscillator,” *Phys. Scr*, vol. 73, p. 62, 2005.
- [27] R. Roman-Ancheyta, O. de los Santos-Sanchez, and C. Gonzalez-Gutierrez, “Damped casimir radiation and photon correlation measurements,” *J. Opt. Soc. Am. B*, vol. 35, p. 523, 2018.
- [28] A. J. Macfarlane, “On q-analogues of the quantum harmonic oscillator and the quantum group SU(2)_q,” *J. Phys. A: Math. Gen.*, vol. 22, p. 4581, 1989.
- [29] I. S. Sogami, K. Koizumi, and R. M. Mir-Kasimov, “q-deformed and c-deformed harmonic oscillators,” *Prog. Theor. Phys.*, vol. 110, p. 819, 2003.
- [30] A. Lorek, A. Ruffing, and J. Wess, “A q-deformation of the harmonic oscillator,” *Zeitschrift für Physik C Particles and Fields*, vol. 74, p. 369, 1997.
- [31] M. P. Jayakrishnan, S. Dey, M. Faizal, and C. Sudheesh, “q-deformed quadrature operator and optical tomogram,” *Annals Phys.*, vol. 385, p. 584, 2017.
- [32] Q. Zeng, J. Ge, H. Luo, and Y. Luo, “Thermal Radiation Laws of a q-deformed Boson System in m Dimensions,” *Int. J. Theor. Phys.*, vol. 56, p. 2738, 2017.
- [33] M. A. Martin-Delgado, “Planck distribution for a q-boson gas,” *J. Phys. A: Math. Gen.*, vol. 24, p. L1285, 1991.
- [34] A. A. Marinho, F. F. Brito, and C. Chesman, “Application of Fibonacci oscillators in the Debye model,” *J. Phys. Conf. Ser.*, vol. 568, no. 1, p. 012009, 2014.
- [35] A. A. Marinho, F. A. Brito, and C. Chesman, “Fibonacci oscillators in the Landau diamagnetism problem,” *Physica A: Statistical Mechanics and its Applications*, vol. 411, p. 74, 2014.

- [36] A. Pradeep, S. Anupama, and C. Sudheesh, “Dynamics of observables in a q -deformed harmonic oscillator,” *Eur. Phys. J. D*, vol. 74, p. 3, 2020.
- [37] V. I. Manko, G. Marmo, S. Solimeno, and F. Zaccaria, “Physical nonlinear aspects of classical and quantum q -oscillators,” *Int. J. Mod. Phys. A*, vol. 08, p. 3577, 1993.
- [38] J. L. Gruver, “ q -deformed dynamics of q -deformed oscillators,” *Phys. Lett. A*, vol. 254, p. 1, 1999.
- [39] A. A. Altintas, F. Ozaydin, C. Yesilyurt, S. Bugu, and M. Arik, “Constructing quantum logic gates using q -deformed harmonic oscillator algebras,” *Quantum Inf. Process.*, vol. 13, p. 1035, 2014.
- [40] Q. J. Zeng, Z. Cheng, and J. H. Yuan, “Thermostatistical properties of a q -deformed bosonic exciton gas,” *Eur. Phys. J. B*, vol. 81, p. 275, 2011.
- [41] A. M. Gavrilik and M. P. Rebesh, “Deformed gas of (p,q) -bosons: virial expansion and virial coefficients,” *Mod. Phys. Lett. B*, vol. 26, p. 1150030, 2012.
- [42] E. Dil and E. Kolay, “Solution of deformed einstein equations and quantum black holes,” *Adv. High Energy Phys.*, vol. 2016, p. 3973706, 2016.
- [43] A. Algin and A. S. Arikan, “Effective approach for taking into account interactions of quasiparticles from the low-temperature behavior of a deformed fermion-gas model,” *J. Stat. Mech.*, vol. 2017, p. 043105, 2017.
- [44] J. Katriel and A. I. Solomon, “Generalized q -bosons and their squeezed states,” *J. Phys. A: Math. Gen.*, vol. 24, p. 2093, 1991.
- [45] K. Mendoza, S. Dey, and V. Hussin, “Generalized squeezed states,” *Phys. Lett. A*, vol. 382, p. 3369, 2018.
- [46] M. Arik and D. D. Coon, “Hilbert spaces of analytic functions and generalized coherent states,” *J. Math. Phys.*, vol. 17, p. 524, 1976.
- [47] S. Dey and S. S. Nair, “Generalized photon-subtracted squeezed vacuum states,” *J. Phys. A: Math. Theor.*, vol. 53, no. 38, p. 385305, 2020.
- [48] P. A. M. Dirac, *The Principles of Quantum Mechanics*. Clarendon Press, 1981.
- [49] K. Suresh and C. Sudheesh, “Disappearance of squeezing in superposition states and its manifestation in the energy density,” *Phys. B: At. Mol. Opt. Phys.*, vol. 55, 2022.

- [50] K. Berrada and H. Eleuch, “Noncommutative deformed cat states under decoherence,” *Phys. Rev. D*, vol. 100, p. 016020, 2019.
- [51] S. Dey, “q-deformed noncommutative cat states and their nonclassical properties,” *Phys. Rev. D*, vol. 91, p. 044024, 2015.
- [52] J. Batouli, M. El Baz, and A. Maaouni, “Optical properties of the superposition of q-deformed coherent states,” *Mod. Phys. Lett. A*, vol. 31, p. 1650190, 2016.
- [53] C. Anastopoulos and B. Hu, “Quantum superposition of two gravitational cat states,” *Class. Quant. Grav.*, vol. 37, p. 235012, 2020.
- [54] S. Kannan, M. Rohith, and C. Sudheesh, “Nonlinear dynamics of superposition of wavepackets,” *Eur. Phys. J. Plus*, vol. 137, p. 471, 2022.
- [55] L. C. Kwek and D. Kiang, “Nonlinear squeezed states,” *J. Opt. B: Quantum Semi-class. Opt.*, vol. 5, p. 383, 2003.
- [56] A. NoormandiPour and M. K. Tavassoly, “f-deformed squeezed vacuum and first excited states, their superposition and corresponding nonclassical properties,” *Commun. Theor. Phys*, vol. 61, p. 521, 2014.
- [57] C. Sudheesh, S. Lakshmibala, and V. Balakrishnan, “Dynamics of quantum observables in entangled states,” *Phys. Lett. A*, vol. 373, no. 32, p. 2814, 2009.
- [58] Sudheesh, C., Lakshmibala, S., and Balakrishnan, V., “Recurrence statistics of observables in quantum-mechanical wave packet dynamics,” *EPL*, vol. 90, p. 50001, 2010.
- [59] A. Shankar, L. Swaminathan, and V. Balakrishnan, “Dynamics of an open quantum system interacting with a quantum environment,” *J. Phys. B: Atom. Mol. Phys.*, vol. 47, 2014.
- [60] K. Berrada and S. Abdel-Khalek, “Entanglement of atom–field interaction for nonlinear optical fields,” *Physica E Low Dimens. Syst. Nanostruct.*, vol. 44, p. 628, 2011.
- [61] E. M. Khalil, A. B. A. Mohamed, A. S. F. Obada, and S. K. Elagan, “Nonlinear optical tomography of q-deformed entangled pair coherent states,” *Results in Physics*, vol. 20, p. 103720, 2021.

- [62] N. O’Dea, F. Burnell, A. Chandran, and V. Khemani, “From tunnels to towers: Quantum scars from lie algebras and q-deformed lie algebras,” *Phys. Rev. Research*, vol. 2, p. 043305, 2020.
- [63] J. Audretsch, *Entangled Systems*. John Wiley, 2007.
- [64] P. Agrawal and A. Pati, “Perfect teleportation and superdense coding with w states,” *Phys. Rev. A*, vol. 74, p. 062320, 2006.
- [65] K. Berrada, S. A. Khalek, and C. H. R. Ooi, “Quantum metrology with entangled spin-coherent states of two modes,” *Phys. Rev. A*, vol. 86, p. 033823, 2012.
- [66] S. S. Mizrahi, J. P. Camargo Lima, and V. V. Dodonov, “Energy spectrum, potential and inertia functions of a generalized f-oscillator,” *J. Phys. A: Math. Gen.*, vol. 37, p. 3707, 2004.
- [67] V. I. Manko, G. Marmo, E. C. G. Sudarshan, and F. Zaccaria, “f-oscillators and nonlinear coherent states,” *Phys. Scr.*, vol. 55, p. 528, 1997.
- [68] R. Chakrabarti and R. Jagannathan, “A (p, q) -oscillator realization of two-parameter quantum algebras,” *J. Phys. A: Math. Gen.*, vol. 24, p. L711, 1991.
- [69] L. C. Biedenharn, “The quantum group $SU_q(2)$ and a q-analogue of the boson operators,” *J. Phys. A: Math. Gen.*, vol. 22, p. L873, 1989.
- [70] C. Quesne, K. A. Penson, and V. M. Tkachuk, “Maths-type q-deformed coherent states for $q > 1$,” *Phys. Lett. A*, vol. 313, no. 1, p. 29, 2003.
- [71] T. Brzeziński, I. L. Egusquiza, and A. J. Macfarlane, “Generalised harmonic oscillator systems and their fock space description,” *Phys. Lett. B*, vol. 311, p. 202, 1993.
- [72] A. J. Macfarlane, “Algebraic structure of parabose fock space. i. the green’s ansatz revisited,” *J. Math. Phys.*, vol. 35, p. 1054, 1994.
- [73] B. Bagchi and A. Fring, “Minimal length in quantum mechanics and non-Hermitian Hamiltonian systems,” *Phys. Lett. A*, vol. 373, p. 4307, 2009.
- [74] S. Dey, A. Fring, L. Gouba, and P. G. Castro, “Time-dependent q-deformed coherent states for generalized uncertainty relations,” *Phys. Rev. D*, vol. 87, p. 084033, 2013.
- [75] W. Vogel and J. Grabow, “Statistics of difference events in homodyne detection,” *Phys. Rev. A*, vol. 47, p. 4227, 1993.

- [76] B. Yurke and D. Stoler, “Measurement of amplitude probability distributions for photon-number-operator eigenstates,” *Phys. Rev. A*, vol. 36, p. 1955, 1987.
- [77] H. Yuen and J. Shapiro, “Optical communication with two-photon coherent states—part iii: Quantum measurements realizable with photoemissive detectors,” *IEEE Transactions on Information Theory*, vol. 26, p. 78, 1980.
- [78] H. P. Yuen and V. W. S. Chan, “Noise in homodyne and heterodyne detection,” *Opt. Lett.*, vol. 8, p. 177, 1983.
- [79] T. S. Chihara, *An introduction to orthogonal polynomials*. Gordon and Breach, 1978.
- [80] G. E. Andrews, *q-Series: Their development and application in analysis, number theory, combinatorics, physics, and computer algebra*. American Mathematical Soc., 1986, vol. 66.
- [81] V. G. Drinfeld, “Quantum groups,” *Zap. Nauchn. Semin.*, vol. 155, p. 18, 1986.
- [82] M. Jimbo, “Introduction to the Yang-Baxter equation,” *Int. Jour. Mod. Phys. A*, vol. 04, p. 3759, 1989.
- [83] D. T. Smithey, M. Beck, A. Faridani, and M. G. Raymer, “Measurement of the wigner distribution and the density matrix of a light mode by using optical homodyne tomography: application to squeezed states and vacuum,” in *Quantum Electronics and Laser Science Conference*. Optica Publishing Group, 1993, p. QThF7.
- [84] M. Rohith and C. Sudheesh, “Visualizing revivals and fractional revivals in a kerr medium using an optical tomogram,” *Phys. Rev. A*, vol. 92, p. 053828, 2015.
- [85] P. Laha, S. Lakshmibala, and V. Balakrishnan, “Estimation of nonclassical properties of multiphoton coherent states from optical tomograms,” *J. Mod. Opt.*, vol. 65, p. 1466, 2018.
- [86] B. Sharmila, K. Saumitran, S. Lakshmibala, and V. Balakrishnan, “Signatures of nonclassical effects in optical tomograms,” *J. Phys. B: At. Mol. Opt. Phys.*, vol. 50, p. 045501, 2017.
- [87] S. H. Dong, *Factorization Method in Quantum Mechanics*. Springer, 2007.
- [88] D. F. Walls, “Squeezed states of light,” *Nature*, vol. 306, p. 141, 1983.

- [89] B. e. a. Caron, “The virgo interferometer,” *Classical and quantum gravity*, vol. 14, p. 1461, 1997.
- [90] M. Vasilyev and N. Stelmakh, “Squeezing in fiber-optic communications,” *Int. J. Mod. Phys. B*, vol. 20, p. 1536, 2006.
- [91] Y. Shevy, B. Crosignani, and A. Yariv, “Quantum fluctuations of the optical forces on atoms in a squeezed vacuum,” *Phys. Rev. A*, vol. 46, p. 1421, 1992.
- [92] G. J. Milburn and S. L. Braunstein, “Quantum teleportation with squeezed vacuum states,” *Phys. Rev. A*, vol. 60, p. 937, 1999.
- [93] C. Gerry and P. Knight, *Introductory Quantum Optics*. Cambridge University Press, 2004.
- [94] C. K. Hong and L. Mandel, “Higher-order squeezing of a quantum field,” *Phys. Rev. Lett.*, vol. 54, p. 323, 1985.
- [95] L. Mandel, “Sub-Poissonian photon statistics in resonance fluorescence,” *Opt. Lett.*, vol. 4, no. 7, p. 205, 1979.
- [96] K. Husimi, “Some formal properties of the density matrix,” *Proc. Phys.-Math. Soc. Jpn.*, vol. 22, p. 264, 1940.
- [97] Y. Kano, “A new phase-space distribution function in the statistical theory of the electromagnetic field,” *J. Math. Phys.*, vol. 6, p. 1913, 1965.
- [98] R. E. Slusher, L. W. Hollberg, B. Yurke, J. C. Mertz, and J. F. Valley, “Observation of squeezed states generated by four-wave mixing in an optical cavity,” *Phys. Rev. Lett.*, vol. 55, p. 2409, 1985.
- [99] K. Zelaya, S. Dey, and V. Hussin, “Generalized squeezed states,” *Phys. Lett. A*, vol. 382, p. 3369, 2018.
- [100] B. J. Lawrie, P. D. Lett, A. M. Marino, and R. C. Pooser, “Quantum sensing with squeezed light,” *ACS Photonics*, vol. 6, no. 6, pp. 1307–1318, 2019.
- [101] K. Jeong, J. Kim, and S. Y. Lee, “Gaussian private quantum channel with squeezed coherent states,” *Sci. Rep.*, vol. 5, p. 13974, 2015.

- [102] Y. A. Barbosa, G. C. Marques, and B. Baseia, “Generalized superposition of two squeezed states: generation and statistical properties,” *Phys. A: Stat. Mech. Appl.*, vol. 280, p. 346, 2000.
- [103] S. Dey and V. Hussin, “Entangled squeezed states in noncommutative spaces with minimal length uncertainty relations,” *Phys. Rev. D*, vol. 91, p. 124017, 2015.
- [104] A. Hertz, S. Dey, V. Hussin, and H. Eleuch, “Higher order nonclassicality from nonlinear coherent states for models with quadratic spectrum,” *Symmetry*, vol. 8, 2016.
- [105] C. Sudheesh, S. Lakshmibala, and V. Balakrishnan, “Squeezing and higher-order squeezing of photon-added coherent states propagating in a Kerr-like medium,” *J. Opt. B: Quantum Semiclass. Opt.*, vol. 7, no. 12, p. S728, 2005.
- [106] S. Sivakumar, “Studies on nonlinear coherent states,” *J. Opt. B: Quantum Semiclass. Opt.*, vol. 2, p. R61, 2000.
- [107] J. Récamier, M. Gorayeb, W. L. Mochán, and J. L. Paz, “Nonlinear coherent states and some of their properties,” *Int. J. Theor. Phys.*, vol. 47, p. 673, 2008.
- [108] C. Sudheesh, S. Lakshmibala, and V. Balakrishnan, “Manifestations of wave packet revivals in the moments of observables,” *Phys. Lett. A*, vol. 329, p. 14, 2004.
- [109] V. V. Eremin and A. A. Meldianov, “The q-deformed harmonic oscillator, coherent states, and the uncertainty relation,” *Theor. Math. Phys.*, vol. 147, p. 709, 2006.
- [110] N. Marwan, R. M. Carmen, M. Thiel, and J. Kurths, “Recurrence plots for the analysis of complex systems,” *Phys. Rep.*, vol. 438, p. 237, 2007.
- [111] R. S. Dumont and P. Brumer, “Characteristics of power spectra for regular and chaotic systems,” *J. Chem. Phys.*, vol. 88, p. 1481, 1988.
- [112] G. Baxter, “Mark kac, probability and related topics in physical sciences,” *Bull. Am. Math. Soc.*, vol. 66, p. 472, 1960.
- [113] M. T. Rosenstein, J. J. Collins, and C. J. De Luca, “A practical method for calculating largest Lyapunov exponents from small data sets,” *Physica D*, vol. 65, p. 117, 1993.
- [114] A. Wolf, W. B. Swift, H. L. Swinney, and J. A. Vastano, “Determining Lyapunov exponents from a time series,” *Physica D*, vol. 16, p. 285, 1985.

- [115] B. Vladimír, “Dynamics of a q-analogue of the quantum harmonic oscillator,” *J. Mod. Opt.*, vol. 38, p. 801, 1991.
- [116] N. Zou, “Quantum entanglement and its application in quantum communication,” *J. Phys. Conf. Ser.*, vol. 1827, p. 012120, 2021.
- [117] J. Yin, Y. Li, and S. e. a. Liao, “Entanglement-based secure quantum cryptography,” *Nature*, vol. 582, p. 501, 2020.
- [118] A. Barenco and A. K. Ekert, “Dense coding based on quantum entanglement,” *Journal of Modern Optics*, vol. 42, p. 1253, 1995.
- [119] Abdel-Khalek, S., Berrada, K., and Obada, A.S.F., “Quantum Fisher information for a single qubit system,” *Eur. Phys. J. D*, vol. 66, p. 69, 2012.
- [120] C. Sudheesh, S. Lakshmibala, and V. Balakrishnan, “Wave packet dynamics of entangled two-mode states,” *J. Phys. B: At. Mol. Opt. Phys.*, vol. 39, p. 3345, 2006.
- [121] L. G. Joneckis and J. H. Shapiro, “Quantum propagation in a Kerr medium: lossless, dispersionless fiber,” *J. Opt. Soc. Am. B.*, vol. 10, p. 1102, 1993.
- [122] G. S. Agarwal and R. R. Puri, “Collapse and revival phenomenon in the evolution of a resonant field in a Kerr-like medium,” *Phys. Rev. A*, vol. 39, p. 2969, 1989.

List of Publications

Refereed Journals

1. A. Pradeep, S. Anupama and C. Sudheesh, "Dynamics of observables in a q -deformed harmonic oscillator", *Eur. Phys. J. D*, vol. 74, p. 3, 2020.

Author contribution statement(from the paper): AditiPradeep and S. Anupama have carried out the work and contributed equally to this work as first authors.

2. S. Anupama , A. Pradeep, A. Pal and C. Sudheesh, "Quadrature operator eigenstates and energy eigenfunctions of f -deformed oscillators". *Indian J. Phys.*, vol. 96, p. 3559, 2022.
3. S. Anupama , S. Kannan and C. Sudheesh "Squeezing and nonclassicality of q -deformed superposition states". *Eur. Phys. J. D*, vol. 76, p. 11, 2022.

Manuscript under preparation:

1. S. Anupama , M. Rohith and C. Sudheesh "Entanglement dynamics of q -deformed states in a nonlinear medium".

Appendix A

The calculation of Husimi Q-function for the state $|\xi\rangle_q^m$

As discussed in the Chapter (3), the q -deformed Husimi function Q is

$$Q(\alpha) = \frac{1}{\pi^m} \langle \alpha | \rho | \alpha \rangle_q^m, \quad (\text{A.1})$$

where ρ is the density operator and $|\alpha\rangle_q^m$ is the q -deformed coherent state given by

$$\rho = |\xi\rangle_q^m \langle \xi| \quad (\text{A.2})$$

and

$$|\alpha\rangle_q^m = \frac{1}{\sqrt{e_q}} \sum_{n=0}^{\infty} \frac{(\alpha)^n}{\sqrt{[n]_q^m!}} |n\rangle_q^m, \quad (\text{A.3})$$

where

$$e_q = \sum_{n=0}^{\infty} \frac{(\bullet)^n}{[n]_q^m!}. \quad (\text{A.4})$$

Now,

$$\begin{aligned} Q(\alpha) &= \frac{1}{\pi^m} \langle \alpha | \xi \rangle_q^m \langle \xi | \alpha \rangle_q^m \\ &= \frac{1}{\pi^m} |\langle \alpha | \xi \rangle_q^m|^2. \end{aligned} \quad (\text{A.5})$$

Let us evaluate the term ${}^m\langle \alpha | \xi \rangle_q^m$.

$${}^m\langle \alpha | \xi \rangle_q^m = \frac{1}{\sqrt{e_q}} \left\{ \sum_{m=0}^{\infty} \frac{(\alpha^*)^m}{\sqrt{[m]_q^m!}} \langle m | \rangle_q^m N_q^m \left\{ \sum_{n=0}^{\infty} (-e^{i\theta} \tanh r)^n \sqrt{\frac{[2n-1]_q^m!!}{[2n]_q^m!!}} |2n\rangle_q^m \right\} \right\}. \quad (\text{A.6})$$

The above given relation exists only when $m = 2n$. Thus,

$${}^m_q \langle \alpha | \xi \rangle_q^m = \frac{1}{\sqrt{e_q}} \sum_{m=0}^{\infty} N_q^m \frac{(\alpha^*)^{2n}}{\sqrt{[2n]_q^m!}} (-1)^n (e^{i\theta} \tanh r)^n \sqrt{\frac{[2n-1]_q^{m!!}}{[2n]_q^{m!!}}}. \quad (\text{A.7})$$

Now, substituting (A.7) in (A.5), we get

$$Q(\alpha) = \frac{1}{\pi e_q} |N_q^m \sum_{m=0}^{\infty} \frac{(\alpha^*)^{2n}}{\sqrt{[2n]_q^m!}} (-1)^n (e^{i\theta} \tanh r)^n \sqrt{\frac{[2n-1]_q^{m!!}}{[2n]_q^{m!!}}}|^2. \quad (\text{A.8})$$

Appendix B

The calculation of $\langle X_q^{m^2} \rangle$ for the deformed squeezed superposition state $|\alpha, \xi\rangle_{s,q}^m$

We have,

$$X_q^m = \frac{\sqrt{1+q^2}}{2}(A_q^{m\dagger} + A_q^m). \quad (\text{B.1})$$

Thus,

$$\langle X_q^{m^2} \rangle = \frac{1+q^2}{4}(\langle A_q^{m^2} \rangle + \langle (A_q^{m\dagger})^2 \rangle + (1+q^2)\langle A_q^{m\dagger} A_q^m \rangle + 1). \quad (\text{B.2})$$

Now, let us evaluate each term in equation (B.2) separately.

$$\begin{aligned} \langle A_q^{m^2} \rangle &= \langle (A_q^{m\dagger})^2 \rangle \\ &= {}^m_{s,q} \langle \alpha, \xi | A_q^{m^2} | \alpha, \xi \rangle_{s,q}^m \\ &= N_{s,q}^{m^2} \left({}^m_q \langle \alpha, \xi | A_q^{m^2} | \alpha, \xi \rangle_q^m + {}^m_q \langle \alpha, \xi | A_q^{m^2} | \alpha, -\xi \rangle_q^m \right. \\ &\quad \left. + {}^m_q \langle \alpha, -\xi | A_q^{m^2} | \alpha, \xi \rangle_q^m + {}^m_q \langle \alpha, -\xi | A_q^{m^2} | \alpha, -\xi \rangle_q^m \right) \\ &= N_{s,q}^{m^2} \left(N_q^{m^2}(\alpha, \xi) \sum_{n=0}^{\infty} \frac{I(\alpha, \xi, n+2)I(\alpha, \xi, n)}{[n]_q^{m!}} \right. \\ &\quad \left. + N_q^m(\alpha, \xi)N_q^m(\alpha, -\xi) \sum_{n=0}^{\infty} \frac{I(\alpha, \xi, n+2)I(\alpha, -\xi, n)}{[n]_q^{m!}} \right. \\ &\quad \left. + N_q^m(\alpha, -\xi)N_q^m(\alpha, \xi) \sum_{n=0}^{\infty} \frac{I(\alpha, -\xi, n+2)I(\alpha, \xi, n)}{[n]_q^{m!}} \right. \\ &\quad \left. + N_q^{m^2}(\alpha, -\xi) \sum_{n=0}^{\infty} \frac{I(\alpha, -\xi, n+2)I(\alpha, -\xi, n)}{[n]_q^{m!}} \right), \quad (\text{B.3}) \end{aligned}$$

where $N_q^{m^2}(\alpha, \xi)$ and $N_{s,q}^{m^2}(\alpha, \xi)$ are given by (3.24) and (3.27) respectively.

Also,

$$\begin{aligned}
\langle A_q^{m^\dagger} A_q^m \rangle &= N_{s,q}^{m^2} \left(N_q^{m^2}(\alpha, \xi) \sum_{n=0}^{\infty} \frac{I^2(\alpha, \xi, n)}{[n-1]_q^{m!}} \right. \\
&\quad + N_q^{m^2}(\alpha, -\xi) \sum_{n=0}^{\infty} \frac{I^2(\alpha, -\xi, n)}{[n-1]_q^{m!}} \\
&\quad \left. + 2N_q^m(\alpha, \xi)N_q^m(\alpha, -\xi) \sum_{n=0}^{\infty} \frac{I(\alpha, \xi, n)I(\alpha, -\xi, n)}{[n-1]_q^{m!}} \right). \quad (\text{B.4})
\end{aligned}$$

Now substituting equations (B.3) and (B.4) in (B.2), we get

$$\begin{aligned}
\langle X_q^{m^2} \rangle &= \left(\frac{1+q^2}{4} \right) N_{s,q}^{m^2} \left[N_q^{m^2}(\alpha, \xi) \left(\sum_{n=0}^{\infty} \frac{I(\alpha, \xi, n+2)I(\alpha, \xi, n)}{[n]_q^{m!}} + (1+q^2) \sum_{n=0}^{\infty} \frac{I^2(\alpha, \xi, n)}{[n-1]_q^{m!}} \right) \right. \\
&\quad + N_q^{m^2}(\alpha, -\xi) \left(\sum_{n=0}^{\infty} \frac{I(\alpha, -\xi, n+2)I(\alpha, -\xi, n)}{[n]_q^{m!}} + (1+q^2) \sum_{n=0}^{\infty} \frac{I^2(\alpha, -\xi, n)}{[n-1]_q^{m!}} \right) \\
&\quad + N_q^m(\alpha, \xi)N_q^m(\alpha, -\xi) \left(\sum_{n=0}^{\infty} \frac{I(\alpha, \xi, n+2)I(\alpha, -\xi, n)}{[n]_q^{m!}} + \sum_{n=0}^{\infty} \frac{I(\alpha, -\xi, n+2)I(\alpha, \xi, n)}{[n]_q^{m!}} \right. \\
&\quad \left. + 2(1+q^2) \sum_{n=0}^{\infty} \frac{I(\alpha, \xi, n)I(\alpha, -\xi, n)}{[n-1]_q^{m!}} \right) \left. \right] + \left(\frac{1+q^2}{4} \right). \quad (\text{B.5})
\end{aligned}$$

Appendix C

Calculation of reduced density matrix for the system with initial state $|N_q^m; 0\rangle$

The time-evolved density matrix can be calculated as

$$\begin{aligned}
 \rho_{tot}(t) &= |\psi(t)\rangle\langle\psi(t)| \\
 &= \sum_{N=0}^{\infty} \sum_{s=0}^N \sum_{N'=0}^{\infty} \sum_{s'=0}^{N'} e^{-i(\lambda_{Ns}-\lambda_{N's'})t} \\
 &\quad \langle\psi_{Ns}|\psi(0)\rangle\langle\psi(0)|\psi_{N's'}\rangle|\psi_{Ns}\rangle\langle\psi_{N's'}|
 \end{aligned} \tag{C.1}$$

For the field initially in the Fock state $|N\rangle_q^m$ and the atom be in the ground state $|0\rangle$, we have

$$\begin{aligned}
 \rho(t) &= \sum_{s=0}^N \sum_{s'=0}^N e^{-i(\lambda_{Ns}-\lambda_{N's'})t} \langle\psi_{Ns}|N_q^m; 0\rangle\langle N_q^m; 0|\psi_{N's'}\rangle|\psi_{Ns}\rangle\langle\psi_{N's'}| \\
 &= \sum_{s=0}^N \sum_{s'=0}^N e^{-i(\lambda_{Ns}-\lambda_{N's'})t} C_0^{Ns} C_0^{N's'} |\psi_{Ns}\rangle\langle\psi_{N's'}|,
 \end{aligned} \tag{C.2}$$

where $C_n^{Ns} = \langle\psi_{Ns}|(N-n)_q^m; n\rangle$.

The reduced density matrix $\rho_k(t)$ is,

$$\begin{aligned}
\rho_q^m(t) &= Tr_a[\rho(t)] \\
&= \sum_{n=0}^{\infty} {}_a\langle n|\rho(t)|n\rangle_a \\
&= \sum_{n=0}^N \sum_{s=0}^N \sum_{s'=0}^N e^{-i(\lambda_{Ns}-\lambda_{N's'})t} C_0^{Ns} C_0^{Ns'} \langle (N-n)_q^m; n|\psi_{Ns}\rangle \langle \psi_{Ns'}|(N-n)_q^m; n\rangle |N-n\rangle_q^{mm} \langle N-n| \\
&= \sum_{n=0}^N \sum_{s=0}^N \sum_{s'=0}^N e^{-i(\lambda_{Ns}-\lambda_{N's'})t} C_0^{Ns} C_0^{Ns'} C_{N-n}^{Ns} C_{N-n}^{Ns'} |N-n\rangle_q^{mm} \langle N-n| \tag{C.3}
\end{aligned}$$

and

$$\begin{aligned}
\rho_a(t) &= Tr_q[\rho(t)] \\
&= \sum_{n=0}^{\infty} {}_q^m\langle n|\rho(t)|n\rangle_q^m \\
&= \sum_{n=0}^N \sum_{s=0}^N \sum_{s'=0}^N e^{-i(\lambda_{Ns}-\lambda_{N's'})t} C_0^{Ns} C_0^{Ns'} \langle n_q^m; N-n|\psi_{Ns}\rangle \langle \psi_{Ns'}|n_q^m; N-n\rangle |N-n\rangle_{aa} \langle N-n| \\
&= \sum_{n=0}^N \sum_{s=0}^N \sum_{s'=0}^N e^{-i(\lambda_{Ns}-\lambda_{N's'})t} C_0^{Ns} C_0^{Ns'} C_n^{Ns} C_n^{Ns'} |N-n\rangle_{aa} \langle N-n|. \tag{C.4}
\end{aligned}$$